

**Advanced Aero Engine Common Preliminary  
Design Environment**  
**for the Automatic Construction of Secondary Air  
System and Thermal Models**

Von der Fakultät für Maschinenbau, Elektrotechnik und Wirtschaftsingenieurwesen der  
Brandenburgischen Technischen Universität Cottbus-Senftenberg zur Erlangung  
des akademischen Grades eines Doktor-Ingenieurs genehmigte Dissertation

vorgelegt von

**Diplom-Ingenieur**  
**Jose María Rey Villazón**

geboren am 10.09.1982 in Madrid

Vorsitzender: Prof. Dr.-Ing. Heiko Schmidt

Gutachter: Prof. Dr.-Ing. Arnold Kühhorn

Gutachter: Prof. Dr.-Ing. Klaus Höschler

Tag der mündlichen Prüfung: 29.04.2015



“Weniger ist mehr”. L. Mies van der Rohe; R. Posse; L. Rey Arnaiz.



# Vorwort

Die vorliegende Dissertation beinhaltet die Ergebnisse meiner Arbeit als wissenschaftlicher Mitarbeiter am Lehrstuhl für Strukturmechanik und Fahrzeugschwingungen (SMF) im Institut für Verkehrstechnik der Brandenburgischen Technischen Universität Cottbus-Senftenberg (BTU). Sie wurde von Herrn Prof. Dr.-Ing. Arnold Kühhorn als Leiter des Lehrstuhls angeregt, dem ich für die wohlwollende Unterstützung, das in mich gesetzte Vertrauen und sein leitendes Vorbild ausdrücklich danken möchte. Herrn Prof. Dr.-Ing. Klaus Höschler gilt mein besonderer Dank für die hilfreichen Korrekturen und die Begutachtung dieser Dissertation. Weiterhin möchte ich mich bei Herrn Prof. Dr.-Ing. Heiko Schmidt für den Vorsitz im Promotionsausschuss bedanken.

Die Arbeit entstand im Rahmen des Programms ViT3 (Virtuelles Triebwerk 3) als Kooperation zwischen der BTU und Rolls-Royce Deutschland (RRD). Dabei hat das Team von RRD einen besonderen Beitrag zum Fachverständnis und der Koordination dieses Projekts geleistet. Hiermit möchte ich Dr.-Ing. Roland Parchem, Robert Benton und Dr.-Ing. Roland Wilhelm für ihre einzigartige Förderung, Unterstützung und Motivation danken. Zum Gelingen dieser Arbeit beigetragen haben auch meine ehemaligen Kollegen Thomas Weiß, Stephan Weinold, Ronja Nazir, Tom Barker und Antonio Guijarro. Die erfolgreiche Fertigstellung meiner Dissertation hat mir mein aktueller Vorgesetzter Günter Wilfert bei GE Aviation erleichtert.

Besonders bedanken möchte ich mich außerdem bei meinen ViT3 Kollegen, vor allem bei meinen Promotionsbrüdern Behnam Nouri, Andreas Angersbach, Philipp Amtsfeld und Moritz Albert. Mein Dank gilt natürlich auch allen anderen Kollegen am Lehrstuhl – unter anderem Bernd Beïrow, Tina de Silva, Thomas Giersch, Georg Rauer, Markus Kober. Mark Gölze hat die Computer-Technik für diese Dissertation ermöglicht und Katrin Weyer hat mir bei allen Verwaltungsangelegenheiten tatkräftig geholfen. Das Fundament meiner Leidenschaft für die Luft- und Raumfahrt wurde von meinen Freunden und den Professoren an der ETSI Aeronáuticos der Universidad Politécnica de Madrid gelegt.

Natürlich gilt ein ganz herzlicher Dank meiner Frau Julia für Ihre grenzlose Unterstützung und nun tiefen Kenntnisse von Luftsystemkavitäten. Meinen Eltern, Luilli und den Niederländern möchte ich besonders danken, sowie meinen Schwiegereltern und Dirk, die mir den nötigen Rückhalt gegeben und mich stets geleitet und unterstützt haben.

Letztendlich gilt diese Danksagung zum Lob und zur Motivation meiner Studenten während des ViT3: D. Grasselt, H. Brammer, M. Berthold, F. Hein, J. Garcia Revillo, V. Kovalchuk, S. Bochmann, M. Reichelt, T. Eydam und Toni Wildow.

Es gibt keine schönere Zeit für einen Forscher als die erste Woche seiner Promotion ...



## **Kurzfassung**

### **Integrierte Vorauslegungsumgebung zur automatisierten Erzeugung von Sekundärluftsystem- und Thermalmodellen für Flugtriebwerke**

Schlüsselwörter: Triebwerkskonstruktion, Sekundärluftsystem, Thermal-Modellierung, Prozessintegration.

Der Stand der Technik in der Triebwerkskonstruktion und -berechnung sind ausgereifte Methoden, die über Jahrzehnte entwickelt und in Computerprogrammen umgesetzt wurden. Nach dem klassischen Ansatz der Vorauslegung von Flugtriebwerken wird der komplexe Entwicklungsprozess in Disziplinen und Teilaufgaben aufgeteilt. Dadurch führen verschiedene Fachleute die zeitaufwendigen Modellierungsarbeiten durch. Aufgrund der steigenden Anforderungen an die Leistung eines Flugtriebwerks und zur Reduzierung der Entwicklungszeiten entwickeln sich Prozessintegration, Modellgenauigkeit und Prozessgeschwindigkeit zu Schlüsselfaktoren.

Mit dieser Arbeit soll gezeigt werden, wie fachübergreifende Integration, Automatisierung und CFD-erweiterte Thermalmodellierungsmethoden zur effizienten Unterstützung in der Triebwerksvorauslegung eingesetzt werden können. Dafür wurde eine Java-basierte Vorauslegungsumgebung für die Integration der Disziplinen Sekundärluftsystemauslegung, Turbinenscheibenkonstruktion und Wärmeübergang entwickelt, welche die automatisierte Erzeugung von CAD-, Strömungsnetzwerk- und Thermalmodellen ermöglicht.

Der implementierte Prozess wird auf eine existierende Hochdruckturbinen als Bezugsfall angewendet, wodurch die Verbesserung der Prozessgeschwindigkeit und der Genauigkeit der Temperaturvorhersage aufgezeigt wird. Zur Validierung dieser Arbeit wird die Vorauslegung des Bezugsfalls nachgebildet. Dabei wird deutlich, dass mit diesem automatisierten Prozess die gleiche Modelltreue erreicht werden kann, wie mit dem bisher genutzten manuellen Prozess. Außerdem konnte mittels der CFD-erweiterten Thermalmodellierung die Temperaturvorhersage für Turbinenscheiben in der Vorauslegungsphase verbessert werden.

## **Abstract**

# **Advanced Aero Engine Common Preliminary Design Environment for the Automatic Construction of Secondary Air System and Thermal Models**

Key words: aero engine design, secondary air system, turbine rotors, thermal modelling, process integration.

The state of the art in aero engine design and analysis methods is based on mature computer programs, which have been developed during several decades. The classical approach to the preliminary design phase of engine subsystems is to split the complex engineering process into disciplines and subtasks. Different experts manage the time-consuming modelling work. Due to the increasing demand for higher aero engine performance and design cycle time reduction, process integration, accuracy and agility have become key assets of the engineering work-flow.

The intention of this work is to show how multi-disciplinary integration, work-flow automation and CFD-enhanced thermal modelling methods can be used efficiently to support the aero engine preliminary design phase, with focus on the high pressure turbine subsystem. A Java based common design environment for the engine secondary air system, rotors and thermal design disciplines has been developed. This design environment enables the automatic generation of CAD, flow network and thermal models.

The improvements in terms of process agility and model prediction accuracy are demonstrated with the application of the implemented process to a reference high pressure turbine subsystem. For validation purposes, the preliminary design definition of the reference turbine case is reproduced. The automatically generated secondary air system and thermal models can replicate the same level of detail as the previous manual approach. It was found that the CFD-enhanced thermal model improves the prediction accuracy in the preliminary design stage, when no engine test data is available.



# Contents

---

<b>List of Symbols</b>	<b>v</b>
<b>Abbreviations</b>	<b>ix</b>
<b>1. Introduction</b>	<b>1</b>
1.1. The Aero Engine and its Subsystems . . . . .	2
1.1.1. Working principles . . . . .	4
1.1.2. Aero engine design . . . . .	6
1.2. Internal Heat Management . . . . .	11
1.3. Design Philosophy of the Secondary Air System . . . . .	13
1.4. Structure of the Thesis . . . . .	17
<b>2. State of the Art Review</b>	<b>18</b>
2.1. Future Aero Engine Requirements . . . . .	18
2.2. Engine Preliminary Design Process . . . . .	20
2.3. Modelling of the Secondary Air System . . . . .	24
2.4. Thermal Modelling and CFD Developments . . . . .	26
<b>3. Fundamentals of Secondary Air System and Rotor Thermal Modelling</b>	<b>32</b>
3.1. Rotor and Secondary Air System Design . . . . .	32
3.1.1. Rotor design . . . . .	33
3.1.2. Secondary Air System design . . . . .	36
3.2. Flow Phenomena in the Secondary Air System . . . . .	42
3.2.1. The free disc system . . . . .	42
3.2.2. The enclosed disc system . . . . .	46
3.2.3. Frictional losses of rotating components: Windage . . . . .	49
3.2.4. Pumping losses of rotating channels . . . . .	50

---

3.3. Flow Network Modelling . . . . .	51
3.3.1. Flow network analysis . . . . .	53
3.3.2. Flow network elements . . . . .	57
3.4. Thermal FE-Modelling . . . . .	59
3.4.1. Example of turbine rotor-stator cavity thermal model . . . . .	62
3.4.2. Extraction of CFD Data for Thermal FE-Modelling . . . . .	65
<b>4. Advanced Turbine Design Environment and Automated Work-flow</b>	<b>68</b>
4.1. Common Design Environment . . . . .	69
4.2. Automated Work-flow for SAS and Thermal Simulation . . . . .	77
4.2.1. Database of Modelling Instructions . . . . .	79
4.3. Geometry Model . . . . .	79
4.3.1. Geometry generation sequence . . . . .	81
4.4. Secondary Air System Model . . . . .	81
4.4.1. Flow network recognition sequence . . . . .	82
4.4.2. 1D flow network model generation and solver sequence . . . . .	84
4.5. Thermal FE-Model . . . . .	85
4.5.1. Thermal FE-model inputs generation sequence . . . . .	85
4.5.2. Thermal FE-model base file construction and solver . . . . .	86
<b>5. Implementation of the Automated Design and Analysis Processes</b>	<b>87</b>
5.1. Object Oriented Data Modelling . . . . .	87
5.2. CAD Geometry Interface . . . . .	89
5.2.1. Modelling of rotor structures . . . . .	89
5.2.2. Modelling of static structures . . . . .	90
5.3. Automated Flow Network Recognition . . . . .	92
5.4. Flow Network Model Construction . . . . .	94
5.4.1. 1D flow network model assembly method . . . . .	94
5.5. Thermal FE-Model Construction . . . . .	96
5.5.1. Thermal boundary conditions template engine . . . . .	96
5.5.2. Thermal FE-model domains allocation . . . . .	98

---

<b>6. Application on an HP Turbine Subsystem</b>	<b>99</b>
6.1. Application Case Description . . . . .	100
6.2. Rotors and SAS Design using the CSI environment . . . . .	102
6.3. Automated SAS Model Construction and Results . . . . .	107
6.4. Automated Thermal FE-Model Construction and Results . . . . .	112
6.5. Design Variation Study . . . . .	120
6.6. Results Discussion . . . . .	122
<b>7. Conclusions &amp; Outlook</b>	<b>127</b>
7.1. Conclusions . . . . .	127
7.2. Outlook . . . . .	131
<b>Appendix</b>	<b>133</b>
<b>A. Appendix on Applied Thermal FE-Modelling</b>	<b>133</b>
A.1. Categorisation of thermal boundary conditions . . . . .	134
A.2. CFD-enhanced Thermal FE-Modelling . . . . .	135
A.3. Rotor-Stator cavity application of CFD-enhanced thermal functions . . . . .	135
A.4. Cycle scaling of CFD-enhanced thermal boundary conditions . . . . .	138
<b>Bibliography</b>	<b>141</b>
<b>Lebenslauf CV</b>	<b>152</b>



## List of Symbols

### Latin Symbols

$A$	Area
$a_i$	Coefficient
$b$	Axial gap in a rotor-stator cavity
$BPR$	Bypass ratio
$c_m$	Moment coefficient
$c_p$	Specific heat at constant pressure
$c_s$	Specific heat for solids
$c_w$	Through flow coefficient
$D$	Drag
$E$	Young's elasticity modulus
$\hat{E}$	Total energy
$F$	Force; Uninstalled engine thrust
$G$	Axial gap ratio
$G_c$	Shroud clearance ratio
$g_c$	Newton's gravity constant
$\dot{H}$	Total enthalpy rate
$HPU$	Heat pick up rate
$HTC$	Heat transfer coefficient
$k$	Conductivity constant
$K_f$	Flow friction resistance coefficient
$K_{rot}$	Rotating flow resistance coefficient
$K_{ij}$	Head loss factor for flow link ij
$M$	Disc moment or torque
$\dot{m}$	Mass flow rate
$Nu$	Nusselt number
$Nu_{av}$	Radially averaged Nusselt number
$p$	Pressure

$Pr$	Prandtl number
$\dot{Q}$	Heat rate
$\dot{q}_0$	Heat rate per unit area
$r$	Radial coordinate
$Re$	Reynolds number
$Re_\varphi$	Rotational Reynolds number
$R^f$	Recovery factor
$RPi$	Location reference point i
$s$	Axial distance to disc wall
$s_c$	Clearance between shroud and rotor
$T$	Temperature; Installed engine thrust
$Tc^{ref}$	Reference normalising temperature of the incoming coolant flow into a rotor-stator cavity
$t$	Time
$u$	Velocity component in x-direction
$V$	Volume
$U$	Internal energy
$v$	Velocity component in y-direction
$\dot{W}$	Power
$w$	Velocity component in z-direction
$x$	X-Coordinate
$y$	Y-Coordinate
$z$	Z-Coordinate

## Greek Symbols

$\alpha$	Coefficient of thermal expansion
$\beta$	dimensionless swirl ratio
$\epsilon$	Radiating emissivity
$\gamma$	Heat capacity ratio or isentropic expansion factor
$\sigma_B$	Stefan–Boltzmann constant
$\eta_P$	Propulsive efficiency
$\eta_T$	Thermal efficiency
$\eta_O$	Overall efficiency
$\lambda$	turbulent flow parameter
$\varphi$	Tangential coordinate
$\rho$	Material density
$\tau$	fluid shear stress
$\bar{\tau}$	complete stress tensor
$\hat{\tau}$	fluid shear stress tensor
$\mu$	Dynamic viscosity
$\nu$	kinematic viscosity
$\nu_P$	Poisson ratio
$\Omega$	Rotational Speed

## Superscript indices

<i>Exp</i>	Experimental value
<i>input</i>	Thermal boundary condition input
<i>Model</i>	Model calculated value
<i>prelim</i>	Previous preliminary design method
<i>ref</i>	Reference value taken for normalisation

## Subscript indices

0	Fluid conditions over disc wall
1	Cavity inlet
2	Cavity outlet
0,1,2,...,9	Locations in the engine
$\infty$	fluid conditions outside the boundary layer
<i>f</i>	Fuel
<i>I</i>	Inlet conditions
<i>sup</i>	Superposed flow
<i>t</i>	Total or stagnation conditions
<i>s</i>	Static conditions
<i>ref-op</i>	Reference operating conditions



## Abbreviations

BC	Boundary Condition
CAD	Computer Aided Design
CE	Concurrent Engineering
CFD	Computational Fluid Dynamics
$CO_2$	Carbon dioxide
CSI	Component System Integration (engineering environment developed within this work)
FE	Finite Element
HP	High pressure
HPT	High pressure turbine
IP	Intermediate pressure
JNLF	FE-tool journal file
LCF	Low cycle fatigue
LES	Large eddy simulation
LP	Low pressure
N	Spool speed
NBM	Netbeans Module
NGV	Nozzle Guided Vane
NH	High pressure spool speed
NL	Low pressure spool speed
$NO_x$	Mono-nitrogen oxides
OOP	Object Oriented Programming
OPR	Overall Pressure Ratio
P3	HP compressor outlet pressure
P34	Combustor outlet pressure
RANS	Reynolds-averaged Navier–Stokes equations
RIT	rotor inlet temperature
SAS	Secondary Air System

SFC	Specific Fuel Consumption
SMART	Subsystem MultidisciplinARy design Tool
TLC's	Through Life Costs
T3	HP compressor outlet temperature
T4	Combustor outlet temperature
UDF	User Defined Feature
W26	Engine core compressor main annulus mass flow
$\dot{W}_{SAS}$	Whole power loss of the HPT front SAS
$\dot{W}_{HP}$	Overall power of the HP subsystem
XML	Extensible Markup Language

---

# 1

## Introduction

---

The European Commission has published the proposal “Flightpath 2050: Europe’s Vision for Aviation” pointing out the key assets and research challenges in quality & affordability, safety, environment, and European air transport system. The propulsion system is involved in these challenges in terms of advanced design methods, validation through modelling and simulation, concurrent engineering, probability and risk analysis, noise reduction, emission reduction, and better aircraft-engine integration. The vision also suggests that the temperatures and pressures in the core of the engine should increase and it calls for new ways to reach peak efficiency during the whole flight. In order to reach these objectives, the aero engine industries need to improve the state of the art in design systems technology.

The design and development process of an aero engine is a complex and time-consuming task that involves many disciplines and company departments with different objectives and requirements. The initial stage of the design process, commonly known as preliminary design, is a phase where multiple concepts are assessed in order to select technologies for a competitive product. During this phase, the decisions taken in the concept creation and specification of requirements will have a high impact in the overall performance of the system during its full life cycle. The biggest opportunities for cost reduction lie at this initial phase of the product design, as analysed in the concurrent engineering (CE) approach for total quality design of advanced technologies from ROYAL AERONAUTICAL SOCIETY (1995). Figure 1.0.1 on page 3

shows a plot of typical resource usage in an engine development program, guided by a plan of engineering review gates. In order to use the potential of the early design stages, the current engineering practice shifts resources into the preliminary design phase. To support this shift of resources, it is well worth investing in preliminary design tools that improve concept flexibility, while delivering the best possible accuracy.

Furthermore, the engine design process, which was traditionally subdivided into modular component tasks, is now considered as a multi-disciplinary approach. Having recognised the need for developing advanced preliminary design tools, this thesis focuses on improving the integration of turbine design disciplines and the accuracy of models, as well as on shortening the time to generate models. The presented methods facilitate an agile evaluation of multiple architectures of the turbine Secondary Air System (SAS). This is accomplished with a novel Java based approach to define the design of turbine discs and SAS features. Additionally, a newly developed engineering work-flow is presented, which automates the generation of SAS flow network models and turbine discs thermal FE-models.

The following sections of this chapter introduce the fundamentals of aero engine design. Therein, the derivation of parameters that are relevant to the engine propulsive and thermal efficiencies provide background on the main engine and SAS design contributors. The second part of the chapter describes the principles of the engine heat management system and the role of the secondary air system. The final part of the chapter presents an overview of the structure of this work and gives an insight into the research purpose, methods and conclusions.

## **1.1. The Aero Engine and its Subsystems**

Jet propulsion systems can be divided into two broad categories: air-breathing and non-air-breathing. This work focuses on the air-breathing propulsion system for aircraft, commonly known as the aero engine. The core of the engine is the gas generator, whose purpose is to supply high temperature and high pressure gas. In turn, the total energy of the gas generator exhaust gases can be converted into mechanical energy and then used to provide power. In an aero engine, the gas generator is typically a gas turbine.

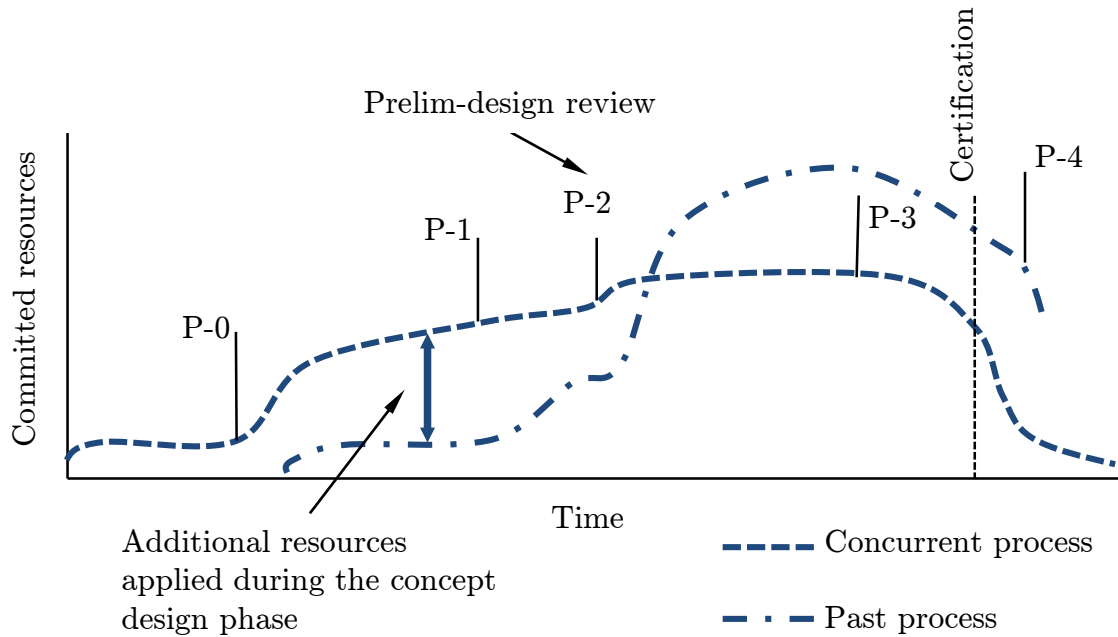


Figure 1.0.1.: Resource usage in a typical engine development program, as described in PANCHENKO et. al. (2003). P-i represent the engineering cycle review gates.

The remaining energy after the turbine can be converted into thrust, defined in MATTINGLY et. al. (2002) as the force on the fluid in one direction to create a reaction in the opposite direction (Newton's principle of action-reaction). Thrust moves the aero engine, and the aircraft it is attached to, in the opposite direction of the mass flow of the fluid. The uninstalled engine thrust  $F$  refers to the thrust of the engine without nacelle and unattached to an aircraft. This thrust can be evaluated with the momentum equation applied to the control volume of the fluid that goes through the engine, shown in Figure 1.1.1 on page 4. Since thrust is the sum of the forces acting on the internal surface of the engine and the stream that contains the air flowing into the engine, it can be expressed in terms of the momentum flux, as in (1.1.1). The installed engine thrust  $T$  is produced by both engine and nacelle, and is therefore the uninstalled thrust minus the drag  $D$  on the external nacelle surface and the pressure force on the external stream tube  $T = F - D$ .

$$\text{Uninstalled Engine Thrust } F = \dot{m}_9 v_9 - \dot{m}_0 v_0 + (P_9 - P_0)A_9 - \int_{A_0}^{A_9} P_{ext} dA \quad (1.1.1)$$

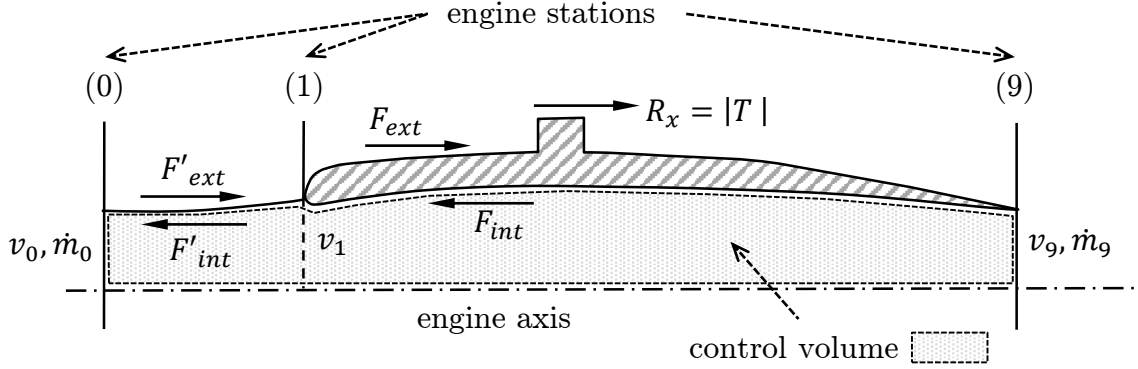


Figure 1.1.1.: The thrust control volume of an aero engine

In the case that the exhaust nozzle is not choked, which occurs when the exhaust jet speed  $v_9$  is lower than the speed of sound, the exit and inlet pressures are equal to the ambient pressure and the exit pressure thrust term on (1.1.1) is no longer considered. This case is known as momentum thrust, where the engine thrust can only be increased by a larger mass flow  $\dot{m}_9$  or higher jet speed  $v_9$ , for a given flight speed  $v_0$ . However, higher mass flow is associated to larger engine frontal area and higher jet speed  $v_9$  usually increases fuel consumption (see (1.1.2)) and noise. Therefore, the aero engine designer must find trade-offs between these performance parameters in order to optimally meet the thrust requirements of the aircraft customer.

### 1.1.1. Working principles

The purpose of the aero engine is to produce propulsive power. Thus, the propulsive efficiency of the engine is the ratio of the propulsive power to the total power output. The total power output is the net rate of kinetic energy increase of the fluid passing through the engine per unit time. Since the kinetic energy increase is the result of the energy transfer mechanisms from the processes in the engine cycle, the propulsive efficiency  $\eta_P$  can be expressed by (1.1.2).

$$\eta_P = \frac{T \cdot v_0}{\dot{W}_{output}} = \frac{T \cdot v_0}{\frac{1}{2} [(\dot{m}_0 + \dot{m}_f)v_9^2 - \dot{m}_0 v_0^2]} \quad (1.1.2)$$

$$\eta_P = \frac{2}{v_9/v_0 + 1} \quad (1.1.3)$$

For an engine where the fuel mass flow rate is much lower than the one of the air, exit pressure is equal to the ambient pressure, and has a single inlet and exhaust, the propulsive efficiency can be simplified to (1.1.3). Thus, high propulsive efficiencies require exhaust velocities similar to the flight velocity.

The Brayton cycle is a simplified thermodynamic model of the working cycle of an aero engine for an ideal gas. It is a varying volume cycle with four stages: compression, combustion, expansion, and exhaust. The air enters through the intake (1), it is compressed (2) to (3), heated after mixing with fuel in the combustor (3) to (4), expanded in the turbine to produce power (4) to (5), and exhausted in the nozzle to the final jet velocity (9). Figure 1.1.2 on page 6 shows the enthalpy and entropy evolution of the fluid along an ideal Brayton cycle.

Assuming a calorific perfect gas, the rate of energy transfer of each component in the Brayton cycle can be expressed with the following equations (1.1.4):

$$\begin{cases} \dot{W}_c = \dot{m}c_p(T_3 - T_2); & \dot{W}_t = \dot{m}c_p(T_4 - T_9) \\ \dot{Q}_{in} = \dot{m}c_p(T_4 - T_3); & \dot{Q}_{out} = \dot{m}c_p(T_9 - T_2) \end{cases} \quad (1.1.4)$$

$$Net \dot{W}_{output} = \dot{m}c_p(T_4 - T_9 - T_3 + T_2) \quad (1.1.5)$$

For an ideal gas circulating in the Brayton cycle,  $T_3/T_2 = T_4/T_9 = (P_3/P_2)^{(\gamma-1)/\gamma}$ , where  $\gamma$  is the isentropic expansion ratio. The pressure ratio of the engine is defined as  $PR = P_3/P_2$ . From the above formulation, it can be derived that the thermal efficiency of the cycle  $\eta_T$  is:

$$\eta_T = \frac{Net \dot{W}_{output}}{\dot{Q}_{in}} = 1 - \left( \frac{1}{PR} \right)^{(\gamma-1)/\gamma} \quad (1.1.6)$$

For an ideal Brayton cycle, it can be demonstrated that there is an optimum compressor pressure ratio that maximises work of the gas generator and leads to:

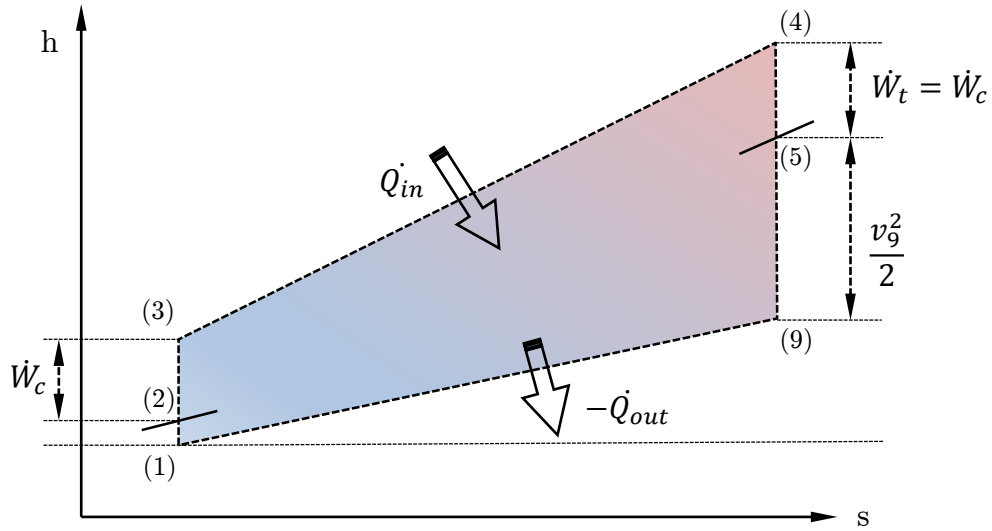


Figure 1.1.2.: Brayton cycle ideal h-s diagram

$$\left(\frac{T_3}{T_4}\right)_{max\ work} = \sqrt{\frac{T_4}{T_2}} \quad (1.1.7)$$

Therefore, the respective net power output per unit mass flow is given by:

$$Net\ \dot{W}_{output} = \dot{m} \cdot c_p T_2 \left( \sqrt{\frac{T_4}{T_2}} - 1 \right)^2 \quad (1.1.8)$$

In summary, the thermal efficiency  $\eta_T$  of the gas generator is directly related to the overall pressure ratio  $PR$  of the engine, (1.1.6), and the net specific power is proportional to the ratio of combustor exit temperature to inlet temperature  $T_4/T_2$ , (1.1.8).

Finally, the overall efficiency of the engine is the combination of the propulsive and thermal efficiencies.

$$\eta_O = \eta_P \cdot \eta_T = \frac{T \cdot v_0}{\dot{Q}_{in}} \quad (1.1.9)$$

### 1.1.2. Aero engine design

The engine design process begins with the aircraft design definition. It starts with the overall



engine system level, followed by the more detailed design of sub-systems, and down to the design of specific parts at the component level. The manufacturing process moves forward in the opposite direction, from the components to the system level.

There are three main phases in the design process: concept design, preliminary design, and detail design. As previously introduced, this work deals with the preliminary design phase. In this phase, several concepts are evaluated, which have been previously selected as high potential in the concept design phase. The outcome of the preliminary phase is the selection of the engine architecture and main design parameters leading into the detail design phase.

When designing an aero engine, the engineering teams are guided by a review process, which stretches over the full life-cycle of the product. A thorough overview of the engine review approach can be found in ROLLS ROYCE (2005). Traditionally, this process is split in seven stages: innovation and opportunity selection, concept and preliminary design, full concept design, product realisation (also called development), production service support, and disposal.

### Subsystems and disciplines

The design process is grounded in physical principles, which are categorised in so called engineering disciplines. Along the process, there are many discipline interactions and inherited contradictions that make the engineering task a challenge. For example, the introduction of advanced turbine cooling systems leads to higher thermodynamic cycle efficiencies, but it also increases the cost due to manufacturing complexity and the installed weight of the engine. Figure 1.1.3 on page 8 presents an overview of the levels and disciplines that support the engine design.

The next paragraphs describe briefly the function and design of each of the engine subsystems. Furthermore, the main system level disciplines are introduced: fluid systems and control systems. Fluid systems include the air, oil and fuel systems, which are the fundamental parts of the heat management system. A more detailed explanation of the engine subsystems and components can be found in BRÄUNLING, WILLY J. G (2009).

- The **inlet** captures the surrounding air and reduces its entering velocity to a level that is adequate for the compressor. The main design parameters are its air compression

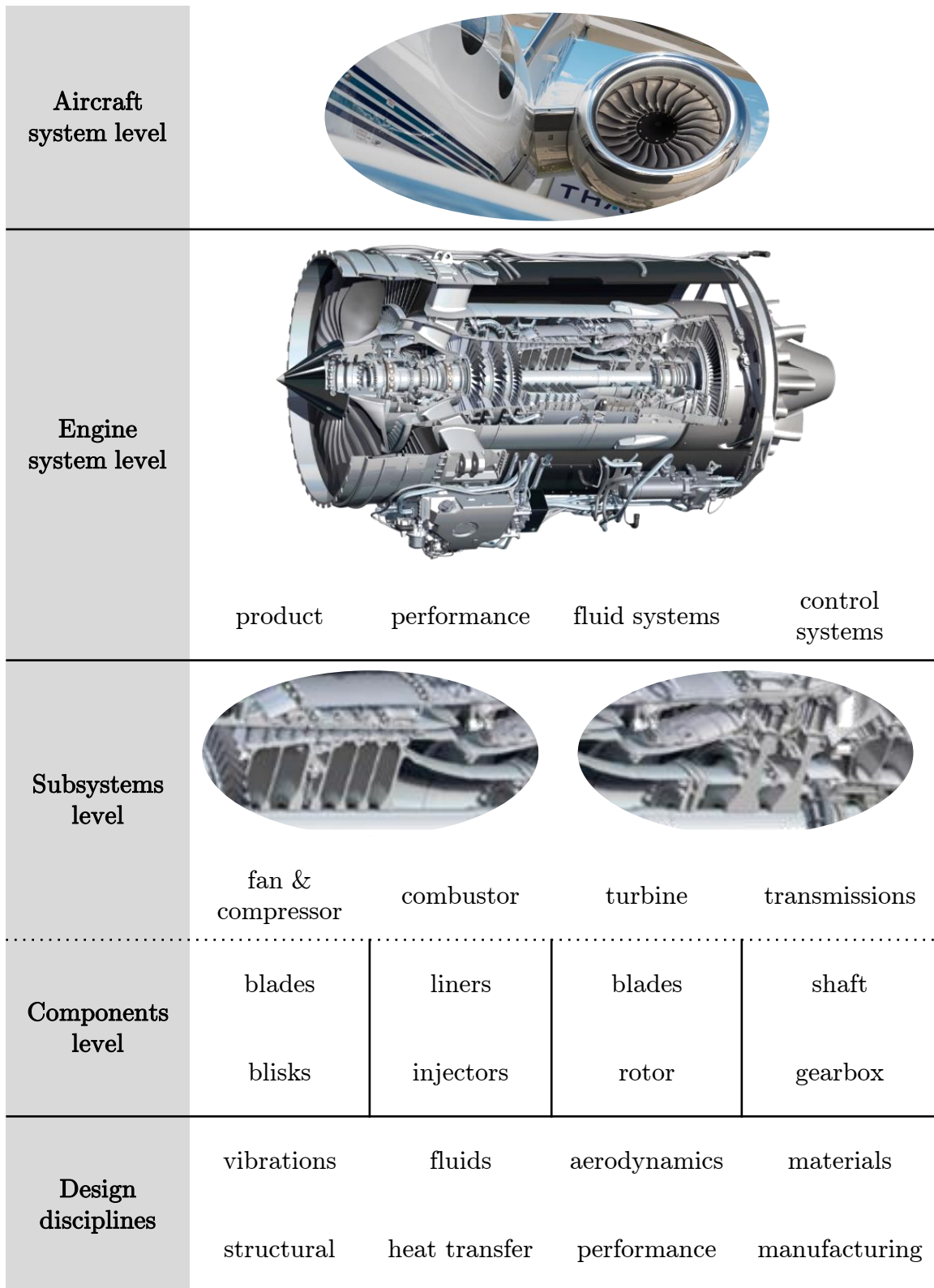


Figure 1.1.3.: Main engine product design levels and disciplines, demonstrated for Rolls-Royce BR725 (printed by courtesy of Rolls-Royce Deutschland)

efficiency, the external drag, and the mass flow entering the engine. The inlet type is commonly categorised into subsonic and supersonic.

- The **fan** blades at the front of the engine are the main contributors to the thrust of the system. The fan also has a compression function and in turbofans it is the stage after which the flow is split into primary and secondary bypass flow.
- The **compressor** increases the pressure of the air exiting the inlet, so that the combustion process can be performed efficiently. Compressors are categorised into axial and centrifugal operation. Currently, axial compressors are commonly used for aero engines, partly because they have a smaller frontal area than centrifugal compressors. The air in an axial compressor flows in axial direction through a series of rotating (rotor) blades and stationary (stator) vanes. Each set of blades or vanes is known as a stage.
- The **combustor** transforms the chemical energy in the fuel and air mixture into thermal energy for expansion in the turbine. Additionally, the combustor tailors the temperature profile of the hot gases at the exit plane. The combustor exit profile must be designed to prevent the turbine components from exceeding the permissible structural temperature levels.
- The **turbine** produces the power to operate the compressor, fan, and various engine accessories. Aero engines commonly use axial flow turbines, which consists of several stages of stationary vanes and rotor wheels (discs) with blades. The vanes are also known as Nozzle Guided Vanes (NGVs), since they form a series of small nozzles that discharge the flow into the rotating blades. The rotor blades then transform the kinetic energy of the incoming flow into mechanical work transmitted through the turbine discs to the shaft.
- The **exhaust** nozzle increases the velocity of the exhaust gases and straightens the flow from the turbine. The typical types of nozzles used in aero engines are the convergent and convergent-divergent nozzles. The latter ones have a throat at the duct position where the cross-sectional area is a minimum, and they are usually employed in supersonic aircraft.
- The **transmissions** subsystem is responsible for distributing the power output of the turbine into useful mechanical work. It has two common goals: the transfer of mechanical

power and the support of the rotating components within the engine. The main requirement of the transmissions subsystem is its high reliability during the entire product life cycle.

- The lubrication or **oil system** is responsible for lubrication and cooling of the gears, bearings and splines. Common for gas turbine engines is a recirculation lubrication system, where the oil is distributed around the engine by pumps. The pressure and temperature conditions of the oil are critical for the operation of the engine. Additionally, the oil system plays a decisive role in heat management, which is further explained in Section 1.2, and in the vibration dynamics<sup>1</sup> of the engine.
- The **fuel system** function is to supply the engine with fuel in a form suitable for combustion and to control the flow to the required quantity necessary for easy starting, acceleration and stable running, at all engine operating conditions. Fuel pumps are used to deliver the fuel to the fuel spray nozzles, which inject it into the combustion system in the form of an atomized spray.
- The engine **secondary air system** (SAS) is defined as those airflows which do not directly contribute to the engine thrust. The air system functions include internal engine and accessory unit cooling, bearing chamber sealing, prevention of hot gas ingestion into the turbine disc cavities, control of bearing axial loads, control of turbine blade tip clearances and engine anti-icing. This system also supplies air for the aircraft services. As a general rule, up to one fifth of the total engine core mass flow is used for these various functions.
- The **control system** monitors and controls the operation of the engine. It continuously makes adjustments to the operational parameters, which are essential for the safety and efficient performance of the engine. This system manages hundreds of measurements, with inputs such as the shaft speeds, engine gas temperatures, oil pressures, or actuator positions. In turn, it adjusts a set of variables, such as fuel flow, stator vanes incidence angle, or air system flows through the bleed valves, according to the power setting that

---

<sup>1</sup>As an example of vibration control using the oil system, the design of the oil film squeeze film dampers is used to adjust the rotor-dynamics of each engine spool and the way that resonances are transmitted between rotors, stator casing and the mounting to the aircraft.

the engine operator has selected.

The next section explains the importance of each engine module in the heat management system. It describes the heat sources and sinks that the engine designer needs to combine and optimise. Furthermore, it presents the role of the SAS in the design for heat management.

## 1.2. Internal Heat Management

As a direct consequence of employing the Brayton cycle, the gas turbine thermal efficiency is proportional to the turbine rotor inlet temperature (RIT). Thus, in order to achieve a competitive specific power output in the aero engine industry, a heat source inside the engine needs to supply the energy to quickly increase the fluid temperature level right after the compressor. The combustor is that heat source, as it converts the chemical energy bound in the fuel into thermal energy. However, the current combustor technology operates efficiently at temperatures much higher than the component material limits. Therefore, there is also a need for a heat sink in the engine.

The task of the heat management system is to optimise the heat sources and sinks. To this effect, the engine designer looks for a heat balance between the oil, fuel and air systems. Already introduced in the previous section, the cooling and lubricating functions of the oil system are essential to guarantee the reliability of the transmission components, the bearings, couplings, and the internal and external gearboxes. This implicates that the oil acts as a heat sink for the power transmission mechanisms. Thus, the heat collected by the oil flow must be given away in another area of the engine, so the lubrication and cooling capacity of the oil does not degrade in its recirculation. Furthermore, the heat that the oil evacuates is proportional to the efficiency losses of the engine. Higher heat transfer rates to the oil system are associated with lower efficiencies of the engine subsystems. Nonetheless, the heat that the oil system collects can be further transferred to the fuel system. An adequate pre-heating of the fuel before injection in the combustor leads to improved engine thermal efficiency, since the heat energy remains in the thermodynamic cycle as it is transferred between internal sources and sinks.

Not only the oil, but also several components in the engine need continuous or partial cooling. The combustor and high pressure turbine components are the main areas where continuous

cooling is required. Sometimes even the low pressure turbine is actively cooled. The combustor is mostly cooled with the main annulus stream from the compressor, and a complex aerothermal design of gas mixing and dilution zones is used to control the combustion chemical process. Five basic features are the basis of a modern combustor design: a primary zone, a secondary zone, a dilution zone, the wall jets, and the management of heat transfer at the combustor boundary.

The heat management of turbine components is solved with the internal or also called secondary air system. The temperature level and gradients on the components of the turbine have to be designed carefully, since the fluid temperatures that the combustor can deliver are well above the current material integrity levels. Current turbine blade technology allows operation at temperatures above the material limits, and the fact that the combustor can supply more energy reveals that there are still opportunities for improvement. There is therefore a need for evacuating heat in the hot end components of the engine. With this purpose, air is extracted from the compressor stages to cool the turbine. The engine designer must take into account that the cooling air poses a penalty on the thermal efficiency, since a portion of the work that could have been done by the turbine blades is lost or transferred as heat in the internal SAS components.

The main turbine components that require specific design for cooling are the blade airfoils and platforms, the upper disc post features, the casing segments above the rotor blades, and the rim sealing features. Turbine discs and shafts heat up through heat conduction from the main annulus, due to the temperature difference between the blade rows and the cooler internal parts. Another requirement is that the turbine parts should operate with limited temperature gradients to avoid high thermally induced stresses. This is of particular importance for the diaphragm and inner radii of the turbine discs. At the disc cob, it is sometimes desirable to have higher temperature levels in order to avoid big temperature differences along the disc radius. The design goal of the engine cooling system is to find an optimum for the maximum temperature levels and gradients that comply with the life target of the engine.

There are highly sophisticated cooling technologies that allow the engine designer to achieve high combustor outlet temperatures while complying with the metal material limits. For example, turbine blade cooling techniques include film cooling, impingement cooling, and augmented convective cooling. A state of the art description of turbine cooling concepts and heat

transfer methods can be found in HAN et. al. (2013).

The heat management in the oil system is also linked with the secondary air system. The oil mist in the power transmission components, such as bearings, has a narrow operating temperature band. High temperatures in the bearings quickly degrade their life and increase the probability of oil fire events. The temperature of the bearings is a function of oil temperature, oil flow and air-oil mixture. Thus, a cooling air flow from the secondary air system is required to control the temperature levels in the bearing housing, especially in the area located in the hot end section of the engine.

In summary, the heat management system has interfaces with most subsystems of the engine and requires coupled design consideration of the air, oil and fuel systems. In the next section, the design fundamentals of the secondary air system are explained.

### 1.3. Design Philosophy of the Secondary Air System

The secondary air system (SAS) is defined as those air flows not directly contributing to engine thrust. There are two types of air system:

- The internal cooling and sealing air.
- The external bleed systems for aircraft anti-icing, cabin pressurisation, and handling bleeds.

This work deals with the internal cooling and sealing air, and in particular, how it provides **cavity ventilation** for the turbine discs. Figure 1.3.1 on page 14 shows a typical cross-section diagram of the SAS flows at the turbine area in an aero engine. The rotating components in gas turbines are highly stressed purely as a result of the centrifugal loading. A main function of the SAS is to ensure that the rotor discs are surrounded by air from the coolest available source, which minimises the degrading of the rotor material properties. An additional problem is that thermally induced stresses can be caused by temperature gradients, which result from a much higher rate of heat transfer in one part of a component relative to another. The cavity ventilation flows have to be designed in such a way that the temperature gradients along the rotating components are minimised.

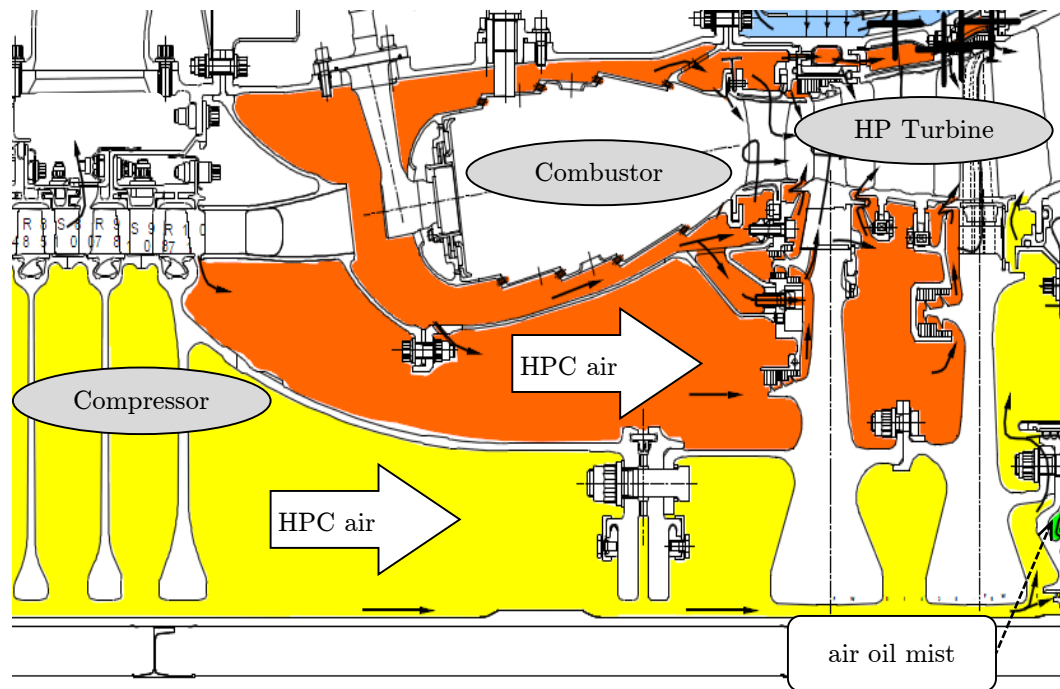


Figure 1.3.1.: SAS cross-section diagram of the flows in the turbine subsystem. Courtesy of Rolls-Royce Deutschland.

The SAS is also responsible for the **blade cooling supply**. Aerofoil cooling air is necessary at least for the first high pressure turbine rotor and nozzle guide vanes (NGVs). This allows higher temperatures to be reached in the engine cycle and therefore an increase in efficiency. However, it is important that the amount of cooling air required for this purpose is minimised. Another important function of the internal air is to prevent that hot gas from the main annulus enters the disc rotor cavities. This function is called **rim sealing** and its intention is to keep the air environment as cool as possible for the highly stressed rotating components. The hot gas ingestion is excluded by means of an outflow of cooling air, which “purges” the disc’s rim cavity. This rim sealing flow degrades the efficiency of the turbine and an optimum mass flow compromise needs to be found.

Additionally, the SAS provides **bearing chamber sealing**. The turbine rotors are supported on rolling element bearings that are lubricated with oil. The oil is retained in the bearing chamber by a flow of air inwards to the chamber through close clearance labyrinth seals.

Rotor **thrust load balance** is a whole engine system function that the internal air system performs. The net load in the thrust bearings can be adjusted by positioning the internal



air seals at suitable radii. Compensating the cavity pressures provides an additional load to counteract the difference between compressor and turbine aerodynamic loads.

As the cooling air is fed back to the main gas path, its velocity profile and temperature conditions do not match the main flow state. This effect is referred to as **spoiling**, and it degrades the aerodynamic performance of the turbine. The impact of spoiling is hard to predict, as it involves 3D fluid dynamics phenomena, but CFD simulations can give a good understanding of its importance, which was proven in the investigations of ROSIC et. al. (2006). Not only the geometry of the disc rim gaps have a direct influence in this effect, but also the design of the internal air system seals and cavities, which change the enthalpy of the cooling flows via the phenomenon known as **rotor-stator windage**.

The design of the secondary air system should minimise the impact on engine performance. In order to achieve this, the lowest possible pressure source for each cooling function must be chosen. A good practice is therefore to use the same air for several functions. Parasitic flows are to be avoided and margins for variation in engine service have to be taken into account. This is therefore a discipline where reducing the uncertainty in the calculation will very favourably contribute to reduce the impact on overall engine efficiency.

TURNER et. al. (1997) presented an overview of problems and investigations of the SAS in gas turbines. According to his research, an increase of the Specific Fuel Consumption (SFC) by 1% traduces into an increase of the operational costs of the engine by 0.5%. The impact of SAS design is then critical, taking into account that in modern aero engines a 1% secondary air increase, corresponds to a SFC from 0.4% to 0.6%.

In summary of the above, the SAS development process for an engine project needs to follow a holistic approach, where essential requirements for cost, weight and performance are set. To meet compromises between these trades at the initial concept phase, the air system design method needs to interact with each sub-system of the engine. Thus, the preliminary design method would profit from coupled interaction across disciplines and more flexibility of concept variability.

There is a potential benefit to be gained in engine performance by linking the SAS, discs design, and discs thermo-mechanical analysis. The publication REY VILLAZON, J. M. et. al. (2012) highlights the impact of SAS and turbine internal flow parameter variations in the life and design

weight of HP turbine discs. These disciplines have been traditionally split in the turbine design process. However, the life and weight design targets for the turbine discs could be optimised by coupling the variations of the SAS and discs design parameters with the calculation of the discs' thermal and mechanical performance. The state of the art in computing technology now enables an integral coupled process to be employed. Such a process is presented in this work, with a multi-disciplinary secondary air system and turbine discs design approach.

## 1.4. Structure of the Thesis

Following the introduction, the next chapters of this work are structured as follows,

- Chapter 2 begins with an overview of future preliminary design engine requirements and developments in engine design tools. The chapter then introduces the current methods for SAS and thermal modelling, with an insight on how CFD methods are used to support these disciplines.
- Chapter 3 describes the fundamentals of turbine discs and SAS design, and it provides a theoretical understanding of the flow field in turbine internal cavities. Moreover, the governing equations for SAS and thermal modelling are presented, along with an application example in a typical HP turbine.
- Chapter 4 presents the proposed advanced work-flow to gather turbine design data and automatically generate the SAS and thermal models. Within this chapter, the chain of sub-processes and the requirements for the automatic operation of each individual module are specified.
- Chapter 5 begins with the basics of object oriented programming and why it has been chosen for the implementation of the methods in this work. It then describes the implementation of the automated CAD models generation work-flow, as well as the support algorithms needed to automatically generate SAS and thermal FE-models.
- Chapter 6 demonstrates the exemplary application of the proposed work-flow to design and analyse a HP internal turbine subsystem. The output of the automated process is then compared to the predictions of existing validated models of a production 2-stage HP turbine. In the final application stage, a parameter study is presented, which shows how SAS design variations affect the overall power losses of a HP turbine subsystem.
- The last chapter of this work, chapter 7, presents the conclusions of the research. The findings of applying the automated process are highlighted, together with the opportunities of improving the temperature prediction of the turbine rotors at the preliminary design stage. Finally, the outlook gives recommendations for future research in the field of secondary air system heat transfer modelling methods for virtual engine design systems.

---

# 2

## State of the Art Review

---

To set the context for the work, this chapter begins with an overview of future engine design requirements and how this research can contribute to the vision of advanced aero engine design methods. This is followed by the history of aero engine preliminary design methods. Then, the chapter presents a review of the state of the art in internal air system modelling, thermal analysis with CFD developments, and the recent progress in design automation.

### 2.1. Future Aero Engine Requirements

The future requirements of aero engines will very much be decided by their **environmental impact** and the **availability of fuel resources**.

As to the environment, the main impact factors are noise and pollutant emissions. The emissions of major importance to control are the  $CO_2$ ,  $NO_X$ , and water vapour from the engine exhaust. In current turbofans, the  $CO_2$  and  $NO_X$  emissions are a function of OPR, maximum combustion temperature (dependent on the air-fuel-ratio), and fluid time of residence in the combustor, which are at the same time essential performance parameters to improve the efficiency of the engine. Noise emissions are becoming an important design and economic factor, since engines with reduced operation noise are able to get reduced airport charges, better flight routes, and even flight permissions in populated areas. The European authorities are addressing the future

of air flight with very challenging goals for environmental regulation. In the report EUROPEAN COMMISSION (2011), the authorities aim for 75% reduction in  $CO_2$  emissions, 90% reduction in  $NO_X$  emissions, and 65% reduction in perceived aircraft noise.

Fuel resources and alternatives will also shape the future of aero engine design. According to MILLER and SORRELL (2013), the concerns about “peak oil” have reached exceptional limits at the start of the global economic recession in 2007. With the advent of shale oil production in the United States, these concerns have somewhat diminished. However, the oil prices keep on increasing and have almost doubled since 2010. Thus, oil remains critically important, and therefore the requirement for lowering the specific fuel consumption of the engine.

Furthermore, the aero engine designer needs to consider trade-offs between the stakeholders that have an impact on the **engine propulsive and thermal efficiencies**, see (1.1.9). The propulsive efficiency (1.1.2) is mainly a function of the Bypass-ratio and the way that the engine is installed on the aircraft. Whereas the thermal efficiency (1.1.6) is a function of the thermodynamic cycle properties, such as OPR, maximum temperature and the efficiency of each component. The following paragraph describes some opportunities for improvement in the engine thermodynamic cycle, concept design, and the efficiency of each subsystem.

The fan and exhaust jet noise emissions are the main contributors to the total engine noise, and they are a function of the bypass ratio (BPR). An increase in BPR can be achieved by novel propulsion designs, such as the geared turbofan<sup>1</sup>. Very high propulsive efficiencies can be achieved with new concepts such as the open rotor or propfan<sup>2</sup>, described as a technological “game-changer” by PETERS (2010).

Another improvement potential lies in the thermal efficiency, which reduces the SFC of the engine, leading to reductions in combustion emissions and more economical flights. The thermal

---

<sup>1</sup>The geared turbofan uses a reduction gearbox between the fan and the LP turbine. By decoupling the fan and turbine rotational speeds, higher speeds and fewer stages can be used in the LP turbine and the IP compressor, thus increasing efficiency and reducing weight of this components. The downside of this technology is that energy is lost as heat in the gear mechanism. There is also an associated weight penalty due to the extra mass of the power transmission mechanism.

<sup>2</sup>An open rotor engine consists of a gas turbine driving an unshielded propeller like a turboprop. Its propeller is designed with many short, highly twisted blades, which confer the propulsion system properties similar to a turbofan. This concept is intended to have the fuels gains of a turboprop, while delivering the speeds and performance of a turbofan. The challenge is to create low noise designs, since an optimum configuration has two contra rotating fans that generate noise without a nacelle containing noise absorption materials.

efficiency can be improved with innovations in subsystem design. Examples of advances in subsystem engineering include:

- Compressor: surge control, casing aspiration, all blisk rotors.
- Turbine: Ceramic Matrix Composite (CMC), novel blade cooling, turbine blisk, and multidisciplinary integral 3D design with **coupled main annulus, internal cooling, disc, and cavities simulation**.
- Combustor: Lean combustion operates with high air-fuel-ratio that reduces the maximum combustion temperature and consequently  $NO_X$  formation. High fidelity simulation of the combustion process is necessary for advanced combustor design.

Finally, the thermal efficiency of the engine can be highly improved with the employment of unconventional thermodynamic cycles. Such is the case of the intercooled and intercooled recuperated cycles. These cycles can reach higher thermal efficiencies, while keeping the OPR in the currently viable band. A review on advanced core and engine thermodynamic cycle innovations was presented in work of WILFERT G. and SIEBER J. (2007).

In order to take these technological leaps, the engine design process has to become more flexible than ever before. The design tools need to be able to cope with a wider range of alternatives employing fast procedures, which couple the detailed component design with the assessment of the overall system thermodynamic cycle. Such is the approach taken in this thesis, where an automated process is presented that couples the design disciplines of the whole turbine subsystem. The proposed process is implemented in a **common design environment** for main annulus, rotor, and transmission components, which **automates the generation of models for SAS and thermal analysis**.

## 2.2. Engine Preliminary Design Process

The origins of computerised engine design can be traced to WYSONG and TABAKOFF (JUL 1965), who published the methodology of a program for the design calculations of a free vortex turbine. Ten years later, under the guidance of the same author in WYSONG et. al. (NOV 1978), the Turbine Design System (TDS) was presented, which offered a completely computerised interactive design and performance calculation platform for turbines. This software

was implemented in Fortran code and was already a multidisciplinary approach that assembled twelve modules that allowed the assessment of turbine aerodynamics, heat transfer, and mechanical design.

A design software to simulate the full engine system would initially appear in the work of STRICKER J. M. and NORDEN (1991), who developed the **Computerised Preliminary Design** (CPD) that coupled all core components of the engine. Their work led to the conclusion of importance of an integrated process in the conceptual design phase, presented in STRICKER J. M. (1998).

The basis of computerised engine simulation in the German aero engine community was first published by MÜNZZBERG and KURZKE (1977). In a next phase KURZKE (1998) developed GasTurb, which started as an academic tool with the potential to evolve into a commercial software. GasTurb presented already an advanced Graphical User Interface (GUI) and the possibility to assemble a wide range of engine configurations (e.g. turboprop, turbofan with two spools, turbofan with three spools, etc..). JESCHKE et. al. (2002) describes the capabilities of MOPEDS, a commercial development of GasTurb, which was adopted in the MTU<sup>3</sup>. The prototype for the MOPEDS system was presented in the dissertation of SCHABER (2000), who puts special emphasis on the advantages of a preliminary design tool that couples all engine core design disciplines and solves the interdepartmental interfaces in an automated way.

The approach of NASA to **complete numerical simulation** of engine systems was the Numerical Propulsion System Simulation NPSS<sup>4</sup>, first published in CLAUS et. al. (1992). In NPSS, each component is represented by physically equivalent modules that capture the working principles of each discipline. In this tool, CFD simulations are the basis for the calculation, with automatic generation of meshed models (see example in Figure 2.2.1 on page 22 from VERES (1999)). As an essential step on the preparation of each CFD module, a validation phase was carried out, where the CFD results were compared with existing experimental data. The work in LYTLE (1999) describes in more detail the methods behind NPSS and provides examples of its use. Additionally, the latter author gives importance to the concept of multi-fidelity levels of simulation. LYTLE (1999) states that “while the physics could be captured by modelling the

---

<sup>3</sup>MTU Aero Engines AG is a German aircraft engine manufacturer, <http://www.mtu.de>

<sup>4</sup>NPSS turned in 2007 into a consortium, <http://www.swri.org/npss/>

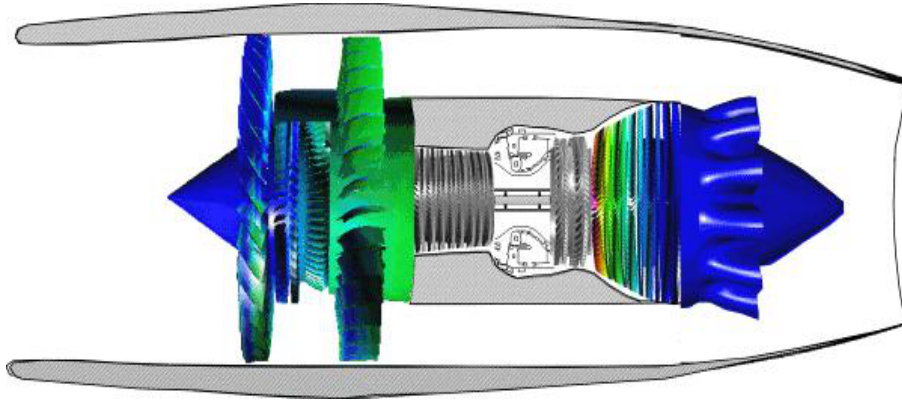


Figure 2.2.1.: Example 3D Navier-Stokes simulation of a low pressure sub-system using NPSS, from VERES (1999).

entire propulsion system at the highest level of fidelity, 3-D, transient and multidisciplinary, two problems prevent this from being a viable option in most cases. First, the level of detailed information needed as boundary and initial conditions to get a converged, validated solution will be extremely difficult to collect. Second, the computational time and cost will be prohibitively high for effective use in a design environment. Therefore, the designer or analyst must tailor the fidelity of the simulation to capture the appropriate physics for each component and discipline”.

Rolls-Royce<sup>5</sup> considered a novel variable into the system: engine affordability and cost, in JONES et. al. (2003). This work introduced the concept of **Through Life Costs** (TLC's), which includes the design, unit, development, in service and disposal costs. These trades of engine capability vs. cost prove to be vital for the design and development of an optimum affordable system.

After the fundamentals for numerical simulation were laid, the state of the art advanced in **multi-disciplinarity** of the tools and robustness of the solution. PANCHENKO et. al. (2003) presented the development of a software system for Pratt & Whitney<sup>6</sup>, with focus on “Preliminary Multi-Disciplinary Optimisation” (PMDO). Then a leap in the programming standards was presented by PRADO et. al. (2005), who proposed a more flexible design system in a Java

<sup>5</sup>Rolls-Royce Holdings plc is a British multinational public holding company that through its subsidiaries, designs, manufactures and distributes power systems

<sup>6</sup>Pratt & Whitney is a U.S.-based aerospace manufacturer, subsidiary of United Technologies Corporation (UTC). It is one of the "big three" aero-engine manufacturers, with General Electric and Rolls-Royce.



(ORACLE (2014)) and XML based platform. The system was modularised in three blocks:

1. The **Java data manager**: comprising the core data processor of the design system, with the data stored and transferred in XML format (also known as MultiServer).
2. The **Java Graphical User Interface**: providing the user access to the data and processes, but programmed as a separate module from the data manager.
3. The commercial **optimisation tool Isight** (SIMULIA (2014)): providing the design variation and optimisation algorithms.

An improvement of the Pratt & Whitney tool was put forward in BROPHY et. al. (2010): PDMO-Lite. Its authors realised that compromises needed to be made between the accuracy of models and the capability to analyse wider ranges of the design space. As stated in BROPHY et. al. (2010), “it is usually more accurate to achieve closure over a wider range of alternatives with a fast procedure that has a lower resolution than to run out of time, fail to achieve closure or miss key strategic decision milestones by using a slower, process that offers a theoretically higher resolution”. This approach opened the field of **surrogate modelling** and approximation functions being used as a replacement of high-fidelity models in some steps of the preliminary design process.

In later years, authors such as CHAUDHARI et. al. (2011) have focused on providing an **integrated preliminary design**, which should reduce design cycle time and improve the fidelity of the engine general arrangement cross-sections. The objectives behind this system are to aid the designer to create components and update the system level model iteratively, while monitoring in an automatic way that the solution meets aerodynamic and mechanical design requirements. Additionally, the system uses a hierarchical database in XML format to store data as objects like engine, modules (i.e. HPC, HPT etc.) and components.

**Probabilistic design** techniques have also proven their high potential for the conceptual phase. Such an approach has been presented by FLASSIG (2011), who used robust design methods embedded into optimisation algorithms to design the blades of an aero engine compressor. These algorithms have been thereafter applied to the design of a complete engine concept by KUPIJAI et. al. (2012), in a Java based preliminary design optimisation system.

The research in this work takes the reviewed state of the art in design systems as a starting point and focuses on improving the aero engine preliminary design process with an advanced

integration of engine components into the air system. The proposed process consist of a **Java and XML based design and simulation environment**, which includes the data model for the main annulus, SAS and rotors design.

## 2.3. Modelling of the Secondary Air System

The secondary air system of an engine is typically modelled as a **one dimensional flow network**, consisting of nodes and links. This abstraction can be viewed as a series of cavities or chambers, linked by flow passages. The approach was originally proposed in CROSS (1936), well before the age of electronic computational engineering, who presented a method based on successive corrections for solving the problem of distribution of flows and loss of pressure head (static pressure) in networks of pipes.

The fundamentals of a computer program to solve the flow network was first published by KUTZ and SPEER (1994) and MAJUMDAR (1998). The program comprised two independent modules:

1. the solver, an algorithm to solve the system of equations in the fluid network with a hybrid numerical method, and
2. the GUI, a user interface to develop the model and construct the network of nodes and links.

The MAJUMDAR (1998) method was already capable of modelling multiple fluids, phase changes, compressible flows, and mixture thermodynamics. It additionally put high importance to the convergence quality and speed of the program. The numerical method originally used was based on the Newton-Raphson algorithm<sup>7</sup> with successive substitution methods. This solver algorithm was simple to implement and proved reliable in most cases. Recent developments in the solver, such as in MERKLER et. al. (2003) and in MULLER and MONNOYER DE GALLAND, F. (2009), have focused in refining the convergence of the solver and in new ways to overcome special criteria that had been previously not taken into account. More specifically, MERKLER

---

<sup>7</sup>Newton-Raphson is a numerical method for finding iteratively better approximations to the roots of a real-valued function, detailed in ATKINSON (2004).

et. al. (2003) presented an strategy particularly developed for the preliminary design phase, which coupled the SAS with the engine performance analysis. The main requirements of the coupled procedure were flexibility of design and rapidity to calculate the impact of the SAS in the engine performance.

In all of the approaches, the key aspect is to abstract the complex engine geometry into a synthesis model, which describes the physical behaviour of the flow passages with basic geometrical properties and flow equations. Since the pattern of the flow in the SAS is 3D or in the simplest cases 2D, the SAS model developer needs to consider these flow characteristics in the one dimensional network. To this effect, experimental results or CFD solutions have been widely used to come up with acceptable correlations that are embedded in the 1D flow network.

In order to make the construction of the flow network manageable, the flow elements are categorised by their operation. Each flow element is characterised by a pressure loss coefficient law, a flow equation, and an energy equation. This data is supplied in form of tables or graphical items that are usually company proprietary data. A publicly available compendium of flow characteristics can be found in MILLER (1984).

Another way of finding suitable flow correlations is by employing **CFD simulation**. The early CFD analysis from GOSMAN (1975) showed it to be a promising approach, and CFD was already considered as a high potential tool for the analysis of the SAS in ZIMMERMANN (1990). Though originally, there was no confidence in the ability to produce validated methods. Nowadays, as stated in CHEW and HILLS (2007), “CFD is used with some confidence in industry and is considered essential as a research tool”. The advances in CFD simulation for the internal air system are directly linked with the developments in thermal modelling, which will be describe in more detail in the next section (2.4).

Another state of the art topic in the modelling of air systems is the one of **automation** and parameter studies. The parametric and **stochastic analysis** of the SAS flow network is of high interest to the gas turbine industry, given the wide range of failure combinations in the SAS and their impact in engine Through-Life-Costs, see TURNER et. al. (1997). Probabilistic analysis of the SAS have been performed by BISCHOFF et. al. (2006) and RAMERTH D. L. et. al. (2010). More recently, ANTINORI et. al. (2013) have published a stochastic analysis of the SAS that combines a sensitivity analysis followed by an uncertainty analysis. The sensitivity analysis

is used to identify the relevant variables and to reduce the number of parameters, whereas the uncertainty propagation analysis is used to determine the robustness of the responses (e.g. pressure loss, mass flows) to the input uncertainties.

Regarding the latest developments in SAS automation for preliminary design systems, ALEXIOU and MATHIOUDAKIS (2009) published an approach for modelling secondary air systems within an **object oriented** environment for gas turbine engine performance simulations. The goal of their work was to compare the performance between different SAS designs of individual components as well as to integrate them automatically in the whole engine performance models. A more advanced system, also object oriented based, is the virtual engine from DI MARE et. al. (2011). The latter authors developed a system that allows simulations of whole gas-turbine engines. The geometry information and physical models are organised in data trees. In this way, the system can handle geometries and three-dimensional boundaries from the parametric representations of gas-turbine features. This allows the automatic generation of full engine cross-sections and the extraction of the SAS. The virtual engine tool was applied to demonstrate the meshing and CFD analysis of a complete aero engine model through a transient operation cycle.

## 2.4. Thermal Modelling and CFD Developments

For the design of aero engine components, thermo-mechanical analyses are used to predict temperatures and displacements. An overview of these types of models can be found in DIXON et. al. (2004). The thermal data is in turn employed for material selection, rotor-stator clearance control, and lifing of components. Traditionally, the thermal boundary conditions have been selected from a number of standard heat transfer solutions, which are then validated against engine experiments equipped with thermocouples. The test measurements are used as reference values to tune calibration factors on the thermal boundary conditions. These calibration or matching factors are needed to adjust the standard boundary condition correlations to realistic engine geometry and operation. However, deviations in secondary flows and geometry from the engine testing can hardly be extrapolated, which limits the ability to use the matched thermal boundary conditions for new designs.

One of the first investigations of the flow and **heat transfer** in SAS disc cavities for turbomachinery is the work of BAYLEY and CONWAY (1964). These authors provided experimental data for use in engine design calculations and investigated the flow field in a narrow cavity between rotating and stationary discs. Moreover, this field of research continued in BAYLEY and OWEN (1970), who investigated the rotating disc cavity flows, and produced a widely used correlation for the minimum flow rate required to prevent hot gas ingestion of main annulus flow into the disc cavity.

The line of research was continued by Owen and others, who extended the investigations to a wide range of cavity topologies, including co-rotating disc cavities. A compendium of this work is described in the two part book: “Flow and heat transfer in rotating-disc systems”, OWEN and ROGERS (1989, 1995). Another early research on rotating disc flows is the one of DORFMAN (1963), whose semi-empirical correlations and theory are frequently used in engineering calculations. Additionally, the work of DAILY and NECE (1958) published measurements and correlations for rotor moment and flow in a sealed shrouded disc system, which has been often used as the basis for evaluation of CFD models.

Given that thermal boundary conditions in the SAS are the result of complex flow physics, **CFD methods** can be used to provide an insight into the flow field solution in SAS cavities with new flow configurations. The aero engine industry is currently applying and developing CFD extensively for the analysis of internal flow systems. CHEW and HILLS (2007) published a review on the state of the art of computational fluid dynamics for turbomachinery internal air systems, which summarised the extent of CFD applications and methods in great detail. In their work, it was stated that: “the performance of CFD for basic axisymmetric rotor/rotor and stator/rotor disc cavities with radial through-flow is largely understood and documented. Incorporation of three-dimensional geometrical features and calculation of unsteady flows are becoming commonplace. Automation of CFD, coupling with thermal models of the solid components, and extension of CFD models to include both air system and main gas path flows are current areas of development”. The main areas of research in CFD methods include:

- solution algorithms,
- parallelisation,
- turbulence modelling, and

- fluid-structure interaction (FSI).

In the field of **solution algorithms**, internal air system flow was originally treated as incompressible. Nowadays, with the advances on computing power, the solution algorithms consist of either pressure correction methods extended to include compressibility effects or density-based methods extended where necessary to low Mach number regimes. A review on the application case of each of these algorithms was presented in CHEW and HILLS (2007).

In terms of developments in **parallelisation**, current high-performance computing uses computational clusters. Thus, the ability to scale CFD models and codes efficiently to a large number of processors has become of great importance. HILLS and CHEW (2009) described the methods to obtain good parallel processor performance for an unstructured CFD code.

Regarding **turbulence** in CFD, Large eddy simulation (LES) is becoming common for research purposes and it is gaining interest in the gas turbine industry, as recently documented in TYACKE et. al. (2014). Nevertheless, most of the current industrial SAS applications of CFD use the Reynolds-averaged Navier–Stokes equations (RANS) with a model of turbulence. In the case of flows with high Reynolds numbers, the conventional  $k - \epsilon$  turbulence model with standard wall function treatment has been accepted as a fast convergence method for most applications, as already demonstrated in VIRR et. al. (1994). However, to be able to analyse heat transfer between solid and fluid domains, the lower Reynolds number flows inside the boundary layer need to be accurately solved. For this practice, it is preferred to use turbulence models resolving the near-wall region such as the two layer realizable  $k - \epsilon$  model or the  $k - \omega$  and  $k - \omega - SST$  models. Such two layer models have been described in DEBUCHY et. al. (2009), and an overview of the recent most frequently used turbulence models has been presented in SCHOBEIRI (2012).

Another desirable analysis capability is that of coupling between the SAS, CFD and FE-thermo-mechanical models. This type of simulations are usually referred to as analyses of **Fluid Structure Interaction** (FSI). According to MULLER and MONNOYER DE GALLAND, F. (2009): “Indeed gas properties, i.e. temperature, pressure and mass flow rate, greatly influence material temperatures, which in turn control the thermal expansion of the engine parts. This effect, redefining blade tip clearance and seal gap characteristics, modifies considerably pressure losses and mass flow rates in the secondary air system. In turn, they impact flow and material

temperatures. The coupling effect, estimated to be strong, must be precisely addressed to come up with a valid secondary air system design". Furthermore, the thermal interactions between structure and secondary air become more relevant as the size of the engine decreases.

**FSI coupled methods** consist on a two-way coupling between the CFD solution and the FE-model solution. The boundary condition information is interchanged between the two models, pursuing continuity of temperature and heat flux at the fluid–solid boundary. Originally, these simulation methods were applied to turbine blade cooling by HESELHAUS et. al. (1992). One of the earliest applications of FSI to analysis of SAS cavities appeared in VERDICCHIO et. al. (2001). Nowadays, state of the art FSI code has been newly developed by CHAQUET et. al. (2011). Moreover, SUN et. al. (2012) have applied the method to model a HPT pre-swirl and cooling system through a full transient engine cycle, and GANINE et. al. (2012) have demonstrated the CFD-thermal coupling application to a turbine model with multiple cavities, illustrated in Figure 2.4.1 on page 30.

An alternative approach to CFD-FE coupling is the **conjugate heat transfer** method, where a single code is used to run the full FSI simulation. The procedure to add conjugate capability to a Navier–Stokes code was described by RIGBY and LEPICOVSKY (2001). This type of FSI calculation has been used by authors, such as STARKE and SCHIFFER (2011), to test and validate simplified heat loss preliminary design methods. However, there is a disadvantage to applying the conjugate method, in that the temperature results may have to be exported to a structural mechanics code for use in stress analysis. This presents an inconvenience for embedding the new methodology in the complex validated design processes of the main engine manufactures.

The field of **automation and design optimisation** is becoming ever more important in the aero engine industry. Automated simulation offers the potential to reduce analysis time and enables the use of multi-physics design optimisation methods. CFD simulation is still limited by a relatively laborious analysis preparation time. Additionally, the results obtained from a CFD analysis may be user-dependent, which presents a standardisation and quality control problem. Aero-thermal analysis automation has been addressed extensively for turbine blading, with state of the art multi-disciplinary process such as in NOURI et. al. (2014). However, the more variable geometries of the SAS have restricted their automation. Nonetheless, CIAMPOLI et. al. (2007) and BAGSHAW et. al. (2010) present examples of automated mesh generation and

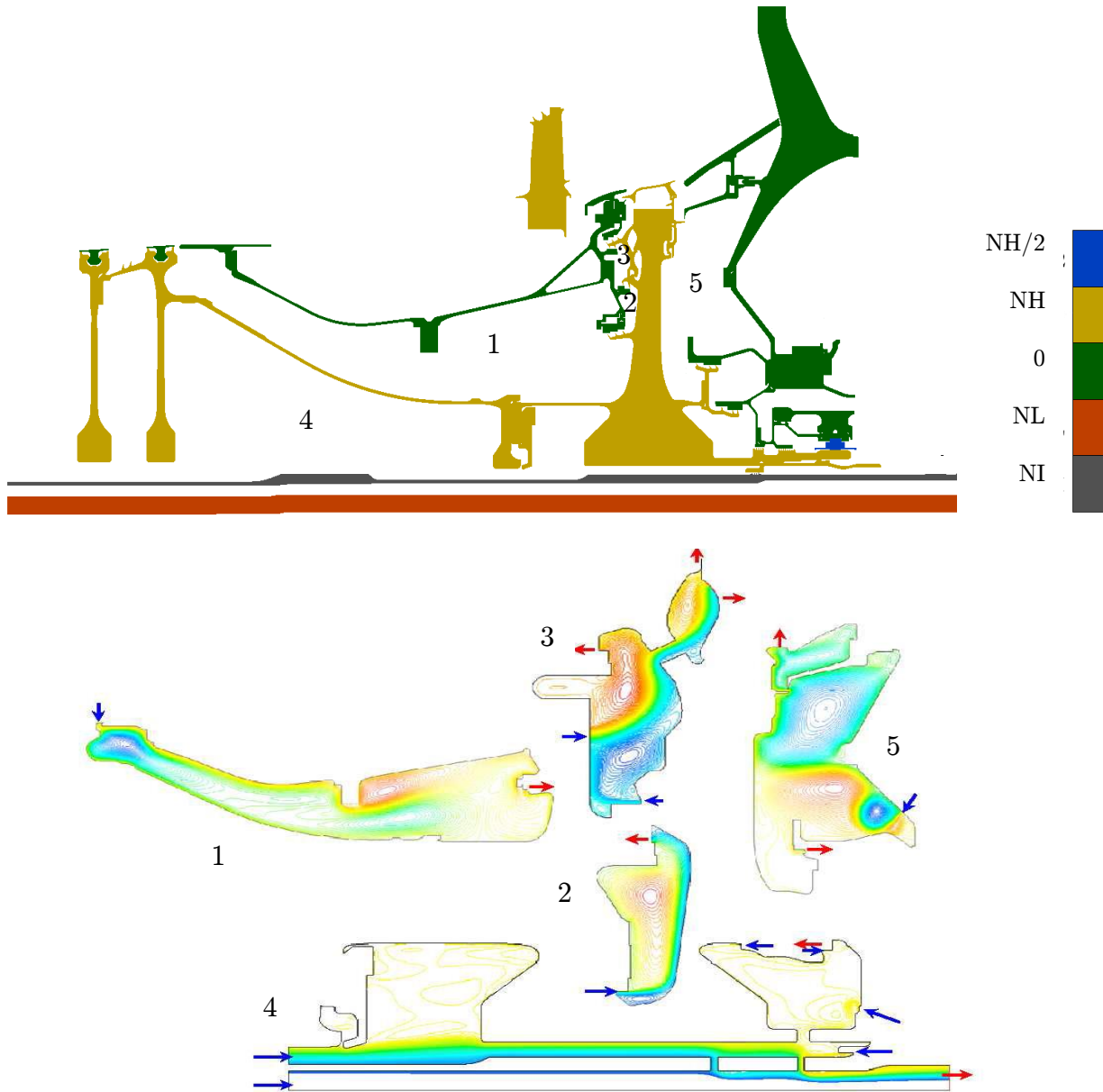


Figure 2.4.1.: Thermal-CFD coupling in multiple cavities demonstrated for a 2D thermal FE-model of HP rotor assembly from GANINE et. al. (2012). The turbine components are coloured by rotational speed (above) and the coupled CFD cavities are numbered 1-5 (below).



CFD analysis of a SAS model, integrated within a design optimisation. The benefits of coupling the SAS, disc design and thermal analysis have also been shown by REY VILLAZON, J. M. et. al. (2012). Furthermore, CFD automated studies have been presented in REY VILLAZON, J. M. et. al. (2013) for the generation of CFD-enhanced thermal boundary conditions suited for the engine preliminary design phase. As a contribution to this work, GRASSELT (2011) automated the complete CFD set-up and simulation process focusing on a non-ventilated HPT cavity, and BERTHOLD (2012) applied the automated CFD process to investigate preliminary design flow scaling methods for HPT rotor-stator cavities.

Even though ideally a FSI approach coupled with the full SAS flow network model of an engine would deliver the highest fidelity level in preliminary design thermal results, such methodology has been considered outside the scope of this thesis due to the high computational cost and complexity of implementing these methods in the time frame of this work. Since the thermal model of a specific engine cavity is very case dependent, there is scarce research to be found in the automation of thermal boundary conditions generation. This thesis presents an automated approach to creating the thermal FE-model of turbine discs, considering that the thermal boundary conditions may source either from engineering experience or advanced CFD simulation. Following the outlook stated in CHEW and HILLS (2009): “Both the attraction and complexity of including the main annulus flow path, the full internal air system and thermo-mechanical modelling in the same calculation are apparent [..]. Coupled modelling of these aspects of the engine is today achieved to some extent through iteration between design groups. More rapid coupling would make unforeseen consequences of design changes less likely and should allow further exploration of design space”.

---

# 3

## Fundamentals of Secondary Air System and Rotor Thermal Modelling

---

The modelling of the secondary air system and the discs temperature field involves a wide range of tools, each offering different levels of model fidelity. This chapter begins with the fundamentals of secondary air system and rotor design methods. As a result of the SAS design configuration, a system of fluid cavities and passages is formed, which defines the flow field around the components of a turbine. A characterisation of these internal flows is presented, together with their effects on heat transfer and power losses in turbine subsystems.

This chapter also explains the fundamentals of thermal analysis via the FE-method. A special case of thermal modelling methods is the use of CFD data for the preparation of thermal boundary conditions. Therefore, the final section focuses on the extraction of CFD data for use in thermal analysis.

### 3.1. Rotor and Secondary Air System Design

The use of rotor discs in turbomachinery is a direct consequence of the need for a component to support the turbine blades and to transmit torque from the turbine to the compressor. Disc design is the immediate step after blade rows design, and the starting point for the configur-

ation of the secondary air system. In due order, this section begins with an overview of rotor design requirements, features and methods. Accordingly follows the design methodology for the secondary air system.

### **3.1.1. Rotor design**

High pressure turbine discs of aero engines are classified as critical parts. Critical parts are those whose failure is defined as likely to have hazardous or even catastrophic effects (e.g. damage to or loss of aircraft structure, injury/loss of the crew/passengers) and therefore require special control in order to achieve an acceptably low probability of individual failure. The design requirements of the turbine discs are set at a very high standard and some of their failure modes can cause that areas of the turbine discs become life limiting features.

Historically, aero engine rotor parts were designed to avoid any failure risks with large safety factors that allow for scatter in different parameters. With the advent of high power computing, the computational time to conduct detailed thermo-mechanical assessments has drastically reduced and is now open for parametric design methods to determine the influence of parameter scatter on life and integrity. In order to use robust design engineering methods, the preliminary design tools need to run automatically, while providing a high level of model fidelity.

In the rotor design process, the geometry is the core of the design activities. At the early stage of the concept design phase, the stakeholders of a project capture the design geometry in a CAD model. The CAD model will then become the basis for the design and analysis steps to follow. The uses of the geometry model include:

- thermal analysis,
- structural analysis,
- component lifing,
- materials and manufacturing process modelling, and
- cost modelling.

Given these broad disciplines of CAD utilization, the requirements for state of the art rotor design methods include: standardisation of design, automation ability, robustness of CAD model to design changes, and model re-usability.

The **rotor design** is organised in a **hierarchy structure** where the disc body acts as the root, or level 1, for the next feature levels. The children feature levels can then be split into categories, where the rule for each level is that it should be possible to directly add it to the previous higher level (e.g. the disc body root for the level 2 features). In turn, deeper levels in the hierarchy, such as level  $i$ , contain geometries that require level  $i-1$  to exist before they can be present. Figure 3.1.1 on page 35 presents a diagram with the typical design features and hierarchies of a turbine rotor component.

According to PAHL et. al. (2007), “a systematic design provides an effective way to rationalise the design and production processes”. In the concept design phase, an structured approach will provide re-usable solutions. This in turn makes it possible to deduce application possibilities from previous projects and to use design libraries. For this purpose, the current engineering CAD design methodology recommends the use of a **parametrisation and tagging convention**.

In order to produce a parametric CAD geometry, state of the art modelling methods include the sketch based approach, the standardised user defined feature (UDF) assembly, and the programmatic design approach. These methods are described in detail in the review synthesis from CHAKRABARTI et. al. (2011) on state of the art for CAD.

In a **sketch based design**, sketches are groups of geometric entities that represent the outline of a feature. The sketch outline can be parametrically controlled with user predefined expressions. These represent parameters with a name and the expression definition, which can be a value, a reference to other parameters or a formula. It presents advantages in that it is a well established modelling method within the engineering designers community, it can be easily understood by users of varying design skills, the geometry is quickly generated, and each sketch can be re-utilised as a UDF. Its downside is that the geometry is not as flexible as the one generated with a programmatic approach, which leads to limitations in robust design automated loops.

The **standard UDF modelling** method was developed by the Technical University of Darmstadt, published in WENZEL et. al. (2013). It is a knowledge-driven approach, where the geometry is constructed from a predefined library of standardised reusable 3D UDF's, and imported via the “Standard Feature Agent”. The features carry design know-how and manufacturing data, which enables component cost and weight calculations. However, it requires a

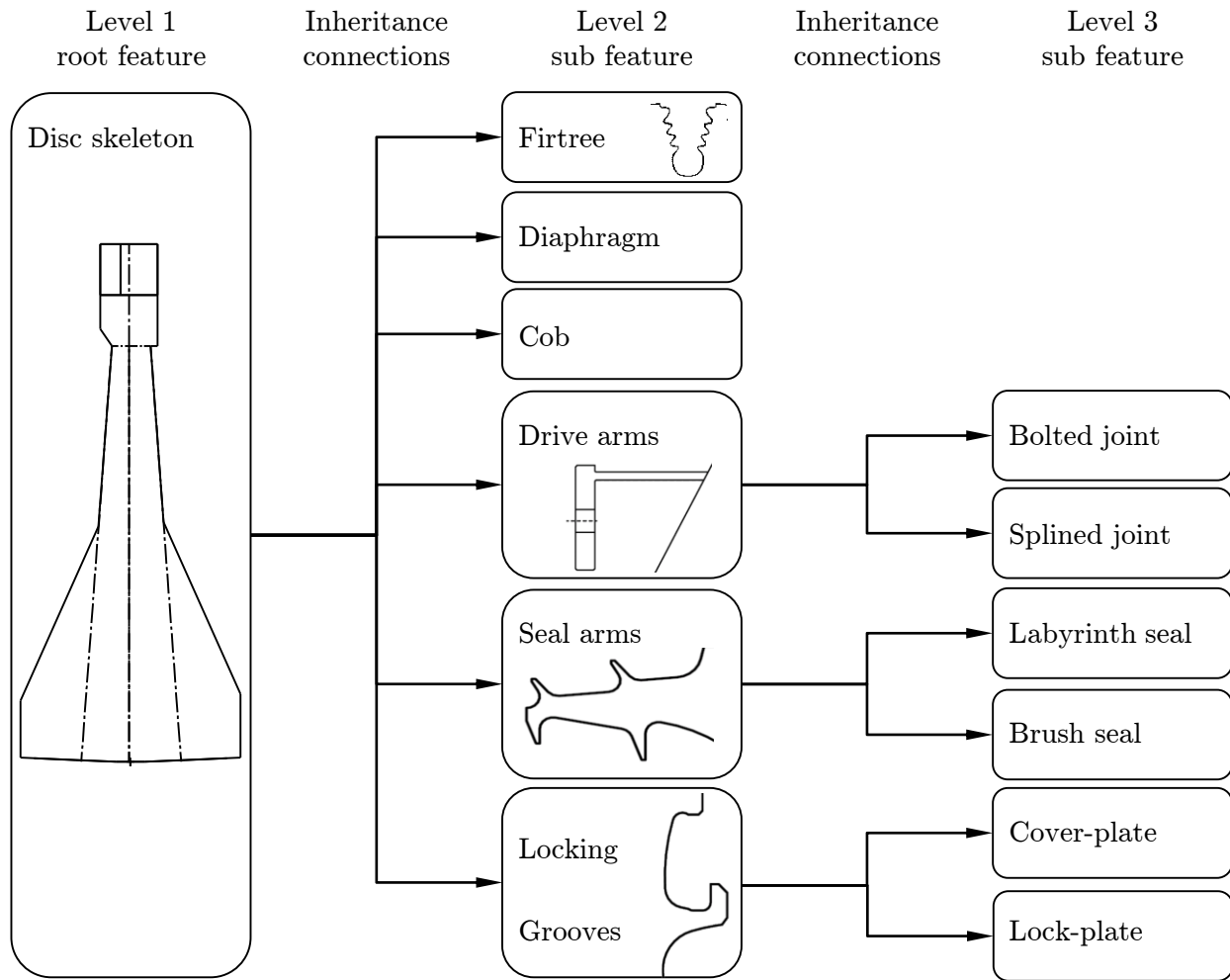


Figure 3.1.1.: Diagram of feature hierarchy levels, demonstrated for the turbine rotor features.

3D geometry, so 2D geometry sections are difficult to extract. This presents some limitation at the preliminary design stage, where commonly thermo-mechanical analysis are based in 2D geometry. Additionally, it requires a high skill level of design abilities to generate the database, and needs high maintenance effort to keep a reliable library of UDF's. A similar knowledge-based master model CAD process for turbomachinery has also been published by SANDBERG et. al. (2011).

In the **programmatic approach**, all geometry is generated with a code command structure. The geometry entities are defined as programming objects and are assigned attributes at the time of construction, e.g tag name, layer, etc. This method is especially well suited for automation, since it allows high control of each entity and post-processing of the geometry for use in further analysis. Such a process was demonstrated for a turbomachinery application by DYE

et. al. (2007), who focused specifically on the cross-section generation for preliminary design. It involves two modelling skills: high end programming users, who are responsible for the coding, and low end design users, who utilise the coded applications. There is a large preparation time frame associated to this method, but once the code is ready, the geometry handling becomes very quick.

Since the geometry is the basis for thermal and structural analyses, its processing will have a direct influence in the ultimate goal of rotor lifing. As a short review of rotor lifing methods, according to REED (2008), the dominant damage mechanism of turbine discs is crack initiation by low cycle fatigue (LCF), followed by crack growth by cycle fatigue propagation. Originally, the typical method for lifing turbine discs was the life-to-first-crack approach. Nowadays, a more cost-effective approach is the damage-tolerance lifing, and more recently the combination of damage-tolerance and probabilistic lifing methods. In the latter case, due to the high number of design iterations, the automated parametric CAD is a key asset to enable probabilistic assessments in an adequate time frame. Furthermore, not only the CAD, but also the flow modelling methods should follow the parametric approach for the design process to be truly fit for probabilistic lifing.

### 3.1.2. Secondary Air System design

This section presents the process and main features of the SAS design, with a brief overview of the inputs from higher level disciplines. It should be noted that unlike the rotor design, traditionally, the SAS design approach has its focus on the flow characteristics rather than the geometric features that guide the flow.

#### Inputs to the secondary air system design

The SAS design starts with the requirements for overall **engine performance** and main annulus aerodynamics. Engine performance is the relationship between power output, revolutions per minute, fuel consumption, and ambient conditions in which an engine operates. The results of the performance analysis are the main flow state properties at predefined stations<sup>1</sup> in the

---

<sup>1</sup>Described in WALSH and FLETCHER (2008), international station numbering and nomenclature standards were developed within the aerospace industry to improve efficiency and quality control of data passed between

engine. The performance input to the SAS comprises the pressures, temperatures, mass flows, and operating speeds of the thermodynamic engine cycle.

The **main annulus aerodynamics** input to the SAS is a more detailed fluid-dynamic description of the flow, including 2D annulus profiles of static pressures, total temperatures, and flow velocities. For the preliminary design aerodynamics, through-flow tools are used to calculate the flow characteristics over the whole annulus height. An explanation on the fundamentals of turbine through-flow aerodynamics can be found in AUNGIER (2006). The state conditions of the fluid at hub and tip positions of the blade row stations are used as boundary conditions for the SAS sources and sinks. Figure 3.1.2 on page 38 shows an example of the initial main annulus geometry and conditions that serve as an input to the SAS and rotor design.

### Interface of SAS and thermal analysis

The design of the SAS is very much coupled with the thermal analysis, as it requires a few iterations in order to converge running clearances and thermal gradients. A change in the SAS will affect the temperature prediction of the thermal model. At the same time, new thermal predictions imply changes in seal gaps and temperature gradient requirements, which need to be fed-back to the SAS design. Furthermore, the engine preliminary design process needs to go through a few iteration loops in order to converge the original performance requirements with the cooling needs of modified SAS configurations.

### Selecting the secondary air system architecture

In order to meet the main gas path cooling and sealing needs, the SAS designer chooses the minimum pressure compressor off-takes that enable feeding of the turbine sinks. When possible, the same off-take is used to feed several sinks. The **selection of compressor off-takes** leads to the configuration of pipes and passages that guides the fluid to the turbine sinks.

In a next step, the number and radial location of **disc seal arms** is selected. The position of seal arms can be adjusted to **optimise bearing loads** and the **discs temperature gradient**. With the selection of disc arms, the type and characteristics of the so called SAS cavities has

---

companies. Station numbers identify locations on the engine and are usually appended to symbols, such as for total pressure, to identify exactly at what point in the engine that value of pressure occurs.

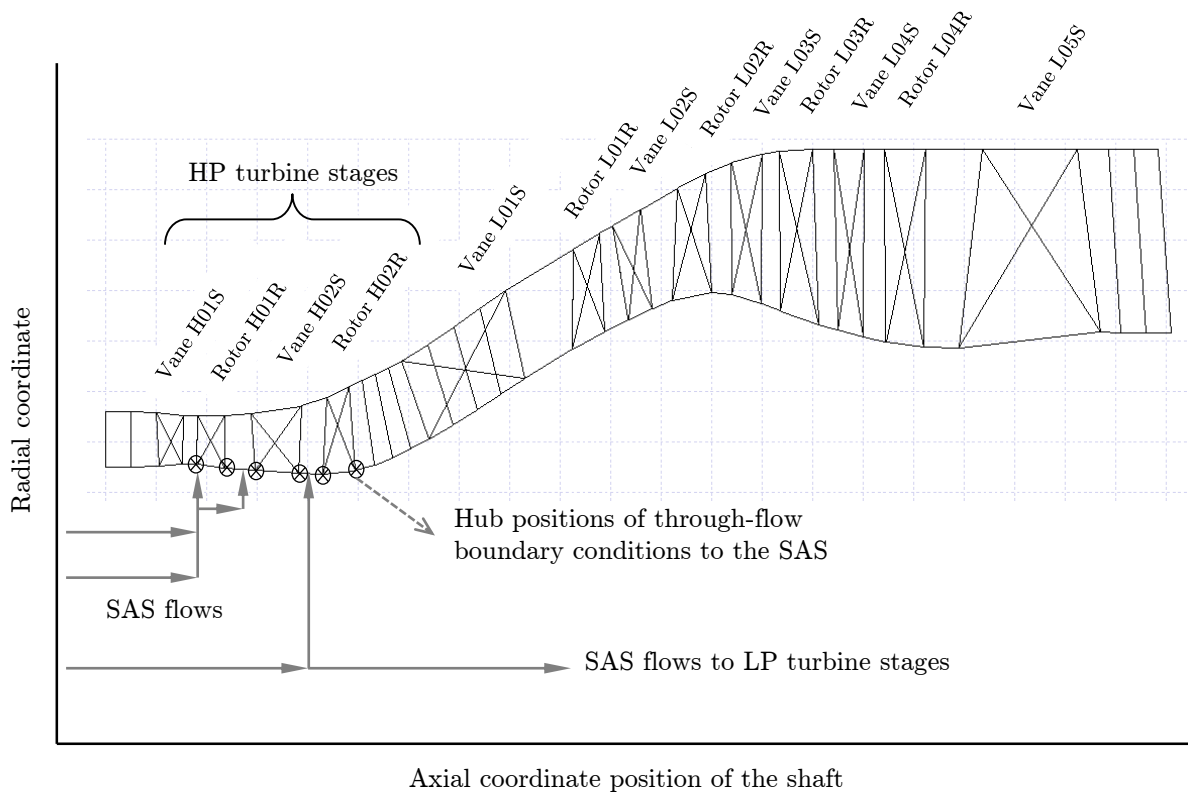


Figure 3.1.2.: Sketch of a typical turbine main annulus geometry for aero through-flow design. The annulus HPT hub locations point out the boundary condition positions for the SAS and rotor layout.

been implicitly fixed. These cavities are the fluid volumes that result from the combination of passages, stationary and rotating walls. Depending on the operation of the walls surrounding the fluid, the SAS cavities are categorised as purely static, rotor-stator, and purely rotating. Once the basic sealing configuration is set, the fluid passages between the cavities are selected to optimally guide the fluid to the turbine sinks. A diagram of a typical SAS cavity with the commonly employed SAS features and their associated flow circulation pattern can be seen in Figure 3.1.3 on page 41.

When configuring the SAS, there should be one controlling restriction wherever possible for each cooling subsystem. This practice favours that if a flow needs to be adjusted there is only one design change to be made. The restriction location is chosen downstream of any potential leaks, while ensuring that the impact on performance is minimised. The SAS features used to control the flow through the internal turbine are described in the rest of this section.



**Flow orifices** are used as flow regulating devices, pressure adjustment, or flow guidance to communicate cavities of different pressure. The flow through orifices is usually described with a discharge coefficient  $C_d$ . However, the design specification is usually the orifice inlet radius, since it leads to a higher and more predictable  $C_d$ , when taking into account the manufacturing tolerances.

**Pre-swirl nozzles** are used to guide flows from a purely static to a rotor-stator cavity, providing the flow a higher level of tangential velocity or swirl. This fluid rotational effect reduces the temperature difference between disc solid wall and fluid in the rotating relative system. There are two types: the simple circular section nozzles and the small vane nozzles. The latter type of nozzle resembles a cascade of turbine nozzle guide vanes. Its performance is somewhat better than the plain nozzle, but it increases the weight and cost of the component.

**Sealing devices** are used to prevent oil leakage from bearing chambers, to control air flows and to prevent hot gas ingestion. They are categorised as contacting and non-contacting, which is of importance in turbomachinery, since contact seals between rotating and static parts are not always practicable due to the high relative speeds.

Among the non-contacting seals, **labyrinth seals** are most common, and they can be of the type: straight-through, inclined fin, stepped, combination seals, double-sided, and overlapping. The labyrinth seal has a series of clearances between rotor and stator. In an ideal seal, the dynamic pressure in each clearance is lost when entering the subsequent chamber. By having a number of sealing clearances in series, the pressure drop across each one is made much smaller than it would be if there were only one clearance to restrict the leakage flow. The labyrinth seal fins is applied in conjunction with a static part, which can be a felt metal lining or a honeycomb lining.

**Contacting seals** are used to prevent mixing of different fluids, for example to keep oil inside a bearing chamber. The constant leakage through a labyrinth seal would not be acceptable, and thus the gap is closed with a rubbing contact. Common types of contact seals include the brush and the ring sealing devices.

Since seals enclose a fluid between a rotating and a static part, they produce windage heating. It is important to consider this effect, since the viscous drag on rotating components represents a loss of energy, and the heating of the fluid requires increased quantities of cooling flow to

maintain an optimal thermal field. Detailed investigations on seal heat transfer effects were performed by MILLWARD and EDWARDS (1996) and WILLENBORG et. al. (2001).

Another key aspect of sealing design is the running clearance. It is necessary to ensure that the intended clearance is accurately maintained under all running conditions. The control of the running clearance must address the multi-disciplinary aspects: manufacturing tolerances, bearing movement, casing vibrations, seal vibrations, strain growth, and thermal expansion. An accurate clearance control requires good knowledge of the thermal field in the components around the seal, and therefore a high fidelity thermal FE-model.

**Heat shields** and cover-plates are used as a way to pump the cooling air into the blade cooling passages, and additionally help to keep the highly loaded disc post shielded from high temperatures at the turbine rim. The cover-plate is a smaller disc attached to the front of the main disc. Its size depends on the required seal and pre-swirl nozzle radii, and the location where this small disc needs to be supported.

**The blade cooling feed system** has to deliver a defined mass flow of cooling air below a critical temperature, which are specified by the turbine blade design team. Since the blade and rotor components are affected by the relative total temperature of the surrounding fluid, pre-swirl systems are used to diminish the relative temperature field. For moderate blade feed pressure, no outer pre-swirl seal is required. In this case, the blade is fed through its shank. However, whenever high feed pressure is needed, drilled air holes are used to guide the fluid from the turbine disc to the bucket groove.

Complex blade root systems can also include the fluid transfer path into the next turbine stage. The **micro-turbine device** achieves such inter-stage cooling air transfer through an air hole in the blade shank that exhausts the air in the opposite direction of blade rotation. This air flow impulse into the next cavity provides some additional percentage of power to the turbine.

**Cooled cooling air:** there is recently a drive to find cooler sources of air to cool the turbine blades. An arrangement with high cooling potential is to take HPC delivery air and cool it in a heat exchanger. With this device, it is possible to cool the air much more than with a pre-swirl system. Another benefit is that it allows to reach parts of the engine which cannot be reached with pre-swirled air. There are high benefits to be gained with this devices, but the disadvantages of high pressure losses, weight and cost are significant.

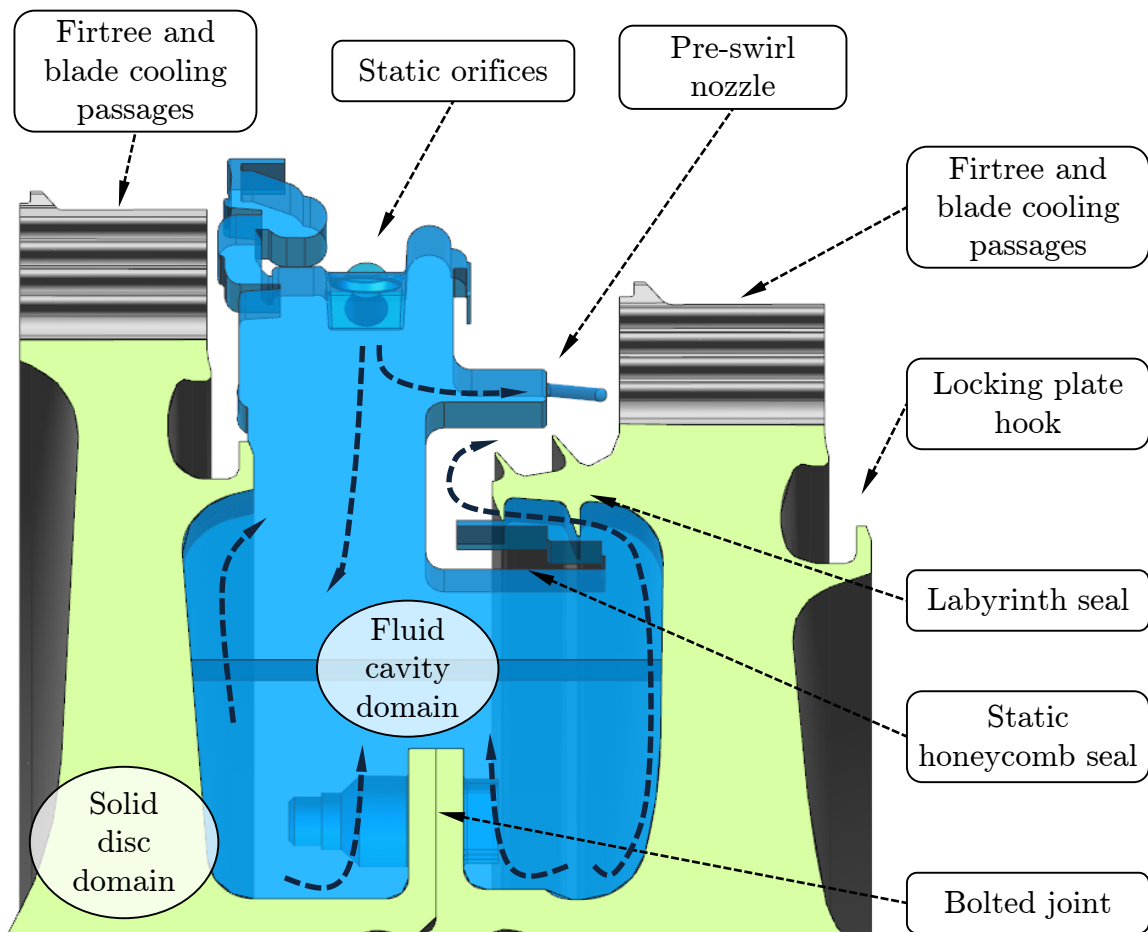


Figure 3.1.3.: Diagram of a typical SAS turbine cavity showing the location of some commonly employed SAS features and the associated flow circulation pattern.

In summary, the number of flow elements and configurations of the SAS is quite large. However, most configurations can be categorised in distinct cavity and flow element families. The next section gives an overview of the flow field and heat transfer phenomena that can be expected in the system of cavities and flow passages of the SAS.

## 3.2. Flow Phenomena in the Secondary Air System

The multiple combinations of features in the SAS yield a wide variety of 3D flow phenomena that lead to complex interactions between all directions of the momentum components. The flow in cavities and the flow through passages is typically analysed separately. This adds some simplicity to analyse the full system, since flow passages, such as orifices or seals, are considered as the inlet and outlet boundaries of a cavity. Another practical flow characterisation distinguishes whether the fluid circulates between rotating or static components, or a combination of both. The flow conditions in most cavities of a turbine SAS will be affected by the rotating disc system.

This section begins with a description of the flow around a free disc and its relevant non-dimensional parameters, as depicted in Figure 3.2.1 on page 43. The enclosed disc flow field is then introduced, as illustrated in Figure 3.2.3 on page 47. The real engine behaviour of the flow over a rotor disc surrounded by a static architecture is in between the theoretical flow field of free and enclosed discs. While disc walls in narrow cavities, with a static part located in their immediate surrounding, will behave like enclosed discs, it can be assumed that disc walls in very wide cavities will be rather similar to the free disc.

Thereafter, the section describes the relevant sources of power losses in the SAS. In this context, the frictional losses of rotor-stator systems and the phenomena known as windage are introduced. An additional source of SAS losses is the pumping power required to guide the flow through narrow channels, such as the passages in the blade cooling feed system.

### 3.2.1. The free disc system

The main assumptions in the free disc system are that the disc rotates in a fluid of infinite extent and the fluid is initially at rest. By applying these boundary conditions, and considering

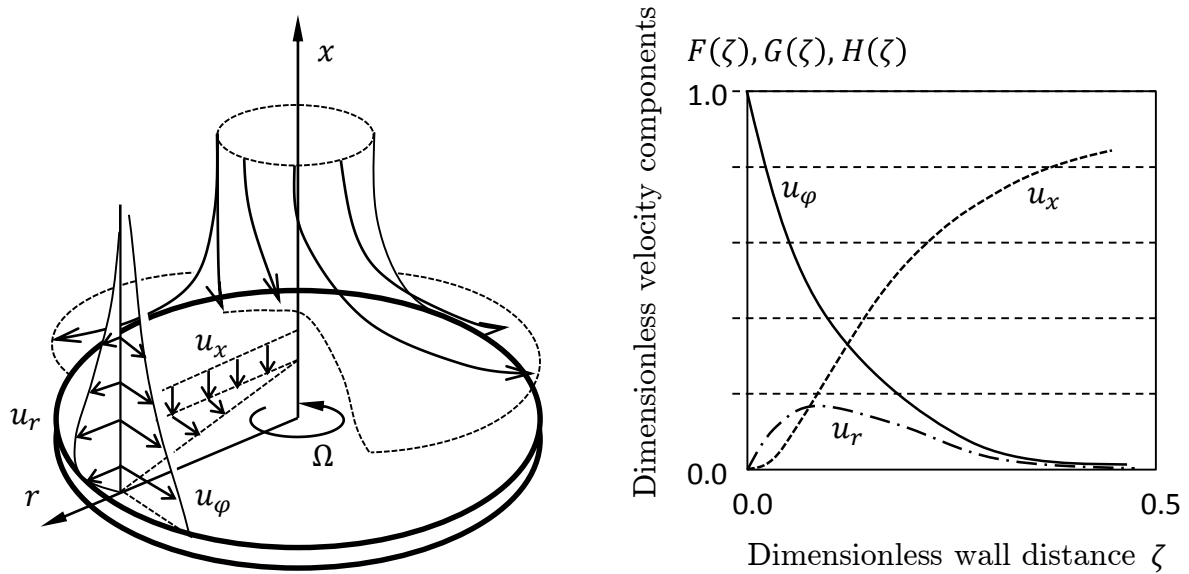


Figure 3.2.1.: Diagram of the flow around a free rotating disc (left) and profile of velocity components with dimensionless wall distance (right), as depicted in OWEN and ROGERS (1989).

incompressible flow  $\rho = \text{constant}$ , with dynamic viscosity  $\mu = \text{constant}$ , KÁRMÁN (1946) solved the Navier-Stokes equations for a free rotating disc. A diagram of the resulting flow field structure and how the velocity components develop along the dimensionless wall distance  $\zeta$  (in  $x$  axis direction) can be seen in Figure 3.2.1 on page 43.

Within the relatively small boundary layer, which may be laminar, transitional or turbulent (depending on the Reynolds number  $Re$ ), there occurs a pumping effect forcing the fluid particles to move radially outwards. In order to satisfy mass flow continuity, additional fluid is entrained axially. Consequently, a three dimensional flow field develops with velocity components in axial, circumferential and radial direction.

The relevant non-dimensional parameters that affect the flow field around the free disc are the rotational Reynolds number  $Re_\phi$  (3.2.1) and the through flow coefficient  $c_w$  (3.2.2). OWEN and ROGERS (1989) describe how these coefficients can be combined in the turbulent flow parameter  $\lambda$  (3.2.3), which compares the through flow with the pumped flow of a free rotating disc. An additional relevant parameter is the dimensionless swirl ratio  $\beta$  (3.2.4), which relates the local circumferential fluid velocity to the angular speed of the rotor. The swirl ratio is useful to compare the inlet condition of the flow and its development along the cavity.

$$Re\varphi = \frac{u_\varphi \cdot r}{\nu} \quad (3.2.1)$$

$$c_w = \frac{\dot{m}}{\mu \cdot r} \quad (3.2.2)$$

$$\lambda = \frac{c_w}{Re\varphi^{0.8}} \quad (3.2.3)$$

$$\beta = \frac{u_\varphi}{\Omega \cdot r} \quad (3.2.4)$$

The experiments carried out by THEODORSEN and REGIER (1944) showed that a laminar boundary layer profile can be expected for  $Re\varphi$  lower than the critical  $Re\varphi^{critical} = 0.5 \cdot 10^5$ . This value marks the beginning of the transition phase. The transition typically takes place between  $0.5 \cdot 10^5 < Re\varphi < 3.1 \cdot 10^5$ . For higher  $Re\varphi$ , the viscous boundary layer under turbulent flow is fully developed. It should be noted that these values also depend on material and manufacturing properties like the disc roughness. In the typical operation of turbine discs,  $Re\varphi$  is sufficiently high that all three boundary layer conditions are present over the disc, with a predominance of viscous layer under turbulent flow.

### Heat transfer in the free disc system

The heat transfer from a free rotating disc depends on the disc temperature distribution  $T_o(r)$  and the Prandtl number<sup>2</sup>  $Pr = c_p\mu/k$ . The energy equation used to determine the temperature distribution within the fluid boundary layer can also be used to determine the heat transfer from the disc and the temperature of the fluid  $T_\infty$  outside the boundary layer. OWEN and ROGERS (1989) describe how the solution of temperature profiles for laminar flow with isothermal and quadratic disc temperature distributions can be determined. The fluid temperature profiles tend to the  $T_\infty$  asymptote with the wall distance, as shown in Figure 3.2.2 on page 45.

---

<sup>2</sup>The Prandtl number is the ratio of momentum diffusivity (kinematic viscosity) to thermal diffusivity.

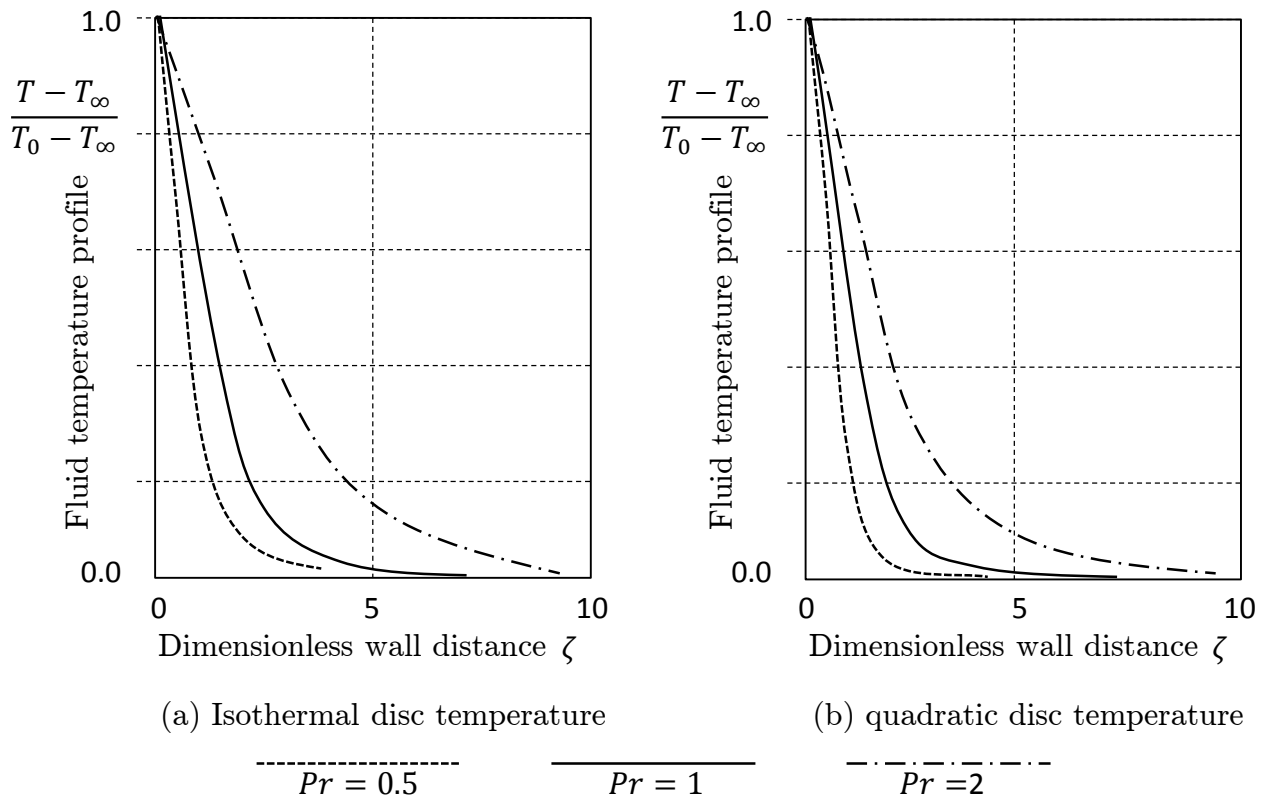


Figure 3.2.2.: Temperature profiles for the free disc under laminar flow, from OWEN and ROGERS (1989). Influence of the  $Pr$  number and the disc solid temperature distribution: isothermal (a) and quadratic (b).

$$Nu = \frac{\dot{q}_0 \cdot r}{k \cdot (T_0 - T_\infty)} \quad (3.2.5)$$

The local Nusselt number<sup>3</sup>  $Nu$ , defined for radial flows in 3.2.5, is used as a measure of convective heat transfer capability over the disc. There is an integral analytical solution for turbulent flow, in the case where the Reynolds analogy is valid. The Reynolds analogy assumes that the boundary layer profiles of heat transfer and wall shear stresses are analogous. The conditions for its validity in rotating discs are that  $Pr = 1$ , the disc temperature distribution is quadratic, and the total enthalpy outside the boundary layer does not depend on the radius  $r$ . A summary of analytical, numerical and experimental results of the variation of  $Nu$  with  $Re_\varphi$  can be found in OWEN and ROGERS (1989). The behaviour of the radially averaged  $Nu_{av}$  can be

<sup>3</sup>The Nusselt number is the ratio of convective to conductive heat transfer across a boundary.

summarised as follows:

- $Nu_{av}$  depends on the  $Pr$  number and the disc solid temperature distribution in an analogous way for laminar and turbulent flow.
- $Nu_{av}$  increases with  $Re\varphi$ , but has a steeper slope dependency in turbulent flow conditions than laminar.

The theoretical solutions for the free disc system provide an understanding of the relevant flow phenomena that can be expected in the SAS cavities. Nevertheless for realistic applications, analytical solutions are commonly not available and CFD is used to simulate the flow field and heat transfer in rotor-stator cavities, which typically include complex 3D features.

### 3.2.2. The enclosed disc system

The enclosed disc system assumes that one disc rotates with angular velocity  $\Omega$  about the x-axis, and has in front of it another stationary disc (the stator side of the cavity). The right side of Figure 3.2.3 on page 47 shows a diagram of the main cavity dimensions and the generic velocity profiles in the enclosed system.

The fundamental research for this type of disc system was performed by DAILY and NECE (1958), who identified four regimens of flow, see left side of Figure 3.2.3 on page 47. The flow pattern mainly depends on the axial gap ratio  $G = s/r_2$  and  $Re\varphi$ . For close cavity clearance, represented by regimes I and III, the boundary layers on the rotor and the stator are merged and the flow inertial terms across the gap are negligible. This type of flow structure is known as a Couette type of flow. To describe the regimes, it is useful to define the gap Reynolds number,  $Re_s$  as in (3.2.6). For  $Re_s \geq 100$ , a rotating inviscid fluid core develops, with sharp velocity gradient near the boundary layer. This is typical of flow regime IV, a Batchelor type of flow structure, which is the most common case found in turbine SAS applications of aero engines.

$$Re_s = \Omega \cdot s^2 / \nu = G^2 \cdot Re\varphi \quad (3.2.6)$$

The enclosed disc flow phenomena are usually classified between system with and without superposed flow. A radial superposed flow is in most cases present in ventilated SAS cavities.



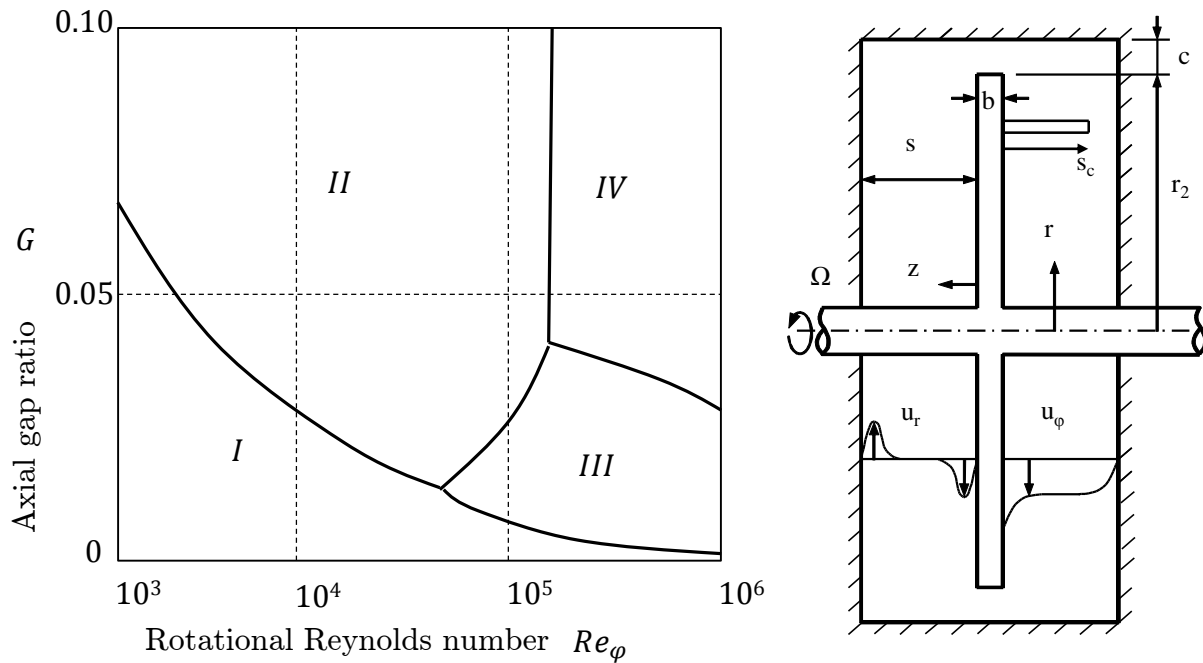


Figure 3.2.3.: Flow regimes of the enclosed disc system (left) and diagram of cavity dimensions and velocity profiles (right), from DAILY and NECE (1958).

This additional inlet flow has an impact on the profiles of the boundary layer and the turbulence intensity. The superposed flow can cause premature transition to turbulent flow. In turbine rotor-stator systems, a superposed radial flow is created by the pressure gradient in between the SAS cavities. At the rim cavities, such a superposed flow prevents hot gas ingestion from the main annulus through the rim seals. When a superposed radial flow is present, the net flow is radially outwards. However, that does not necessarily imply that all of the local flow is directed outwards. In most enclosed disc systems, a local recirculation forms, with opposite flow directions over the stator and disc walls.

The mass flow distribution between the rotor and the stator wall depends on the value of the flow parameter  $\lambda$  and the amount of superposed mass flow  $m_{sup}$ . Typically, the incoming superposed mass flow has some swirl velocity. Under these conditions, there is a source region with a tendency for angular momentum to be conserved. Therefore, the fluid tangential velocity in the core decreases with increasing radius.

## Heat transfer in the enclosed disc system

Extensive research has been performed previous to this work on heat transfer in rotor-stator systems. When no superposed mass flow is present, the  $Nu$  number is defined with a temperature difference relating to the temperature of core  $T_c$ , as in (3.2.7). When a superposed flow is considered,  $Nu$  is defined as in (3.2.8), where the temperature difference is referenced to the temperature of the incoming fluid  $T_I$  or to the adiabatic temperature  $T_{0,ad}$ , as in (3.2.9).

$$Nu = \frac{\dot{q}_0 \cdot r}{k \cdot (T_0 - T_C)} \quad (3.2.7)$$

$$Nu = \frac{\dot{q}_0 \cdot r}{k \cdot (T_0 - T_I)} \quad (3.2.8)$$

$$T_{0,ad} = T_I + R^f \cdot \frac{\Omega^2 \cdot r^2}{2 \cdot c_p} \quad (3.2.9)$$

Historically, the investigations on heat transfer in enclosed discs distinguish between shrouded and unshrouded systems. The shroud refers to an upper horizontal solid boundary, which is usually present in engine SAS in the form of a disc arm or a sealing structure. The shroud clearance ratio  $G_c = s_c \cdot r_2$  is a useful geometrical parameter to describe the impact of the shroud. OWEN and ROGERS (1989) present a thorough summary of numerical and experimental results for heat transfer in rotor-stator systems. The main conclusions of their work, based on the radially averaged Nusselt number  $Nu_{av}$ , can be summarised as follows:

- for unshrouded discs:
  - $Nu_{av}$  increases as  $G$  decreases for small gap ratios and becomes independent of  $G$  for large ones.
  - with large rotational speed,  $Nu_{av}$  tends to the free-disc case as  $Re\varphi$  increases, and with small speeds, the results tend to an asymptote independent of  $Re\varphi$ .
- for shrouded discs:
  - $Nu_{av}$  is higher than the unshrouded disc result, but the dependencies to  $Re\varphi$  and  $G$  remains analogous to the unshrouded case.

–  $Nu_{av}$  decreases with  $G_c$  and increases with the flow coefficient  $c_w$ .

### 3.2.3. Frictional losses of rotating components: Windage

The fluid frictional shear stresses over the disc suppose an additional torque requirement to the turbine subsystem. Since this torque does not contribute to engine thrust, nor to the thermal efficiency of the gas generator, it is considered as a power loss. The frictional shear stresses result from the fluid's viscosity, which generates tangential forces within the boundary layer. The momentum integral equations of a rotating disc can be found in OWEN and ROGERS (1989), and are included in Section A.4.

In practice, the associated forces over the disc can be expressed as the integrated torque  $M$  over one wetted side of the disc, (3.2.10), where the tangential shear stress at the wall,  $\tau_{\varphi,0}$  can be determined by (3.2.11).

$$M = -2\pi \int_{r_1}^{r_2} r^2 \cdot \tau_{\varphi,0} \cdot dr \quad (3.2.10)$$

$$\tau_{\varphi,0} = \mu \frac{du_{\varphi}}{dx} \Big|_0 \quad (3.2.11)$$

For a non-dimensional characterisation, the torque can be described with the moment coefficient  $c_m$  for a complete disc (2 wetted sides), defined in (3.2.12).

$$c_m = \frac{M}{\Omega^2 \cdot r_2^5 \cdot \rho / 2} \quad (3.2.12)$$

The correlations and parameter laws that describe  $c_m$  have been the scope of many investigations, since it can also provide information about the power loss of the disc and the temperature pick up of the fluid in a rotor-stator cavity. Based on the first law of thermodynamics, the sum of the heat rate  $\dot{Q}$  and the power input  $\dot{W}$  equals the difference of total enthalpy rate  $\dot{H}_2 - \dot{H}_1$ , which for a perfect gas is a function of total temperature difference, (3.2.13).

$$\dot{Q} - \dot{W} = \dot{H}_2 - \dot{H}_1 = \dot{m} \cdot c_p \cdot (T_{t,2} - T_{t,1}) \quad (3.2.13)$$

The heat term is associated to convective heat transfer and sometimes even a source of radiation. If the system would be considered to be adiabatic,  $\dot{Q}$  would be zero. The term  $\dot{W}$  is the power that is put into the fluid system by the disc. It includes what is commonly known as viscous heating or windage  $\dot{W} = M \cdot \Omega$ . Windage is therefore defined as the power applied by the rotor moment on the fluid bathing it.

When combining the above formulation, it can be concluded that windage changes the total temperature of the fluid from the inlet to the outlet of the rotor-stator system. There is a direct relation between  $c_m$  and the temperature change of the fluid in the rotor-stator cavity, as expressed in (3.2.14). Therefore, the heat pick up of the fluid per unit area,  $HPU$ , is the sum of the energy input in form of the convective heat rate  $HPU_{conv}$  and the windage power  $HPU_{wind}$ , as in (3.2.15).

$$\Delta T_{windage} = \frac{c_m \cdot \Omega^3 \cdot r_2^5 \cdot \rho / 2}{\dot{m} \cdot c_p} \quad (3.2.14)$$

$$HPU = HPT_{conv} + HPU_{wind} = \frac{\dot{Q} - \dot{W}}{A} \quad (3.2.15)$$

In practice, the heat pick up due to windage can be determined with the correlations for the moment coefficient  $c_m$  (3.2.12) or via CFD analysis. Ultimately,  $c_m$  is a measure of the wall shear stresses, which strongly depend on the flow field properties, the flow field regimes (section 3.2.2) and the associated Reynolds number  $Re_\varphi$ . BERTHOLD (2012) summarises the commonly used  $c_m$  correlations for SAS rotor-stator cavities and seals.

### 3.2.4. Pumping losses of rotating channels

When the fluid enters a rotating channel from a cavity where the swirl number is below 1, power is needed to increase the tangential velocity of the flow and to pump the flow from a lower to a higher radius. The power associated to these pumping effects can be simplistically calculated by the Euler's pump and turbine equation of turbo-machinery (3.2.16).

$$\dot{W} = \dot{m} \cdot (u_{\varphi,2} \cdot \Omega \cdot r_2 - u_{\varphi,1} \cdot \Omega \cdot r_1) \quad (3.2.16)$$

The rotating channel pumping effect can be split in two separate power contributions: the power to increase the fluids swirl and the power to move the fluid radially outwards. When the fluid enters a rotating channel from a cavity, it usually has a different tangential velocity (in most cases lower) than the rotating speed of the channel. Thus, the power needed to accelerate the fluid from a swirl of  $\beta$  to swirl of 1 can be determined with (3.2.17). Once the fluid is inside the rotating channel, its tangential velocity is very close to the rotational speed of the channel walls (not necessarily true for wide channels, but these would fall under the category of rotating cavities). Hence, with the assumption that  $u_\varphi(r) = \Omega \cdot r$ , the power needed for bringing the fluid to a higher radius within the rotating channel can be determined with (3.2.18).

$$\dot{W} = \dot{m} \cdot \Omega^2 \cdot r^2 \cdot (1 - \beta) \quad (3.2.17)$$

$$\dot{W} = \dot{m} \cdot \Omega^2 \cdot (r_2^2 - r_1^2) \quad (3.2.18)$$

The pumping losses within rotating channels can account for a very relevant percentage of the whole SAS power losses. One of the highest contributors is the pumping power required to guide the fluid through the blade cooling system, since the fluid needs to be fed from the lower turbine cavities into the higher radii of the turbine main annulus. The complex system of blade cooling passages supposes a large increase in both radius and swirl for the fluid.

### 3.3. Flow Network Modelling

The tool most commonly used in the analysis of air systems is the 1D flow network model. An introduction to the state of the art and functions of flow network modelling has been presented in Section 2.3. This section describes the fundamentals of this type of modelling program and the general arrangement of typical SAS flow network models.

To create the model, the complex engine geometry needs to be simplified into a 1D synthesis model, which describes the physical behaviour of the flow passages and cavities with basic geometrical properties and flow equations. The computer program to build the 1D flow network requires the air system to be translated into an equivalent network of links, which represent all

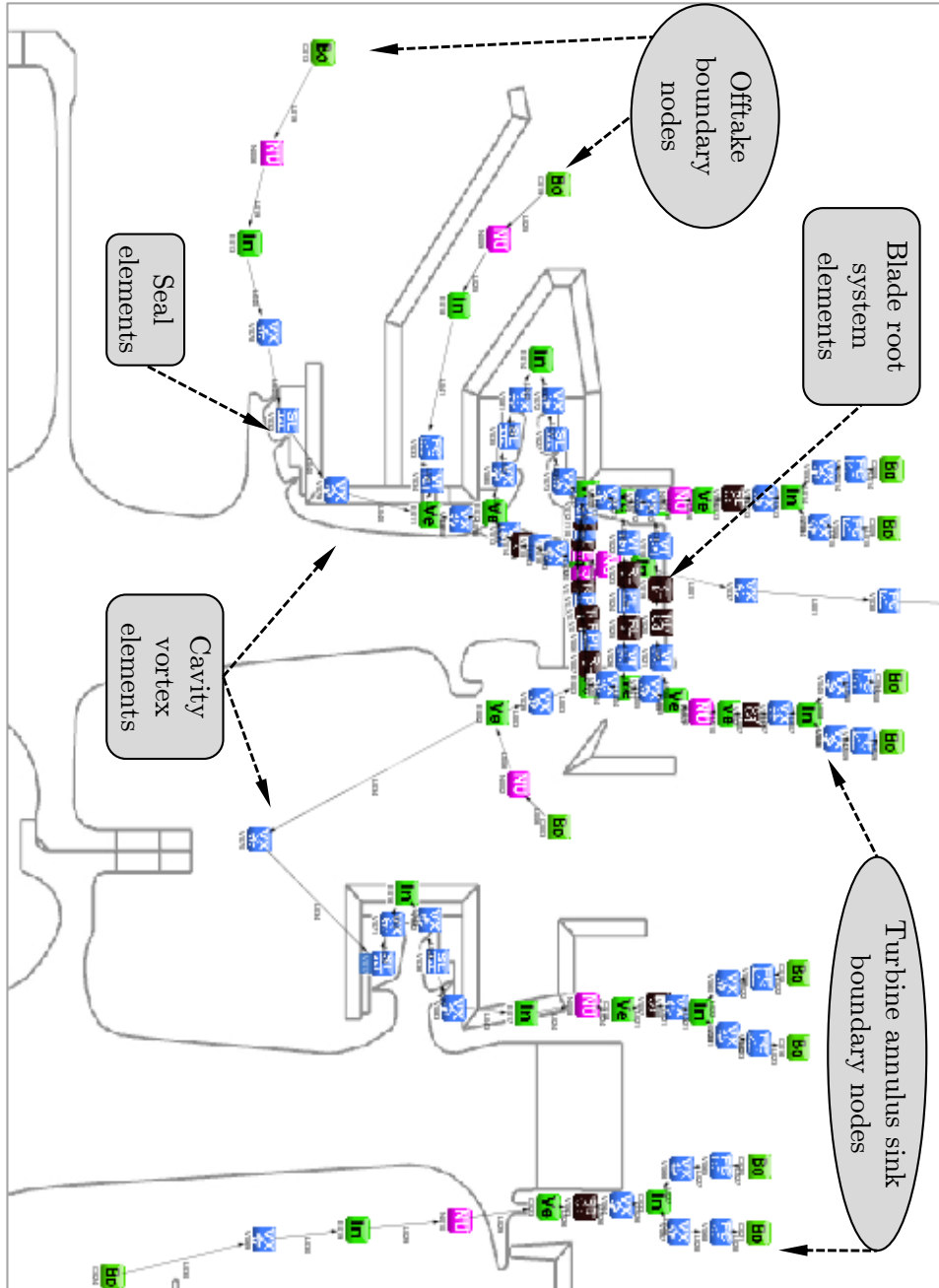


Figure 3.3.1.: Diagram of the 1D flow network model of a typical 2-stage HPT.

of the flow paths, and nodes, where links meet. In order to assemble the network, the modeller needs to go through the SAS design identifying all of the significant flow paths defining the links. Then, one or more elements have to be placed within the links (called bits), which represent the features in the network that produce changes of pressure or enthalpy. Figure 3.3.1 on page 52 shows an example of the 1D flow network model of a typical HP turbine SAS.

### 3.3.1. Flow network analysis

In order to compute the flow, pressure, and temperature in a flow network, the network is discretised into a finite number of control volumes. The conservation equations for mass, momentum, and energy must be accounted for in each control volume. The resulting system of equations is a coupled and non-linear system that is solved by a numerical method.

#### Governing equations

The mass and energy conservation equations are used to solve the state of the fluid in the internal nodes, and the momentum conservation equation is used for the flow rate in each link. Figure 3.3.2 on page 55 shows a diagram of the nodes and links arrangement, together with a typical orientation with respect to the engine axis. The following formulation assumes that the problem is steady state ( $\partial/\partial t = 0$ ). Therefore, whenever a transient cycle analysis with the flow network model is attempted, the solution will be a set of interpolated steady state points.

Mass conservation requires that the net mass flow from a given node must equate to zero. The integral form of mass conservation in a control volume  $V$ , in (3.3.1), shows that the time rate of mass change in the volume  $V$  plus the net rate of mass flow through its surfaces  $A$  must be equal to zero. Thus, for the flow network nodes, it can be formulated as in (3.3.2), where  $\dot{m}_S$  represents a possible term of mass injection.

$$\frac{\partial}{\partial t} \int_V \rho dV + \int_A \rho(\bar{v} \cdot \bar{n}) dA = 0 \quad (3.3.1)$$

$$\sum_{j=1}^n \dot{m}_{ij} + \dot{m}_S = 0 \quad (3.3.2)$$

The momentum conservation equation shows that the fluid body forces  $\bar{X}$  (gravity, inertia, etc.), pressures and viscous stresses on a control volume equal the rate of momentum change in the volume plus the rate of the momentum flow through its surfaces, as in (3.3.3). This can be formulated for a given flow link as (3.3.4), where Inertia, pressure, gravity, friction and centrifugal forces are considered. In addition to these terms, a source term  $S$  is provided in the equation to input pump characteristics or other external force in a given link. The momentum conservation equation requires the knowledge of the density, specific heats and viscosity of the fluid within the branch. These properties are functions of the temperatures and pressures at each node, so an average value is chosen between node  $i$  and  $j$ .

$$\int_V \rho \bar{X} dV + \int_A (\bar{\tau} \cdot \bar{n}) dA = \frac{\partial}{\partial t} \int_V \rho \bar{v} dV + \int_A \rho (\bar{v} \cdot \bar{n}) \bar{v} dA \quad (3.3.3)$$

$$\begin{aligned} \overbrace{\dot{m}_{ij} \cdot (u_j - u_i)}^{\textit{inertia}} = A \cdot \overbrace{(p_i - p_j)}^{\textit{pressure}} - \rho \cdot \overbrace{g_c \cdot V \cdot \cos\theta}^{\textit{gravity}} - K f \overbrace{\dot{m}_{ij} \cdot |\dot{m}_{ij}|}^{\textit{friction}} \cdot A \\ + \frac{\rho \cdot K_{rot}^2 \cdot \Omega^2 \cdot A}{2} \overbrace{(r_j^2 - r_i^2)}^{\textit{centrifugal}} \cdot \cos\theta + \overbrace{S}^{\textit{source}} \end{aligned} \quad (3.3.4)$$

Energy conservation for a control volume as in the first law of thermodynamics, (3.3.5), states that the rate of total energy change plus the energy flow through its surfaces equals to the heat transferred into the volume plus the work applied on the volume. The total energy is defined as the sum of internal, kinetic, potential energies and other terms,  $\hat{E} = U + m\bar{v}^2/2 + mgr$ . Moreover, the power terms can be split into work from body forces, pressures, viscous terms, and from other applied forces, as in (3.3.6). The heat terms  $\dot{Q}$  are then attributed to conduction, convection and radiation across the boundaries, as well as internally generated heat. Additionally, the equation terms can be regroup using the enthalpy of the fluid, which is defined as  $H = U + pV$ , and therefore the specific enthalpy  $h = H/m$ . For the flow network formulation, this means that the net energy flow from a given node must equate to zero. Thus, the total energy leaving a node is equal to the total energy coming into the node from neighbouring nodes plus any external heat and power sources. (3.3.7) presents the energy governing equation for a control volume in the flow network formulation. Energy conservation is applied to each



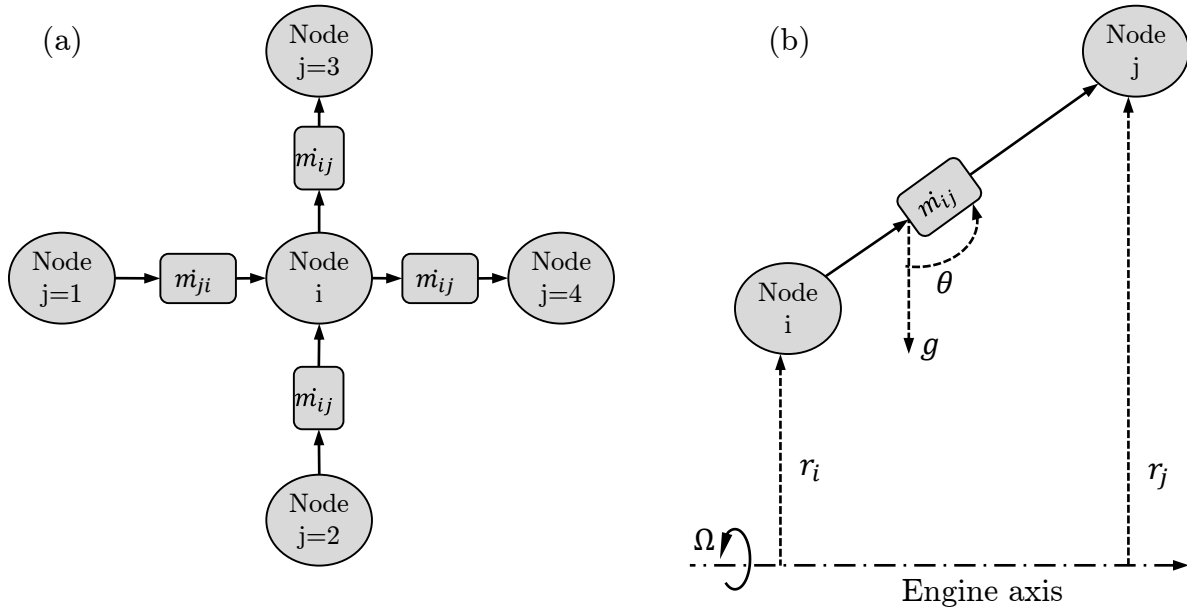


Figure 3.3.2.: Diagram of 1D flow network nodes and flow links arrangement (a), with typical relative position to engine axis (b).

node, and  $n$  is the total number of flow links connected with node  $i$ . The *MAX* operator in (3.3.7) is known as an upwind differencing scheme, which allows the transport of energy only from upstream neighbours, even when the flow direction is an unknown.

$$\dot{Q} + \dot{W} = \frac{\partial}{\partial t} \int_V \rho \left( \frac{U}{m} + \frac{\bar{v}^2}{2} + gh \right) dV + \int_A \rho (\bar{v} \cdot \bar{n}) \left( \frac{U}{m} + \frac{\bar{v}^2}{2} + gh \right) dA \quad (3.3.5)$$

$$\dot{W} = - \int_V \rho \bar{X} \cdot \bar{v} dV - \int_A p (\bar{v} \cdot \bar{n}) dA - \int_A \bar{v} \cdot (\hat{\tau} \cdot \bar{n}) dA \quad (3.3.6)$$

$$\sum_{j=1}^n \left\{ MAX [-\dot{m}_{ij}, 0] h_j - MAX [\dot{m}_{ij}, 0] h_i + \frac{MAX [-\dot{m}_{ij}, 0]}{|\dot{m}_{ij}|} [(p_i - p_j) + K_{ij} \dot{m}_{ij}^2] A_{ij} u_{ij} \right\} + \dot{Q}_i = 0 \quad (3.3.7)$$

## Solver algorithm

A combination of a successive substitution method and the Newton-Raphson method is used to solve the flow network set of equations. The successive substitution method is based on successive correction iterations to the variables until the errors in the conservation laws are minimised. The Newton-Raphson method is a numerical technique that solves the system of equations simultaneously. The mass and momentum conservation equations are solved by the Newton-Raphson method. The energy and constituents (case of multi-fluids) conservation equations are solved by the successive substitution method. In this way, the equations which are more strongly coupled are solved by the Newton-Raphson method, which has a significantly faster convergence rate but requires additional computing memory.

## Initial values

A set of initial values to start the calculation needs to be estimated by the algorithm or given by the user. The algorithm estimate begins by applying ambient temperatures to all internal nodes. The unknown pressures are then estimated by using the Laplacian law of repartition. This algorithm uses the pressure boundary conditions to assign the average of the total pressure values of the adjacent nodes to a given node. Once pressures and temperatures are fixed, an estimate for mass flow rates is computed using the momentum equation. With the guessed unknown variables, the residuals corresponding to each of the conservation equations are computed (mass, energy and momentum equations), which sets the start of the iterative process.

## Convergence criteria

With each solution iteration, the set of equations is locally linearised and solved using the Newton-Raphson method. Two basic conditions are checked at each step:

1. the largest residual of the nodal values at a given iteration  $k$  is less than the largest correction at iterations  $k - 1$  and  $k - 2$ .
2. the largest residual at iteration  $k$  is less than the prescribed convergence value.

These two conditions need to be fulfilled in order to ensure that convergence cannot be accidentally reached if there are significant residual oscillations between consecutive iterations.

### 3.3.2. Flow network elements

The creation of the flow network requires the user to follow a physical abstraction process, where the SAS design features are reduced to categories of flow elements. The process starts by setting the nodes of the flow network and then applying appropriate thermodynamic bits to the flow links, which represent energy and momentum addition terms. Following is a description of the most common elements that are needed to build the turbine flow network.

The basic flow network node types include: **boundary, internal and velocity nodes**. Boundary nodes represent the interface of the model with the not-modelled environment. These nodes can either be set as sink or source, providing state information of pressure and temperature. The internal nodes are the most common nodes in the flow network, representing the internal states of the fluid. Finally, the velocity nodes are internal nodes that allow for changes in the frame of reference. These latter nodes are used in combination with the change-of-reference elements to switch between rotating and stationary reference modelling.

#### Flow elements

Flow elements are characterised by a pressure loss coefficient and a flow equation. As already mentioned in Section 2.3, loss coefficients can be determined either experimentally or via CFD simulation. This data is loaded into the flow network program in the form of tables or diagrams that are usually company proprietary data.

**Orifices** are used as flow regulating devices or for pressure adjustment means. They are modelled with a discharge coefficient  $c_d$ , which is the ratio of actual-to-ideal mass flow. Their constitutive equation relates the mass flow to the pressure drop across the orifice, given by (3.3.8).

$$\frac{\dot{m} \cdot \sqrt{T_{in}}}{c_d \cdot A \cdot p_{in}} = \sqrt{\frac{2\gamma}{\gamma - 1} \cdot \frac{1}{R} \left(\frac{p_{out}}{p_{in}}\right)^{2/\gamma} \left(1 - \left(\frac{p_{out}}{p_{in}}\right)^{\gamma-1/\gamma}\right)} \quad (3.3.8)$$

The **labyrinth seal** flow element approximates the seal as a series of orifices, with a dynamic pressure loss after each fin. This effect is summarized in the carry over factor (COF). The  $c_d$  value for the seal constitutive equation, (3.3.9), depends on different parameters such as: presence of honeycomb and its characteristics, height and width of the fins, shape of the fin

tip, size of the steps, gap between the fin and the honey comb step, and the influence of the Reynolds number.

$$\frac{\dot{m} \cdot \sqrt{T_{in}}}{c_d \cdot A \cdot p_{in}} = COF \cdot \sqrt{\frac{1 - \left(\frac{p_{out}}{p_{in}}\right)^2}{R \cdot \left(n - \ln\left(\frac{p_{out}}{p_{in}}\right)\right)}} \quad (3.3.9)$$

For complex flow elements it is best practice to use experimental measurements or CFD results. Such elements are modelled with a **flow-characteristic**, which provides the pressure losses and mass flow constitutive law of a given element depending on its geometric and operational parameters. The flow-characteristic is employed for complex SAS devices such as pre-swirl nozzles or blade cooling channels.

## Cavities

The flow in SAS cavities is the result of a complex interaction of flow characteristics. In the 1D flow network, they are usually modelled as a combination of simpler thermodynamic effects, such as dynamic head loss, vortex, and change of reference.

**Dynamic head loss** elements model the total pressure losses by a fixed pressure loss coefficient, as fraction of the dynamic head. These elements are used to represent pipe inlets and outlets, sudden restrictions and enlargements, and junctions or bifurcations.

The swirling flows that occur in rotor-stator cavities are modelled with **vortex** elements, which condense the 3D flow field effects into a momentum and power term input into the flow network between two nodes. As a simplistic vortex element, free or forced vortices can be chosen. Forced vortices are characterised by their tangential velocity being proportional to the rotor speed  $u_\varphi = \beta \cdot \Omega r$ . On the other hand, free vortices are usually the result of upstream swirl, such as pre-swirl nozzles, and their tangential velocity is best represented by  $u_\varphi = K/r$ .

Another common cavity element is the **change-of-reference**, which models the transition from the absolute frame of reference to the rotating frame and vice versa. Since the change is performed over an element, the two adjacent nodes of the element are in two different frames of reference.

## 3.4. Thermal FE-Modelling

An introduction to the state of the art and purpose of thermal analysis with the finite element (FE) method has been presented in chapter 2.4. For the research undertaken in this work, the Rolls-Royce in-house FE tool SC03, EDMUNDS (1993), has been used. This section describes the necessary inputs to construct a thermal FE-model, how a solution is obtained, and the type of output data that results from the analysis.

### Creation of the thermal FE-model

To create a thermal FE-model of an engine component, the inputs from several engineering departments are needed as a pre-requisite. The process requires to gather the component's design, performance, air system and material data. Additionally, the thermal engineer follows a process of abstraction of physical principles, where the flow field and heat transfer mechanisms around the component are reduced to thermal boundary conditions.

The **geometry** of the thermal model represents the solid contour of the component to be modelled. The thermal boundary conditions will be assigned to the geometry curves and faces, and the solid material information to the internal geometry domains. The geometry for thermal FE-analysis may be 2D or 3D. This work concentrates on thermal analysis with 2D engine axisymmetric geometries, since 2D thermal models are currently the standard for assessments in the preliminary design phase. A summary of CAD modelling best practices has been presented in chapter 3.1.1. There, the importance of systematic geometry tagging was pointed out, which will be used in the thermal modelling for the association of thermal boundary conditions to model curves.

The thermal FE-model geometry is modulated in **domains**. Each domain definition is an area of the model with distinct solid properties. Usually, domains represent different parts and features of a component. The set of domain properties contains:

- Domain identifier name, used in the program code to associate properties to the domain.
- Material properties, which include information such as Young modulus  $E$ , Poisson ratio  $\nu$ , coefficient of thermal expansion  $\alpha$  and the thermal conductivity  $k$ .
- Rotational speed, defining also whether the component is rotating or static.

- Domain symmetry type, which can be 3D, axisymmetric, plane stress or plane strain. Even 2D models contain non-axisymmetric domains, which represent purely 3D features such as bolts or holes.
- Thickness properties, used only for plane stress or strain domains.
- Thermal loads, used to apply prescribed temperature fields.
- Structural loads, used to apply prescribed mechanical loading of the component.

Additionally, the engine cycle and fluid environment description needs to be loaded in the model. The definition of the **cycle performance data** is the start of the process to set up the fluid boundary data in the thermal model. The performance input to the model comprises the pressures, temperatures, and mass flows at engine stations, plus the operating speeds of the thermodynamic engine cycle. This data is loaded together with an **engine cycle definition**, which in turn defines the time steps and conditions for the analysis of the model. The cycle definition might be a simple time-marching operation between two stabilised conditions (e.g. idle and high power operation) or a complex flight profile suited for component life prediction (e.g. idle, taxi-way, take-off, climb, cruise, approach and landing).

Another necessary set of inputs relating the thermal model to the fluid environment is the **secondary air system data**. Again, this data set needs to be associated to the cycle time steps. It includes the results of the SAS flow network model, and it provides the main cavity pressures, mass flows, and initial temperatures for the boundary conditions of the model. However, it should be noted that the SAS flow description is rather macroscopic, and the thermal designer still needs to determine how to distribute the flows at the local level.

Also cycle dependent, the set of **oil data** is of particular importance for the modelling of bearing chambers. And another set of cycle inputs includes the **aerodynamic loads** from the main annulus blades and vanes. The aerodynamic loads are necessary to determine model displacements, but are not needed for the computation of temperatures.

Once the previous inputs to the thermal design are available, **thermal boundary conditions** have to be applied to the model to be able to simulate the local flow field around the solid parts. Each of these contains a set of properties that describe the flow field in order to compute heat transfer between solid and fluid boundaries. The definition of a thermal boundary condition includes: boundary condition type, mass flow, inlet temperature, inlet pressure, heat pick up,

heat transfer correlation and swirl velocity. Further detail on thermal boundary condition types and their inputs is presented in the appendix Section A.1.

Figure 3.4.1 on page 63 shows a thermal FE-model of a rotor-stator cavity in a typical HPT disc. The lines along the edges of the solid geometry characterise different boundary condition types like streams, ducts and voids.

### Thermal analysis solver

In order to obtain the temperature distribution within the solid, a system of partial differential equations needs to be solved through a time marching steady-state calculation. The finite element method is the basis for solving the thermal model. This method consists on discretizing the solution domain into many small and interconnected elements, which leads to a piece-wise approximation of the governing equations. Thus, the finite element procedure reduces the continuum problem to one with a finite number of unknowns at specified points referred to as FE-nodes. A description of the fundamentals of FE-analysis can be found on RIEG et. al. (2012).

The governing equation to solve the thermal problem in the FE-model is the heat diffusion equation solved at the solids, (3.4.1). Depending on the type of thermal boundary condition, diffusion is solved with either Dirichlet,  $T = T_0$ , or Newmann-like boundary conditions,  $-(k\nabla T) \cdot \bar{n} = q_0$ , at the boundaries.

$$\rho \cdot c_s \frac{\partial T}{\partial t} = \nabla \cdot (k\nabla T) + \dot{Q} \quad (3.4.1)$$

Heat diffusion in the FE-problem is weakly non-linear, since the material properties have a non-linear dependency with the temperature, and the boundary conditions usually include sophisticated correlations of the Nusselt number, which intrinsically depends on  $T$ .

The FE-solver proceeds to solve the equations at the nodes with a temporal discretization, which can be implicit or explicit. At each time step iteration, the material properties, which are temperature dependant, are frozen from the previous step. Additionally, the non-linear boundary condition coefficients, such as in convecting or radiating walls, are linearised by calculating them with the temperatures of the last step. Convective boundary conditions are solved with Newton's law of cooling, (3.4.2), and radiating heat flux is calculated based on the

thermal power emitted by a perfect diffuse radiating grey boundary, (3.4.3).

$$\dot{Q}_0 = A \cdot h \cdot (T_\infty - T_0) \quad (3.4.2)$$

$$\dot{Q} = A \cdot \epsilon \cdot \sigma_B \cdot T_0^4 \quad (3.4.3)$$

### Results of the thermal FE-model

The results of a thermal analysis applied to an engine component over a time cycle are the fields of temperature and displacements at each FE-node. The temperatures are used to assess material integrity and lifing the components, in combination with the structural analysis to determine the distribution of mechanical stresses and strains. The model node displacements are useful to determine running part interfaces and rotor-stator gaps. Furthermore, the thermal gradients are used to better adequate the loading of the component and the heat flux information is fed-back to the SAS model for better assessment of the condition of the SAS flows when they are returned to the main annulus.

#### 3.4.1. Example of turbine rotor-stator cavity thermal model

As a practical application example, a thermal model of a typical turbine rotor-stator system is shown in Figure 3.4.1 on page 63.

The 2D geometry of the example model represents the front features of a HP turbine disc with the static structures around it. The disc is build from a disc body, front and rear drive arms with bolted joints, and two front labyrinth seal arms. Additionally, the disc includes a cooling air hole that guides the fluid to the blade cooling channels. The static structure encloses the cavities in front of the disc, leading to a rotor-stator fluid system. In this application, the static structure holds the honeycomb features associated to the labyrinth seals, and a pre-swirl nozzle that accommodates the air coming into the cavity where the cooling air hole is located.

The 2D solid geometry is broken down into domains. The disc domains are defined as rotating, with rotational speed  $\Omega = NH$ , and the static domains are assigned no speed ( $\Omega = 0$ ). Most



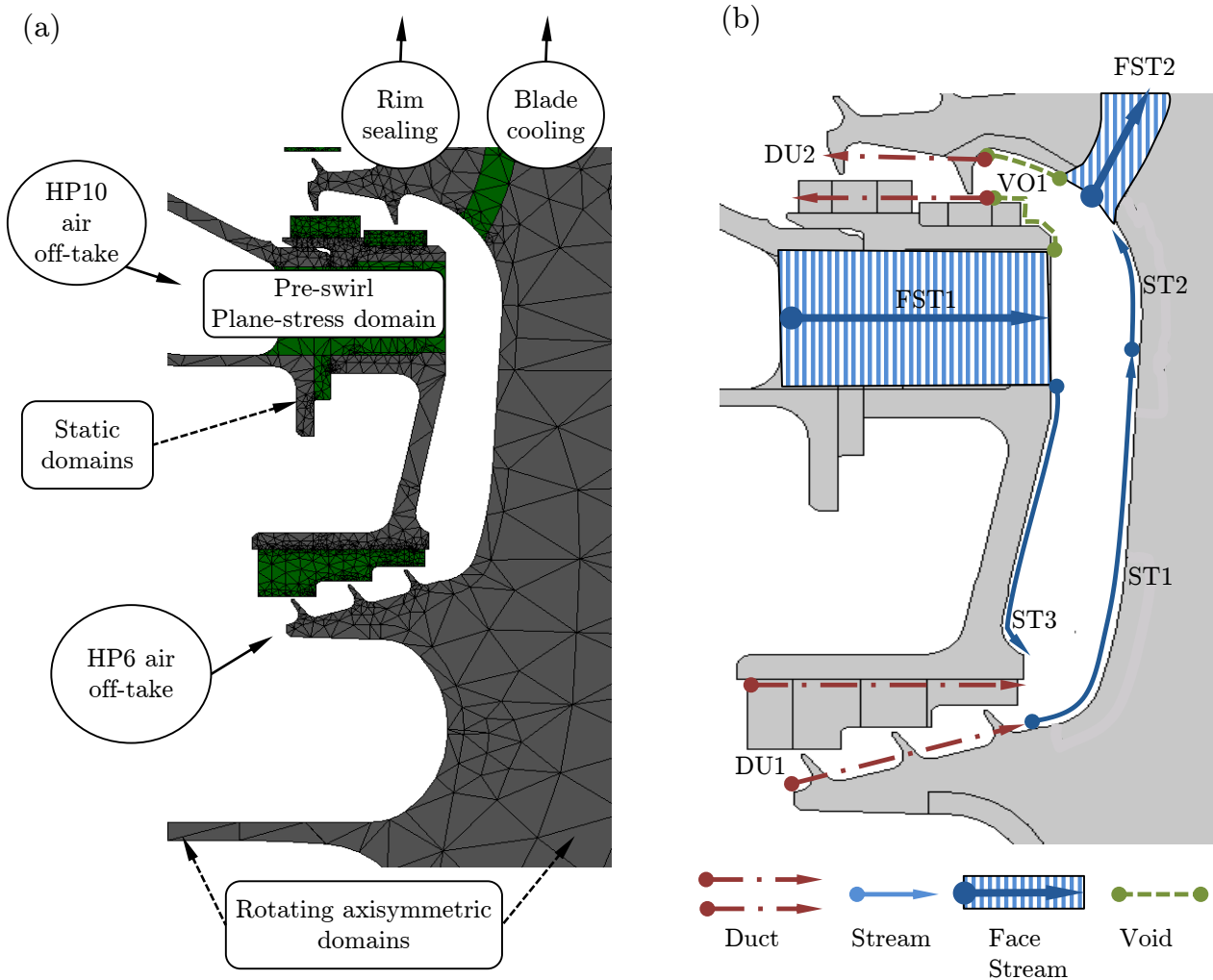


Figure 3.4.1.: Thermal FE-model of a typical HPT disc and front static structure. (a) Definition of 2D geometry, domains and FE-mesh; and (b) diagram of thermal boundary conditions representing the flow field around the FE-model.

of the domains are set with kinematic definition “axisymmetric”, except for the cooling air holes, seal honeycombs, and pre-swirl nozzles, which are set as “plane stress”. The plane stress domains are assigned a user defined thickness property, which is lower than  $2\pi r$ .

In order to perform the FE discretization of the 2D domains, the mesh generation functionality of the FE-tool (SC03) is used. It should be noted that the number of discretization elements needed for thermal analysis is less than for structural analysis. The very fine meshes usually employed for mechanical analysis are not necessary for an accurate resolution of the heat diffusion equation in the solid (3.4.1).

To complete the set of inputs, the performance and SAS data is loaded in the model as a table deck. The performance input includes the spool rotational speeds and the total pressures and temperatures at the main engine stations. The SAS input includes the mass flows from the compressor off-takes flowing into the turbine main annulus, total pressures at the cavities, and the temperatures of the compressor flows that are inlets into this turbine sub-system. Both, the performance and SAS data are cycle dependent, and they are associated to a set of time and operating conditions. In the example shown in Figure 3.4.2 on page 67, the operating cycle consists of an acceleration in 20 s between ambient still condition and a high power condition, followed by stabilisation at the high power condition.

With the previous inputs, it is the task of the thermal designer to model the local flow field effects around the solid parts. Due to the pressure difference specified by the SAS design, the air tends to flow from the inner to the outer cavities. With typical rotational speeds of round  $NH = 1200$  rad/s, radii of the order of 100 to 200 mm, and cavity widths larger than 5mm, the  $Re_\varphi$  is well into the turbulent flow zone. Thus the rotor-stator cavities operate in flow regime IV, see Figure 3.2.3 on page 47. The superposed mass flow in the cavities is provided by the SAS input, which in this case is less than the pumping mass flow that the disc manages to impulse radially outwards. There is therefore flow recirculation in the radial rotor-stator cavities, as depicted in Figure 3.4.1 on page 63.

A categorisation of thermal boundary conditions can be found in the appendix Section A.1. In this example, thermal streams are used as boundary conditions to model the heat transfer of the flows around the disc and static structures in the cavities. Thermal voids are used for small air pockets forming where there is a quick air recirculation mixing zone. Additionally, ducts are used for narrow channels, such as in seals and air holes. Figure 3.4.1 on page 63 shows the location of thermal boundary conditions in the model. For each thermal boundary condition, a set of thermal inputs is specified. The work of BERTHOLD (2012) contains a summary of the inputs that are needed for the thermal boundary conditions and it provides an understanding of the influence of each thermal input on the temperature distribution of a typical turbine rotor-stator cavity.

The results of the thermal analysis include the model prediction of the solid temperature distribution, fluid temperatures along the boundaries, heat fluxes, and the distribution of the heat transfer coefficient. A typical thermal output of solid temperature contours for the HP turbine

example is shown in Figure 3.4.2 on page 67. Additionally, the thermal model provides information on the transient development of temperatures with cycle time, which is of particular importance for the prediction of thermal gradients and their influence on induced stresses.

Focusing on the shown thermal result, both the solid and fluid temperatures increase rapidly during the acceleration phase. During this phase, the thermal boundary condition inputs (e.g. the heat transfer coefficient HTC) change with every time step as a result of their dependency to the operation parameters (e.g. NH). The temperatures however keep on rising, even when the operation parameters are frozen at high power condition. This is due to the diffusion of heat in the solid, which requires a time lag until the heat transfer effects stabilise. Given that the thermal capacity of the solid is much higher than the fluid, the fluid temperatures stabilise quicker than the solid ones. This in turn leads to transient temperature gradients, which need to be accounted for in the lifing methodology of the component.

### 3.4.2. Extraction of CFD Data for Thermal FE-Modelling

As already described in chapter 2.4, CFD methods can be used to provide a more accurate understanding of the flow field in SAS cavities. The thermal modelling data that can be extracted from CFD includes: stream directions, modelling of flow recirculation, local mass flow distribution, swirl number, heat transfer coefficients, and heat pick up due to windage effects. This data can then be used to improve the fidelity of thermal inputs, as well as to better define the orientation and type of boundary conditions (e.g. a new recirculation zone might be considered).

The CFD models can either be used as information means to improve the way thermal boundary conditions are created, or as a module of the thermal model whenever coupled CFD-thermal analysis is employed. Either way, an interface between the CFD and the thermal model needs to be specified. In this work, the automated thermal modelling process is equipped with the capability to use CFD-enhanced thermal boundary conditions, but due to research time limitations CFD-thermal coupling has not been considered within the scope of the work.

#### Interpretation of CFD results

The first step to introduce CFD data into a thermal model is to split the flow field into smaller

parts. This can be attempted based on the knowledge of the flow structure simulated with the CFD model. The next step is to go through all of the zones and to extract the mass flow distribution and the swirl numbers, which fix the flow field in the thermal model. Finally, the windage heating  $HPU$  and the  $HTC$  distribution from the CFD model are translated into correlations that can be applied to the thermal model. This process is described in detail in the appendix Section A.3.

### **Cycle scaling of thermal boundary conditions**

A set of thermal data extracted from a CFD model for a given design operating condition needs a cycle operation scaling rule to be used in thermal transient prediction. It is common to have CFD data available for a single operating point, and the thermal model being used to analyse full complex time cycles, such as engine flight cycles. The methods and effects of scaling the CFD extracted thermal input data to other engine conditions are discussed in the appendix Section A.4. In order to evaluate the validity of scaling the CFD extracted data, it is necessary to assess the changes in the flow field with at least another operating condition. Thus, CFD results should be made available for the design operating point and at least one other operating point, such as an idle condition. In case that the flow field significantly changes between operating conditions, simple scaling equations may not be valid. For these cases, coupled CFD-thermal analysis could provide an adequate level of accuracy.

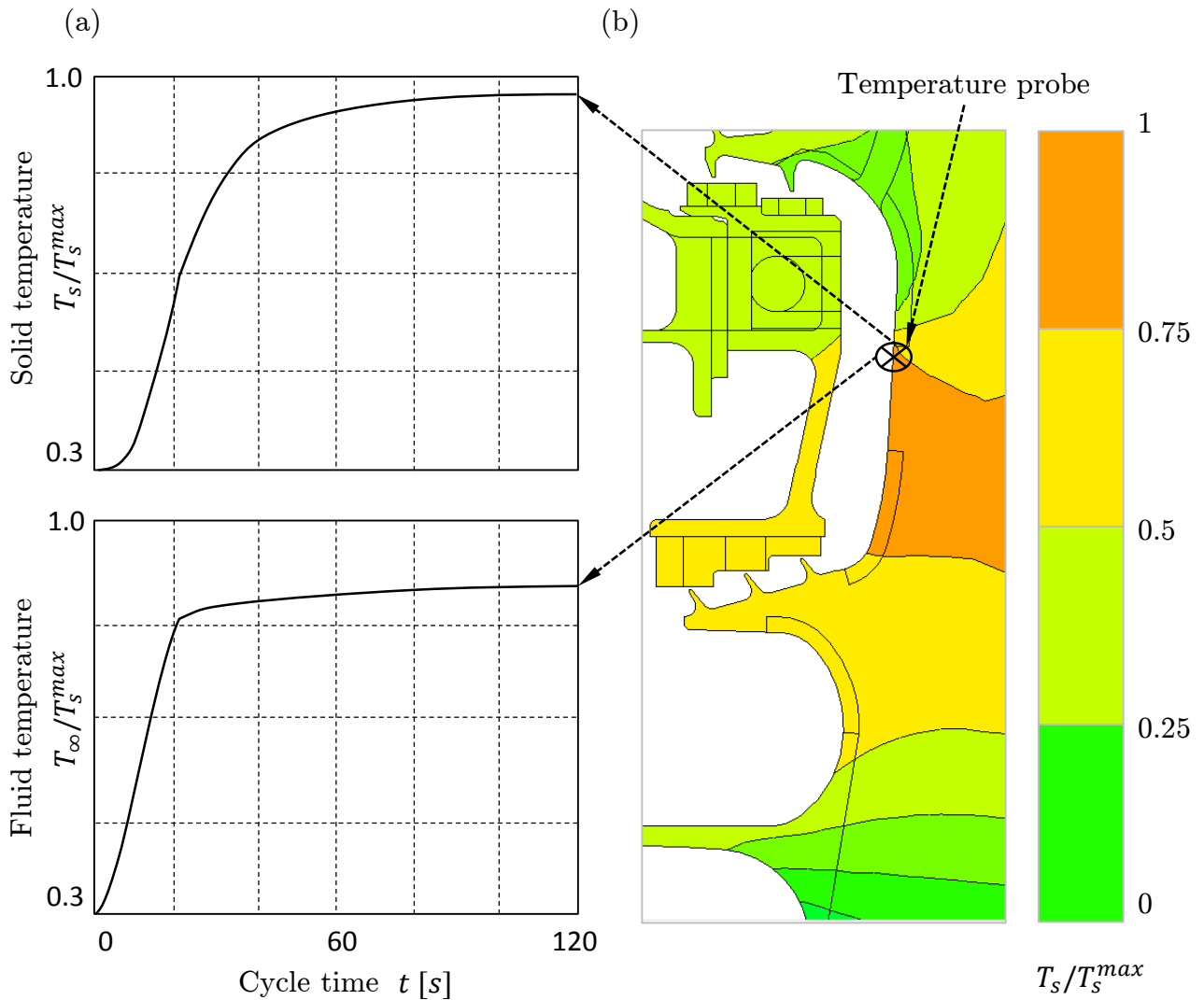


Figure 3.4.2.: Thermal results of a typical HPT front cavity over an operating cycle with acceleration in 20s from ambient still condition to high power condition, followed by stabilisation at the high power condition: (a) transient normalised solid and fluid temperature at a virtual probe point vs. time; and (b) thermal FE-model temperature distribution at the stabilised high power operating condition.

---

# 4

## Advanced Turbine Design Environment and Automated Work-flow

---

The methods developed in this work facilitate an automated SAS and turbine discs preliminary design process implemented in a common design environment. Furthermore, the process of design and model generation should be accelerated via automation of the engineering work-flow. Since the full process is rather complex, the proposed work-flow follows a modular approach, while keeping all disciplines integrated into a single framework. The automated process has been arranged in three main modules:

1. A common design environment, where the design definition and requirements are captured in a programming data-model.
2. A chain of automated processes that can be applied to the data-model to produce the design outputs.
3. A database to gather modelling instructions, which is readily expandable by the engineering departments of each discipline.

This chapter describes the functions of this suite of modules and how they achieve the automation goals. The Rolls-Royce in-house developed preliminary design platform SMART has been taken as a basis to implement the automated processes developed in this work. The SMART platform already contains a design environment for the turbine main annulus. As an extension

to SMART, the array of processes developed within this work have been called the “Component System Integration” (CSI). The engineering work-flows within the CSI framework automate the design of engine components and their integration in simulation environments of the air system (i.e. generation of SAS and thermal models).

This chapter begins presenting the common design environment, with focus on the design of the turbine discs components and the SAS architecture. Next, the automated work-flow to generate the design simulation models is outlined. Then, each of the individual work-flow modules is described in detail. The basis for engine component simulation is the geometry, and thus the automated work-flow for generation of CAD models is described first. Thereafter, the automated processes to generate SAS flow network models and thermal FE-models are explained. Finally, the chapter describes how a database of standardised modelling practices fills in the engineering knowledge within the automated simulation environment.

## 4.1. Common Design Environment

The initial step in the virtual design environment is to capture the design definition from the engineering user in a programmable language. The implementation details of this environment, developed in Java, are further described in Chapter 5. The design data model is saved in a data tree structure containing the engine component features. Each feature contains a list of design parameters, design rules, associated analysis output, and other properties needed in the processes to be performed. Additionally, design features can be associated with one another and can contain sub-features. This feature object-oriented approach can gather the design parameters and requirements in a directly programmable context. The advantage of such a programmable design platform is that it allows design changes to be automatically propagated throughout the design data tree. Furthermore, this approach allows the design features and turbine architecture to be manipulated automatically via programming code.

A Graphical User Interface (GUI) is used to gather the design definition in the data-model. It should be noted that the data-model contains the design details, but it has no processing functionality. To that respect, the processing algorithms in the common design environment are separate functions, which are applied to the data model to perform operations with the design

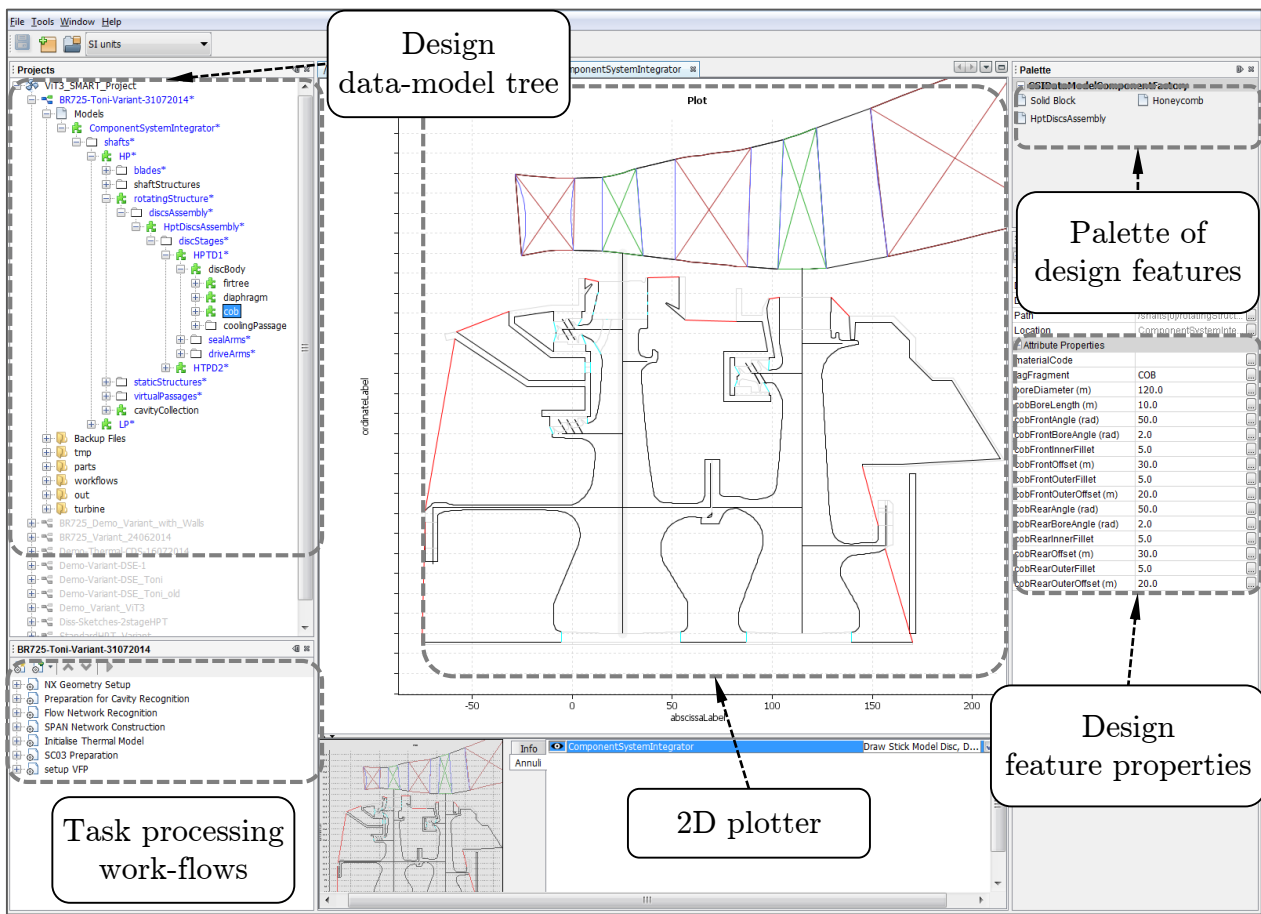


Figure 4.1.1.: GUI arrangement of the CSI common design environment. This platform arrangement shows fields for the engineering user definition of the design data-model in a data tree and 2D sketch plotter format. The arrangement also shows windows for the selection of design features (palette), overview of feature properties, and setting of task work-flows to be applied on the design.

data. Such algorithms can be used for calculating further design parameters or for executing the tasks to generate simulation models. Figure 4.1.1 on page 70 shows a GUI arrangement of the CSI design environment. The data-model definition is supported by a 2D sketch plotter representation. Therein, the design of discs and SAS features can be integrated with the turbine main annulus definition.

Each engine component feature available in the environment contains a programming data package, which is loaded as a plug-in in a NetBeans module (NBM)<sup>1</sup>. The NBM of a design

<sup>1</sup>A NetBeans module is a group of Java classes that provides an application with a specific feature.



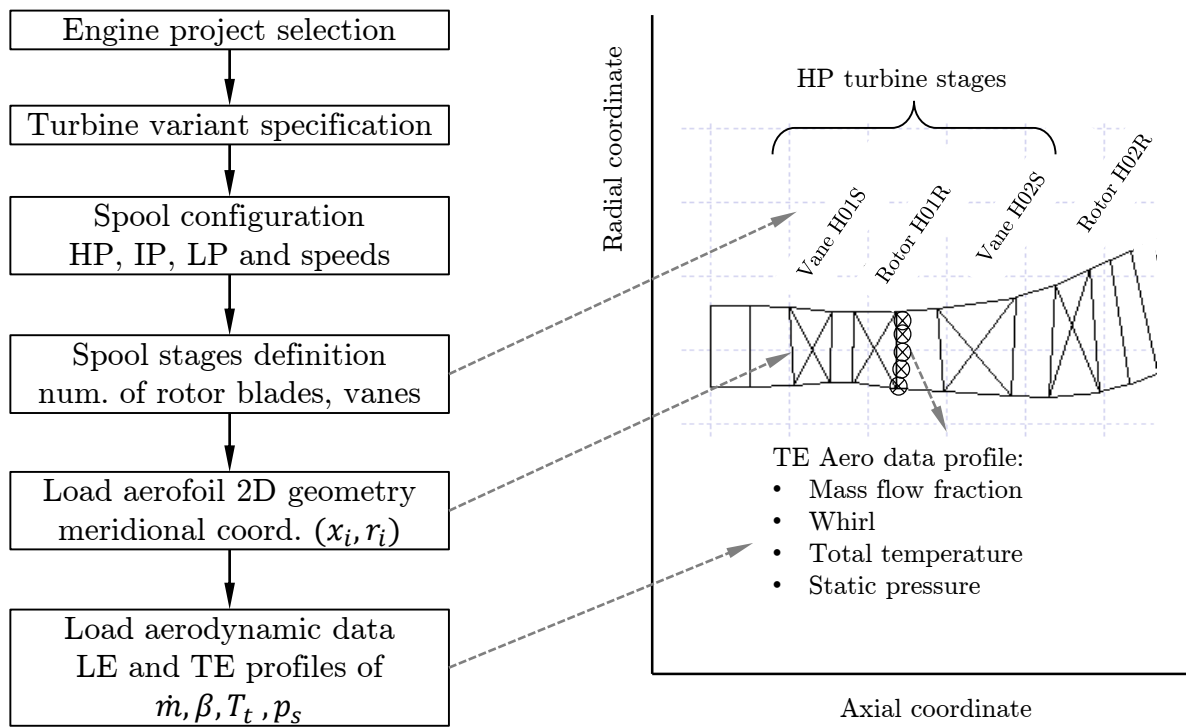


Figure 4.1.2.: Process of CSI project setup and main annulus data definition.

feature includes the instructions to construct its CAD model and to integrate it in the SAS and thermal FE-models. The rest of this section describes the process intended for the CSI designer to follow in order to construct the turbine discs and SAS design data model.

### Main annulus design definition

The turbine main annulus design data is a prerequisite to the turbine discs and SAS design process. The requirements for engine performance and aerodynamic design data for the main annulus have been explained in chapter 3.1.2.

The CSI data-model is prepared to capture a simplistic design definition of the main annulus geometry and aerodynamic data. This simplistic **main annulus model**, together with the **engine performance deck**, constitute the input data to design and model the SAS flows. The turbine radii and the axial positions of aerofoil stages are an envelop to the design of the SAS and disc features. In the CSI platform, the main annulus data can be manually implemented (via GUI) or automatically loaded from an existing turbine aerodynamics model.

The process steps for the CSI main annulus data definition are illustrated in Figure 4.1.2 on page 71.

### **Discs design definition**

Once the turbine blade stages have been defined, the disc design is accommodated to drive the turbine power to the compressor and fan components. The fundamentals of the disc design process have been explained in chapter 3.1.1.

The initial step in the CSI disc design process is the selection of a **disc-assembly** architecture. Disc-assembly templates are available or can be implemented in the engine geometries database. These assemblies are usually spool dependent and each of them has partial flexibility of automatic geometry manipulation. A disc-assembly template can be inserted into the data-model via the GUI drag-and-drop functionality. Each disc assembly template is loaded as a NBM module that includes the association and interface of design features to a parametric CAD model. Thus, the user selection of a specific disc-assembly automatically links it to a parametric CAD geometry. The details of what the **component NBM plug-ins** contain are further explained in chapter Section 4.3.

The process steps for the CSI disc-assembly sub-features definition are illustrated in Figure 4.1.3 on page 73. The system automatically recognises the number of disc stages needed, depending on the previously defined blade rotor stages. For special cases, the user can override the automatic disc stages setting and add or remove discs. The **disc body** parameters are automatically loaded with the user selection of a disc architecture template. The system populates a default set of parameter values, which can then be modified by the user or an automated algorithm. If a different set of parameters would be required, another disc-assembly plug-in should be loaded, either a complete new NBM disc-assembly template or a modification of an existing one. The next step is the definition of the **disc power transmission**, which involves the user selection of number and style of drive arms in the data model. For each drive arm, a joint type can be chosen (e.g. bolted, welded, or splined), as well as its orientation with respect to engine axis.

At this stage, each sub-feature of the disc-assembly has been automatically set with a tag-fragment, which fits its associated CAD model tagging convention. This feature tag-fragment

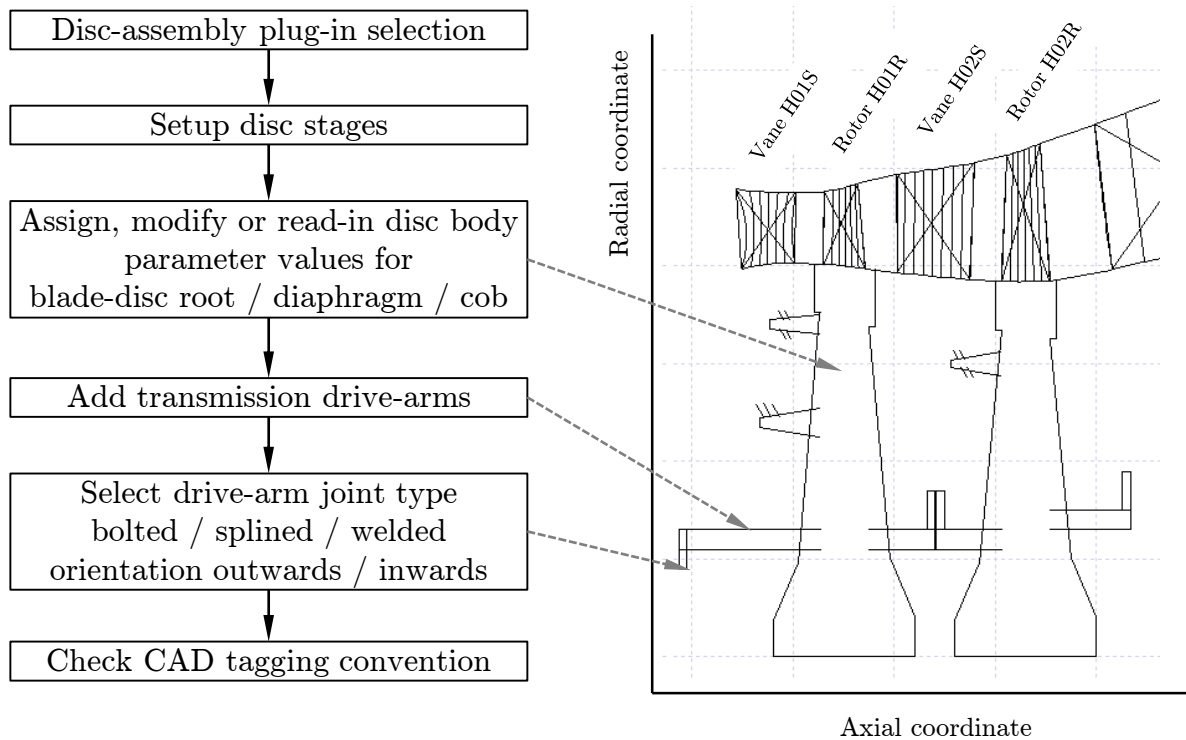


Figure 4.1.3.: Process of CSI disc-assembly data definition.

enables the mapping of geometry curves between the feature in Java and its mirror geometry in the CAD model. The tag-fragment default setting for each feature can also be overridden by the user for special CAD handling tasks.

### SAS design definition

The geometry of the main annulus blade rows and the discs assemblies sets the initial envelop to the construction of a SAS architecture. In this context, the design process to select a SAS concept has been explained in chapter 3.1.2. It is supposed from here on that the choice of SAS compressor off-takes and turbine flow sink requirements has been fixed. This pre-selection might be a user choice or an automated setting from a parametric algorithm, such as for example an iteration of a design optimisation.

The approach in the CSI common design environment is to select directly SAS manufacturable features, which guide the flow in an intended pattern. This approach is somewhat different than the traditional SAS design process, where flow characteristics were first chosen to form a

SAS flow network. This step was then followed by the selection of geometry features that would lead to the chosen flow network. The CSI methodology automatically associates manufacturable features to flow-network model representations, thus enabling the SAS designer to focus on the technology selection.

In the CSI SAS construction process, the SAS features are added to the data-model either by direct insert or via a GUI feature-node dragging functionality. However, not only the SAS flow channels need to be inserted, but also the geometry of static structures leading to the system of rotor-stator cavities. The design functionality developed in this work provides a simplistic definition of turbine internal static structures. This level of static structure's modelling fidelity is sufficient for flow-network and thermal FE-model assessments in the preliminary design phase. It should be noted that the static structures definition in the overall engine design process depends on additional disciplines such as whole engine dynamics, bearing chamber design or oil system design.

The process steps for the CSI SAS features definition are illustrated in Figure 4.1.4 on page 75. First, a disc **feed system for blade cooling** is selected. Then an architecture for the stage front, rear and **interstage cooling** feeding arrangement is chosen. Following, the type of **rim sealing** features, number and location of **sealing arms**, and seal types is specified. Once the SAS concept around the disc-assembly has been fixed, the preliminary **static structure scenery** is defined with block modules. The SAS **flow orifices and pre-swirl nozzles** can then be added to the static blocks. As closing elements, **virtual boundaries** have to be introduced, to represent the boundaries of the modelled sub-system with the non-modelled environment. Also associated to the virtual boundaries, feature solid walls that are not to be considered have to be marked as **external walls**.

Ideally, a complete SAS design would include the definition of all engine components (compressors, combustor, turbines, casings), which would enclose the SAS without the need of a virtual boundary. In practice, it is desirable to be able to model sub-systems independently. Thus, the virtual boundary is used to enclose the fluid walls at the edges of the geometry features that have been left unconnected to a partner component (e.g. turbine disc drive arm left unconnected, due to compressor drum not being modelled). This type of boundary is linked to two geometry points, usually belonging to a static and a rotating geometry. The CSI code will then recognise that no cavities should be considered beyond these edges, and thus the flow

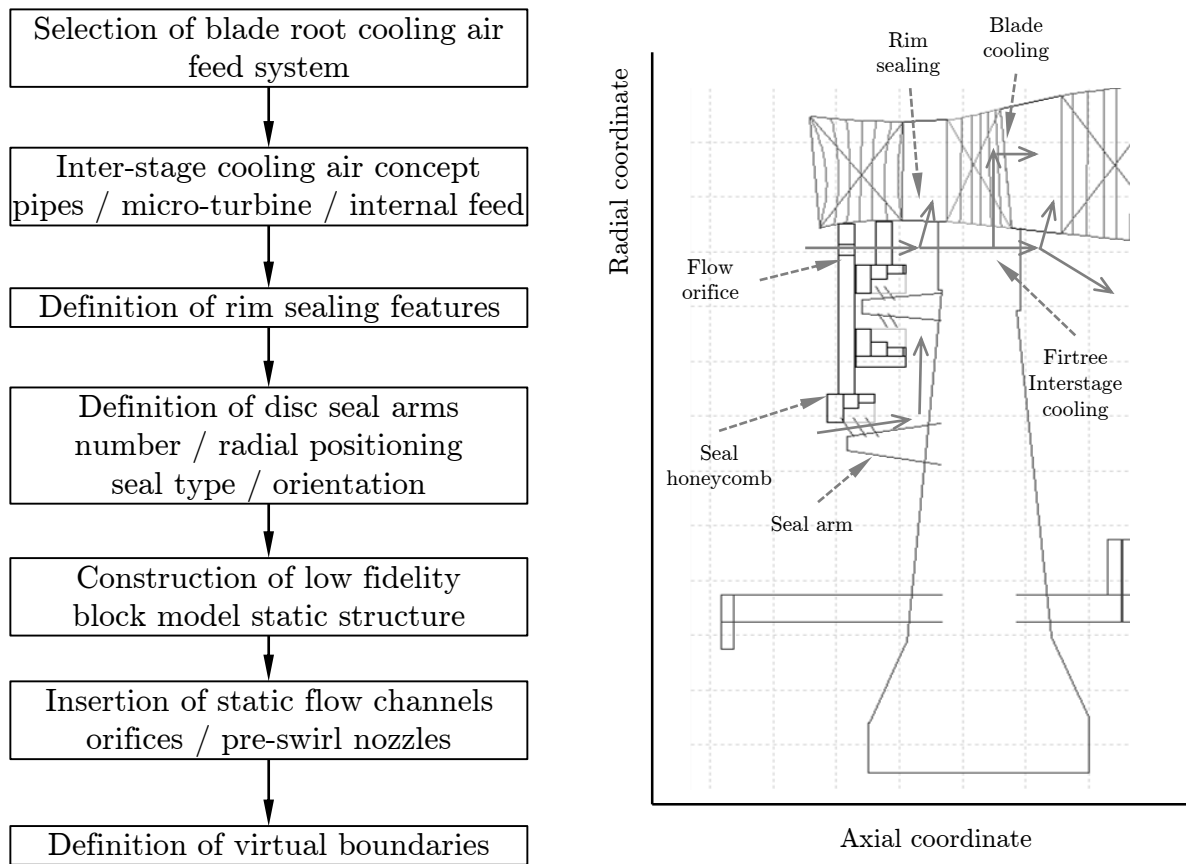


Figure 4.1.4.: Process of CSI SAS data definition.

network will end at this boundary. Moreover, the CSI user can select between several types of virtual boundaries: general boundary, compressor off-take, turbine rim boundary, blade cooling flow, bearing chamber flow, or turbine inter-stage sink.

When a SAS feature is loaded in the data tree, its class definition package carries the required interface code to generate its CAD geometry, to model its associated flow network elements, and to generate its FE-domain and thermal boundary conditions. Further details about the CAD model generation of the SAS features are specified in Section 4.3. A relevant distinction is made between features that belong to rotating disc-assemblies and to static structures. The interface between a feature class and the database of flow network modelling instructions is described in Section 4.4 and Section 4.5.

As a final step in the SAS design definition, an **intended flow orientation** for each flow channel must be selected by the user. For this purpose, the class of SAS flow channels, like

seals or holes, carries an inlet and an outlet fluid wall. The user specifies an initial setting of the fluid wall as inlet or outlet. This setting does not rule out a reverse flow, but it is required for the initialisation of the flow network. In order to aid the initialisation, the coordinates of these fluid walls are automatically calculated based on the geometry of their containing feature.

### **Parametric design connectivity**

Whenever a design modification is introduced, either by a parameter change or by a new feature being introduced, the rest of design features need to be adapted to fit the new geometry. The CSI element **feature-connection** has been introduced to enable the automated propagation of design variations across features. This element imposes a parametric linkage between two location points of different features or the same feature.

The feature-connection function constrains the location of a point in a feature to another point in the CSI design environment. Additionally, a gap parameter in radial and axial coordinate can be specified to keep the connected points at a fixed distance from each other. For example, the origin point of a static block can be connected to the end point of another static block. Likewise, the origin and end points of a single block can be connected with a gap, thus fixing the block length. In this manner, complex chains of connected structures can be build. The connection logic for a structure should be specified by the engineering user, depending on the design modifications that are to be evaluated. Whenever a parameter is modified, the system updates automatically the rest of parameters in the data model to satisfy the connectivities imposed.

As an example application of this functionality, it enables the automated adjustment of static structures when a disc sealing or drive arm radial position is modified. The variation of disc arm radii is common in the preliminary design phase to optimise bearing loads or cavity cooling arrangements. The CSI parametric design connectivity function triggers a chain of parameter modifications, which scales the features in the static structures that have been connected to the disc arms.

## 4.2. Automated Work-flow for SAS and Thermal Simulation

The parametric definition of the component and SAS design leads the way for the application of the automated simulation work-flow. The goal of the process is the generation of the FE-model, progressing through the CAD model generation, the SAS flow network model generation and processing of interface data.

### Starting point

The above described user definition of the subsystem design in the CSI common design environment constitutes the data model to run the automated processes. These prerequisites include:

- performance data,
- main annulus geometry,
- aerodynamic data,
- disc design definition,
- SAS configuration and design parameters.

### Work-flow

The application of automated processes onto the data model is usually performed in either single tasks, a tasks sequence, or a conditional loop of tasks. Each sequence contains a set of algorithms with a processing goal (e.g. producing the CAD model or working with the data model for the recognition of the flow network). The individual tasks can also be operated separately from the rest of the sequence, which adds flexibility at the time of re-using and porting the algorithms.

The **CAD model generation** sequence would typically be launched first, unless a fully prepared parametric CAD model of the design is already available. The CAD sequence starts with processing of the individual feature CAD models. This step involves manipulating the rotor models (discs with transmission and sealing arms) and generating the block models of the

static structures. Then, the individual models are combined in the subsystem model. This latter model goes thereafter through a post-processing algorithm that trims overlapping geometry lines and results in a clean subsystem CAD model fit for FE-analysis.

In order to automatically work out the interaction between fluid and solid boundaries, a **flow network recognition** algorithm has been developed. This algorithm resolves the network of cavities, flow channels, and their connections to one another. As previous steps to the flow network recognition, the CAD model curves are automatically collected in the CSI data model, and the fluid boundaries are initialised. The result of the flow network recognition sequence consists of the list of cavities in the subsystem, their inter-connectivity through flow passages, and the automatically assigned cavity types.

The process to generate a **SAS flow network model** requires the previously described network of cavities to be available in the data model. It is recommendable that the CSI user checks the specific settings of each SAS feature at this point. The automated SAS sequence constructs and exports the SAS 1D flow network model file, followed by solving of the model, and saving of a SAS output file.

The automated **thermal FE-model** process also requires a sequence of tasks. First, the SAS output data needs to be made available to the thermal data model. A thermal sub-model of each flow network feature (cavities and flow passages) is initialised based on a template-engine. Each thermal model contains a list of thermal boundary conditions. The user should check if the default initialisation needs some modification to fulfil the project requirements. Each thermal boundary condition automatically gets a dependency to the list of geometry curve tags where it will be located in the FE-model. Thereafter, the FE-model domains are automatically allocated. The list of domains and thermal boundary conditions are then exported to the FE-tool journal definition file (JNLF), and the FE-geometry file is exported from the CAD model, which still retains the CAD-tagging information. Finally, all input modules of the FE-model are assembled and the model is meshed. The thermal FE-model is at this stage ready to run. Figure 4.2.1 on page 80 presents a full overview of the CSI work-flow process.

## Outputs

After running the above described processes, the user can access various output data in the project folder. The automatically generated data includes:



- CAD models of the discs rotor assembly and integrated disc assembly with static structures scenery. These output CAD models are parametric and tagged.
- The SAS flow network model file and SAS results output file. Additionally, the flow network nodes and cavity types can be accessed in the CSI data model.
- The thermal FE-model base file, the JNLF file with the domains and thermal boundary conditions listing, and the cycle and performance BDD file. Finally, the results file of the FE-model is also made available in the project folder.

#### 4.2.1. Database of Modelling Instructions

The automatic construction of models relies on a database of SAS and thermal modelling instructions. Both, the flow network model and the thermal model of the subsystem, are assembled from smaller standardised feature models. The individual models are structured in categories, such as seals, holes, rotor-stator cavities, etc. In the CSI approach, a database of standardised flow network elements and thermal model templates is the basis for the automatic processes. The requirements that were set for developing the database of modelling instructions include:

- fast accessibility during run time.
- Easy expandability by discipline experts without programming background.
- Moderately compact storage of data.
- Global tracking and version monitoring capability.
- Ability to store modelling methods of different fidelity levels.

### 4.3. Geometry Model

A parametric and tagged CAD geometry model can be automatically generated with the CSI environment, once the user has defined the design data tree. The user selected features in the GUI are a visual representation of the NBM plug-ins containing the part definition and interface code to produce the CAD model. Therefore, the information to generate the CAD

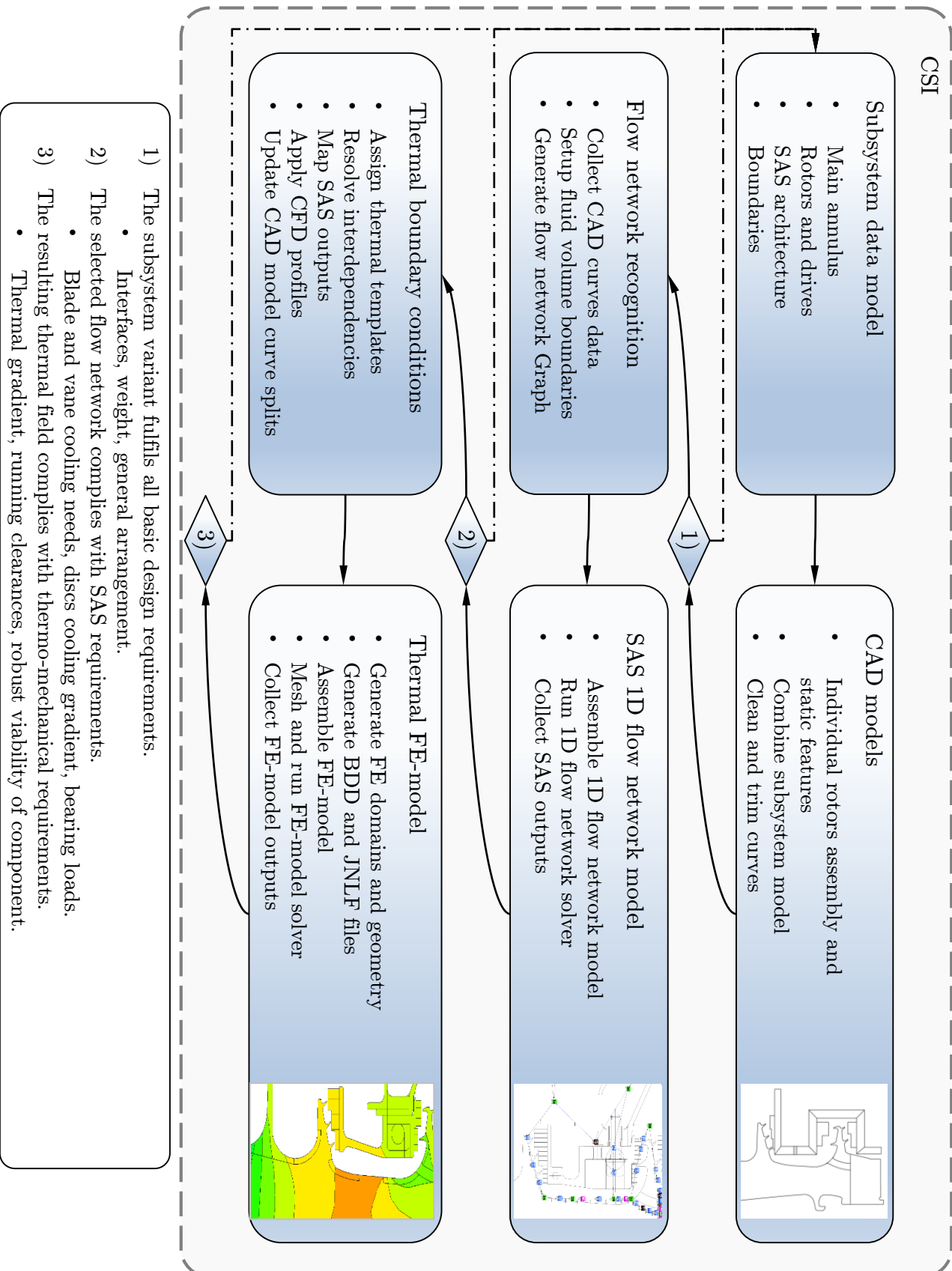


Figure 4.2.1.: Overview of CSI work-flow.

models is already made available to the system as the user adds features to the CSI data tree. Chapter Section 5.2 describes in further detail how the interface of the NBM plug-ins and CAD processing routines have been implemented.

### 4.3.1. Geometry generation sequence

The work-flow sequence to produce a CAD model ready for the subsequent flow network and FE-analysis is described in Table 4.1 on page 81. Firstly, the rotors parameter values are mapped from the CSI data tree to the CAD model of the disc assembly. Secondly, the CAD models of the individual static features are generated. Finally, the rotors and statics geometries are combined and automatically trimmed.

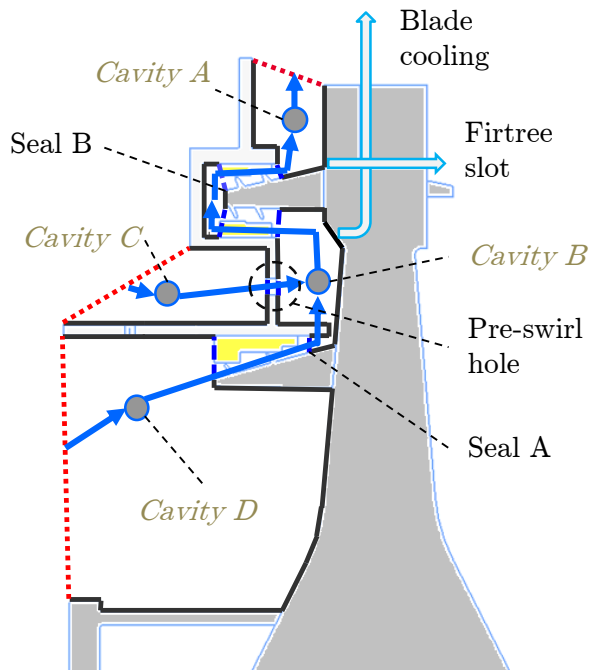
Table 4.1.: CAD geometry model generation work-flow sequence

Sequence	Task	Description
1	Update discs assembly model	Mapping of discs assembly parameter values from CSI to the CAD tool
2	Generate static structure models	Generation of block feature models from a template, followed by mapping of parameter values and curve tag names from CSI to the CAD tool
3	Combine rotor and static structure models	Importing individual static structure block models into the discs assembly model
4	Trim combined model	Cleaning of internal geometry lines for consistency in FE-analysis

## 4.4. Secondary Air System Model

Each SAS feature that the user has previously loaded in the CSI environment is an instance of a class, which carries the interface data to access its flow network modelling instructions. The flow parameters automatically get a default value, which can be modified by the user. Other flow network settings can also be adjusted, such as the source of graphical item data for complex flow characteristics (i.e. pre-swirl nozzle or blade cooling). This section explains the user operability of the CSI SAS model generation utilities. The goal is to automatically generate and run the SAS 1D flow network model.

A) Flow network features



B) 1D flow network model

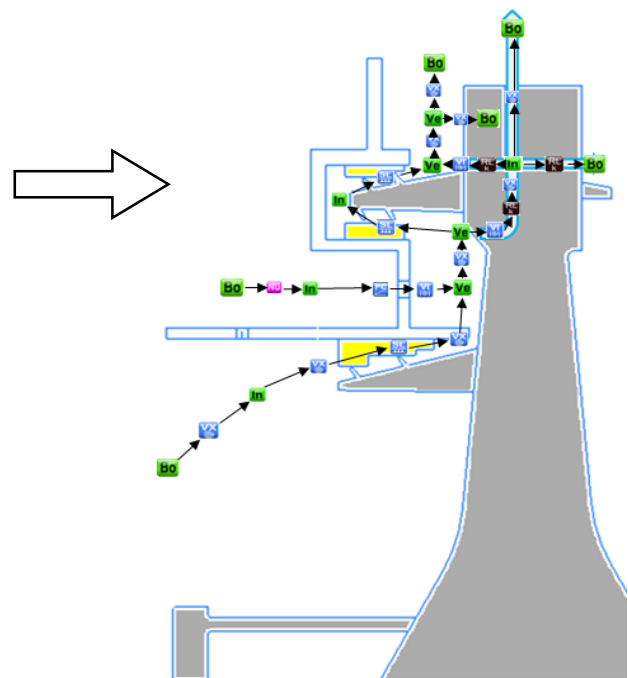


Figure 4.4.1.: Typical HPT front flow network arrangement. A) Diagram of the air system features that are automatically recognised with the CSI algorithms, and B) automatically assembled 1D flow network model.

#### 4.4.1. Flow network recognition sequence

The flow network recognition work-flow takes as a starting point a data model in the CSI environment with available disc-statics combined and trimmed CAD models, as previously described. There are a few preparation tasks that need to be performed before the flow network recognition algorithm is able to operate. The work-flow steps in Table 4.2 on page 83 describe the automatic process to recognise the flow network. The first task involves setting the fluid and solid boundaries for the subsystem that is suppose to be analysed. The user has to define in either a manual or automated way the borders of the engine area in focus. These subsystem boundaries can be defined in the CAD tool, marked with an attribute as “virtual flow passage” and let the following automated algorithms collect them into the data model. Additionally, the component solid walls that are adjacent to the geometry in focus, but should not be taken into account in the flow network, need to be marked as “external”.

In the next step, an automated algorithm collects the curves information from the subsystem

Table 4.2.: Flow network recognition work-flow sequence

Sequence	Task	Description
1	Set up of subsystem boundaries	Defining the fluid and solid external boundaries to the subsystem in focus
2	Collect curves from CAD to CSI	Gathering curve tags, attributes, origin and end coordinates from the CAD tool into CSI
3	Set up of CSI flow passage fluid walls	Setting flow passage inlet and outlet fluid walls coordinates based on the solid information from the CAD model
4	Flow network recognition	Construction of the flow network graph of cavity nodes and flow passage edges, as well as initialisation of cavity types and cavity flow network sub-nodes (inlets, outlets, flow conjunctions inside a cavity).

CAD model. This algorithm establishes an interface between the CSI data model and the CAD model. The curve information being sent to the CSI data model includes tags, attributes and curve origin and end point coordinates. A further automated task is needed to initialise the coordinates and attributes of fluid walls in the CSI data model. These are for example the fluid inlet and outlet of seals or flow orifices. Finally, with all wall and boundary information saved in the CSI data model, the flow network recognition method works out the cavities in the subsystem and how they are interconnected to one another via flow passages. The output of the method is a mathematical graph, where the nodes represent cavities and the edges represent flow passages between cavities. As a visual output of this method, the list of cavities with their associated types is made available in the CSI data model. The default characterisation of cavity types (e.g. rotor-stator outwards flow, rotor-stator axial flow, etc.) can also be overridden by a CSI user. Moreover, each cavity is assigned a list of flow network sub-nodes, which identify inlets, outlets and flow conjunctions inside a cavity.

Figure 4.4.1 on page 82 presents an example of a typical HPT front flow network arrangement that can be automatically recognised using the CSI environment. Further detail on how the algorithm for flow network recognition has been implemented is described in Section 5.3.

Table 4.3.: Flow network generation and solver work-flow sequence

Sequence	Task	Description
1	User check through of SAS settings	User checking of correct flow passage orientation, flow network templates, and cavity definition
2	SAS flow network model generation	Generating the flow network base model and saving it in the project “out” folder
3	SAS flow network model solver	Launching the flow network base model simulation and saving the results file in the project “out” folder

#### 4.4.2. 1D flow network model generation and solver sequence

The work-flow steps in Table 4.3 on page 84 describe the automatic process to generate and solve the 1D flow network model. Before the flow network model generation task is automatically launched, the CSI user should check the specific settings of the SAS features in the data model. This involves making sure that each flow passage has been assigned the desired flow direction<sup>2</sup>, that the available flow network templates for each SAS feature are appropriate for the engine project being modelled, and that the previous flow network recognition algorithm has produced a sensible list of cavities with their associated flow network nodes.

The algorithm to generate the flow network model runs fully automatic in the CSI environment. The output is a flow network base file suitable to be used in a flow network tool. A subsequent task is able to launch the simulation solver of the flow network model and an output results file is made available in the CSI project “out” folder. The 1D flow network solver algorithm has not been considered as part of this work, but an overview of its basic functions has been provided in Section 3.3. Figure 4.4.1 on page 82 presents an example of a typical HPT front 1D flow network model that has been automatically generated using the CSI environment. Moreover, Section 5.4 describes in detail how the instructions to generate the integral flow network model have been implemented.

---

<sup>2</sup>Flow passages such as seals and orifices need a default flow orientation in order to automatically generate their link in the flow network model. This default flow orientation does not rule out reverse flow that could be a possible outcome of a simulation with the flow network model.

## 4.5. Thermal FE-Model

This section explains the user operation of the CSI thermal FE-model generation utilities. In Section 5.5 will be described how the interface of the CSI environment classes with the thermal FE-modelling instructions has been implemented. Generating the full set of inputs to construct a thermal FE-model is currently a time consuming and somewhat complex process. The automated routines developed in this work especially focus on accelerating the process to generate the FE-model domains and thermal boundary conditions.

### 4.5.1. Thermal FE-model inputs generation sequence

The work-flow steps in Table 4.4 on page 85 describe the automatic process to generate all input files needed to assemble the thermal FE-model.

Table 4.4.: Thermal FE-model inputs generation work-flow

Sequence	Task	Description
1	Generate FE domains	Generating the FE domains definition and properties (material, kinematic, speed, etc.)
2	Generate thermal boundary conditions	User or system default selection of thermal model templates for each flow network feature. Automatic mapping of thermal boundary conditions to geometry curve-tags
3	Connect thermal boundary conditions	Resolving boundary condition interdependencies and mapping of flow network outputs into the thermal boundary conditions.
4	BDD file constructor	Exporting performance, oil system, and aero loads data into BDD file format. Additionally exporting the definition of the simulation cycle into the BDD file.
5	JNLF file constructor	Exporting of FE-domain allocation, domain properties, thermal boundary conditions, and analysis settings into JNLF file format.

The key automated steps in this process are the generation of FE-model domains and thermal boundary conditions. The domains are allocated based on the available CAD-curves information. Regarding the thermal boundary conditions, a thermal modelling scheme is assigned to

each flow network feature (e.g. cavities and flow passages). The selection of a thermal model for each cavity category is performed on the basis of pre-stored thermal boundary conditions templates. Furthermore, the CSI environment offers the user the possibility to assign CFD-data profiles to the thermal boundary conditions. A detail explanation of the CSI thermal modelling functionality can be found in Section 5.5.

#### 4.5.2. Thermal FE-model base file construction and solver

Table 4.5 on page 86 describes the work-flow sequence to construct and start the simulation of the thermal FE-model with the previously generated inputs. This involves the assembly of several data sets: the FE-model geometry, the domain allocation, the thermal boundary conditions, and the performance and cycle data. Further details on how the FE-model assembly process has been implemented can be found in Section 5.5.

Table 4.5.: Thermal FE-model construction and solver work-flow

Sequence	Task	Description
1	Load CAD geometry into FE-model	Loading 2D or 3D geometry definition into the FE-tool
3	Load BDD file	Loading BDD file with cycle definition, performance, and various other cycle specific data
4	Load JNLF file	Loading JNLF file with domain definition and thermal boundary conditions list associated to geometry curve-tags
5	Mesh model	Thermal FE-model automated meshing process
6	Start FE-model solver	Solving the thermal FE-model
7	Process thermal results	Processing of thermo-mechanical results

Most of the steps in this process involve loading the automatically generated files in the FE-tool using its scripting programming language. The mesh generation and solver settings are detailed inside the JNLF file. Regarding the meshing and solving processes themselves, these are intrinsic to the FE-tool, so their algorithms have not been considered as part of this work. A brief description of the thermal FE-solver and typical thermal results has been provided in Section 3.4.



---

# 5

## Implementation of the Automated Design and Analysis Processes

---

This chapter describes how the algorithms and methods for the automation of the engineering work-flow have been implemented. The implementation approach is based on Java object oriented programming and a brief overview is given in order to understand the methodology that this implies. The chapter further describes how the CAD modelling interface in the CSI design environment has been solved, providing an insight on the differences between modelling of rotor and static structures. Then, the algorithm to automatically recognize the flow network configuration of a turbine design is explained, and thereon, the steps to construct the 1D flow network model. Finally, the last section focuses on the functionality to automatically generate the thermal FE-model building blocks.

### 5.1. Object Oriented Data Modelling

The fundamentals of object oriented programming (OOP) have been extensively described in previous literature. Java has been chosen in this work to implement the developed methods in an OOP fashion. Even though Java is of course not the only OOP language, its characteristics make it easy to program the functions that are the purpose of this work, and it offers a modular

and efficient way to build interfaces between the preliminary design platform and the rest of tools that need to be automated. A state of the art reference to Java OOP can be found in ULLENBOOM (2012), which describes the Java methods from a design and engineering point of view.

The key to object-oriented software development is how to model objects and how to define their interfaces. Objects are critical to understand object oriented methods and they have three important properties:

- a unique identity as long as the object exists (in runtime),
- their state is stored in fields, and
- their behaviour is exhibited through methods.

A class is a template or blueprint from which individual objects are created (in programming language, instantiated). A class declares two main properties of an object:

- the attributes, which describe the object properties, and
- the operations, which describe the actions that the object can perform.

In this context, classes in OOP can make use of two important functionalities: inheritance and interface. OOP allows classes to inherit state and behaviour from other classes. In Java language, each class can have one direct superclass, and each superclass has the potential to contain an unlimited number of subclasses. The other function, implementing an interface, allows a class to communicate its behaviour with outside classes, which is executed at build time by the compiler.

Every new engineering project can make use of the know-how accumulated in earlier projects, where similar problems were already solved. A great deal of resources, in terms of both economy and time, can be saved when parts are reused in different contexts. Such is the goal of object oriented methods for engineering practices. The re-usability of modules and components of a software is greatly facilitated by object-oriented programming. This approach is further strengthened by the fact that programming classes can be bundled in libraries, with which many thousands of classes can be reused for the implementation of data structures or for the buffering of data streams. The benefits of an object oriented data model structure and programming re-usability apply to the engineering methods developed in this work.

## 5.2. CAD Geometry Interface

The work-flow sequence to automate the generation of subsystem CAD models has been described in Section 4.3. It was explained how the user loads into the CSI design data tree the turbine features, which contain the parametrisation and interface data to create a CAD representation of the geometry. Each turbine feature is an instance of a Java class, which is loaded as an NBM plug-in containing the part definition and interface code to communicate with the CAD tool.

The NBM plug-in of a feature is a data package with the following files:

- a part definition class, which contains the part file naming interface and parameter mapping instruction,
- a plotting class, which contains the feature drawing instructions for the CSI GUI,
- an initialisation class, which contains standardised default instructions for connecting the new added feature with the rest of the parts (e.g. attachment of disc to rotor blade),
- a parametrised and tagged CAD part file, which replicates the feature in the CAD tool.

In order to operate the CAD tool from the CSI environment, a connector class has been programmed that builds a client-server interface between both tools. This allows direct communication with the CAD tool via its own programming classes, while manipulating features within the CSI environment.

### 5.2.1. Modelling of rotor structures

Disc assemblies belong hierarchically to an engine subsystem or spool. In a typical turbofan configuration, each subsystem (i.e. HP, IP, and LP) would have one disc assembly. However, the CSI environment is able to cope with multiple disc assemblies per shaft, which might be an option for advanced aero engine concepts with counter rotating disc assemblies in the same subsystem.

Each disc assembly in CSI is associated to a NBM plug-in including the parametric CAD part file that mirrors it. This predefined disc assembly CAD model should resemble the realistic

geometry as best as possible. The CAD model may include switch-able features, such as seal arms, drive arms, or joint types (e.g. bolted or splined). In this sense, the parametrisation of the model should take into account that the desired design variability will be achieved by modifying expression values. Additionally, the CAD model curve tags should follow a systematic nomenclature, to ensure the appropriate interface of lines with the CSI environment.

The robustness of the CAD model should be checked beforehand. It is important to make sure that the parameter modifications in the desired range do not break the integrity of the model. An approach to ensure CAD model stability for automated parameter studies has been presented in REY VILLAZON, J. M. et. al. (2012).

It should be noted that rotor disc's lifing is very sensitive to the fidelity of the CAD model. This is not as restrictive during the preliminary design phase for the static structures, which work under no centrifugal loading. Therefore, the CSI approach for the modelling of the rotors concentrates in the highest possible model fidelity of rotors for automatic concept studies. The disc assembly model is loaded as a complete CAD part with some design variability. A more flexible approach would consist on building the disc assembly automatically from individual features (e.g. arms, firtree, etc). However, this latter process results in a model that is usually more unstable to later design changes. As an example of the level of fidelity that has been implemented in the automated process, Figure 5.2.2 on page 92 shows a 2D sketch with the disc post of the CAD model assembled in the CSI environment.

Within the category of rotating structures, the CSI environment also enables to plug-in block-built structures. These features might be helpful to represent unconnected shafts when only a subsystem of the engine is intended to be modelled. In a realistic engine, no such structure could exist without a connection to a bearing housing, but for simulation purposes it is sometimes useful to be able to model rotating pipe structures that are unattached to other components.

### **5.2.2. Modelling of static structures**

Static structures are modelled as a chain of interconnected block features. This is a somewhat different approach to the one followed with the discs assembly. The static structure will be build during runtime from the connection of basic features. In the 2D GUI representation, the blocks resemble a bar. As they represent axisymmetric features, in reality each "block" is a

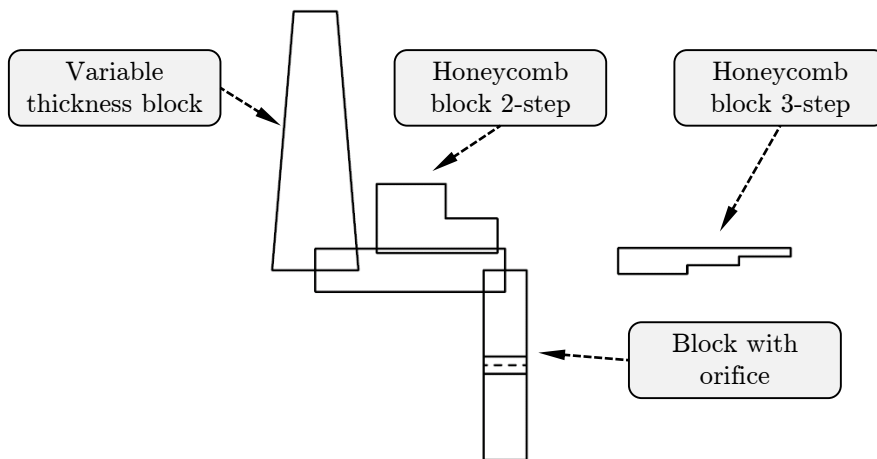


Figure 5.2.1.: CAD model 2D view of static structure block features.

ring shaped casing. The block features can replicate simple pipes with a thickness property, or have some more complex geometries including 3D features such as pre-swirl nozzles and seal honeycombs. A library of structure blocks has been made available. The library contains several CAD UDF's that serve as a template to produce a manifold of structure arrangements. Figure 5.2.1 on page 91 shows some of these static structure block features.

The CSI process to generate the static structures CAD geometry starts by creating the individual blocks and switching of special features. The individual blocks are then inserted as a chain in the discs assembly model. Finally, the combined statics geometry is trimmed automatically to produce clean internal surfaces with no line overlapping. Figure 5.2.2 on page 92 presents a comparison of a combined untrimmed model with a trimmed model, focusing on an area of the discs assembly with a static structure.

Regarding the CAD model representation of the SAS features, it should be distinguished between features that belong to rotating disc assemblies and to static structures. SAS features that belong to a disc-assembly, such as a labyrinth seal, are switched on in the associated CAD model of the disc-assembly. On the other hand, SAS features that belong to a static structure block, are loaded with the individual block part file. Examples of SAS static structure features include the block with an orifice, block with a pre-swirl, or the seal honeycomb

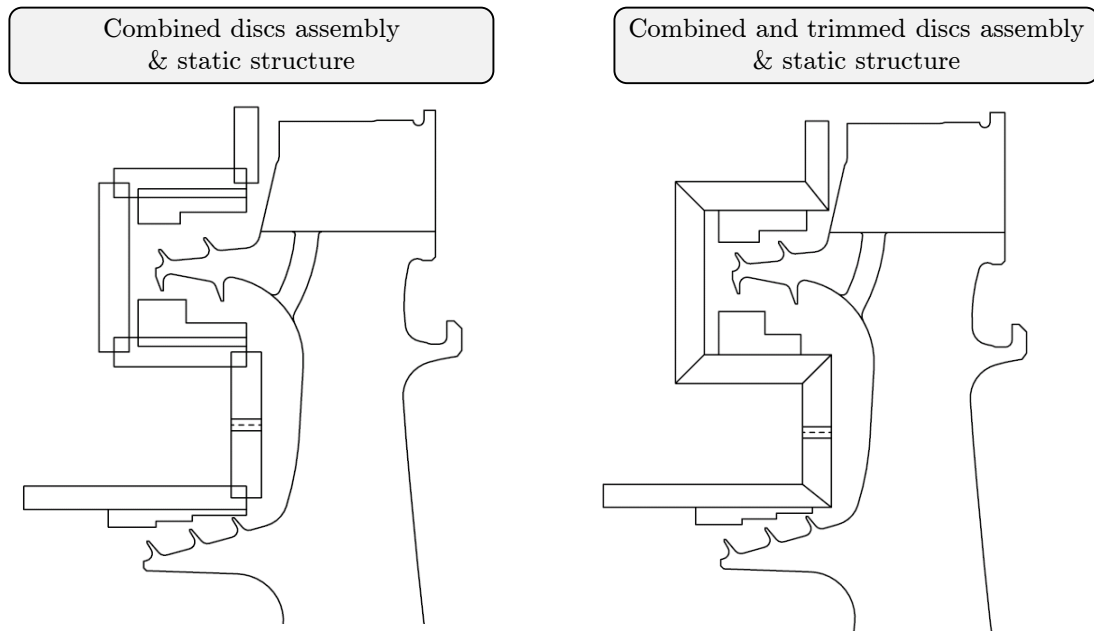


Figure 5.2.2.: CAD model 2D view comparison of a combined untrimmed model with a trimmed model, focusing on an area of the HPT discs assembly with adjacent static structure.

block.

### 5.3. Automated Flow Network Recognition

The flow network recognition algorithm relies on the interdependency rules between the features and their associated walls. Several types of subsystem walls are considered in the CSI data model:

- Solid walls, which can be the contour of a solid feature, internal to a solid feature, or external to the subsystem being considered.
- Fluid walls, which represent inlets and outlets of SAS features (e.g. seals).
- Virtual boundary walls, which define the fluid borders of the subsystem (e.g. rim boundary or upstream off-take).

Another important categorisation of the flow network features is that of cavities and flow passages. The flow passages are fluid devices intended to transfer the fluid between cavities.

In order to abstract the flow architecture information, a mathematical directed multigraph<sup>1</sup> is used to store the information of cavity nodes in the system and flow passage edges connecting cavities. The chosen graph is of type “directed” to keep track of the flow orientation and it can store multiple edges between two nodes in order to capture connections between two cavities of more than one flow passage (e.g. the firtree feature with leakages and interstage flows). This graph entity, which is build in the CSI algorithms during runtime, has been called the flow-network-graph.

The assembly of the flow network graph is performed via a Java-implemented procedure that recognises cavities and the flow passages that link them on the basis of the geometry definition. The cavity class has methods for instantiating objects that contain a list of surrounding walls and have at least one inlet or outlet flow. The flow network recognition algorithm starts by collecting all walls of the subsystem. Thereafter, solid external walls, solid internal walls, and flow passage inlet and outlet walls are filtered out. The procedure then determines which walls are connected to each other and form a graph close loop (enclosed cavity). A new cavity object is then created and added to the data tree. Additionally, the new cavity object is added to the flow network directed graph as a node, with the cavity inlet and outlet flow passages as edges of the graph.

The outcome of the process is the list of cavities found in the enclosed subsystem, including their flow passage connections, and the cavity types. Each cavity type is defined according to the following criteria,

- Operation: rotor-stator, purely rotating, or purely static.
- Flow orientation: radial outwards, radial inwards, or axial.
- Flow passage connections: number and type of inlets and outlets.

The above described information is the basis for the 1D flow network model construction algorithm and for the assignation of a thermal boundary conditions scheme.

---

<sup>1</sup>In mathematical graph theory, a graph is a representation of a set of objects, where some pairs of objects are connected by links. The objects are represented by mathematical abstractions called vertices, and the links that connect some pairs of vertices are called edges. The term “directed” means that the edges have a direction associated with them. The term "multigraph" means that multiple links or edges connecting two vertices (and sometimes loops) are allowed.

## 5.4. Flow Network Model Construction

As a starting point for the SAS 1D flow network model construction, the flow network directed multigraph is constructed automatically as soon as the algorithm is run. The construction algorithm further relies on a database of 1D flow network elements categorised by flow passage type and cavity type. This database is stored in XML format, and its elements need to be previously agreed as best practice standard from the fluid systems engineering department. Following, the model assembly method is described.

### 5.4.1. 1D flow network model assembly method

A diagram of the 1D flow network model assembly process is shown in Figure 5.4.1 on page 95. In the first step of the 1D flow network model assembly, the bits of every flow passage (graph edges) are loaded. Secondly, the procedure iterates through the virtual boundaries to load the model boundary nodes and elements (note that the rim boundary feature contains a complex set of nodes and flow characteristic bits).

The next step in the procedure involves setting up the cavity elements. This begins with loading of internal nodes, with a logic depending on the number and type of inlets and outlets. Then, linking of the internal cavity flow network is performed by adding internal bits, such as vortex or heat-power bits, and by linking the nodes and bits inside the cavity.

In the final step, the system of cavities and flow passage components is linked together. The linking process is based on the connections provided by the flow network graph. In some cases, additional vortex and change of reference frame elements are added, in order to accommodate the radial and rotor to stator flow changes.

The fully linked SAS 1D flow network model represents a customised model fitted to the requirements of the SAS design and features specified in the CSI environment. The parameter information of each SAS element is mapped from the CSI data model into the corresponding 1D flow network element during the model construction process.

During this process, if specified in the cavity definition, CFD derived correlations for modelling of windage and pumping power losses are included in the heat and power elements of the 1D



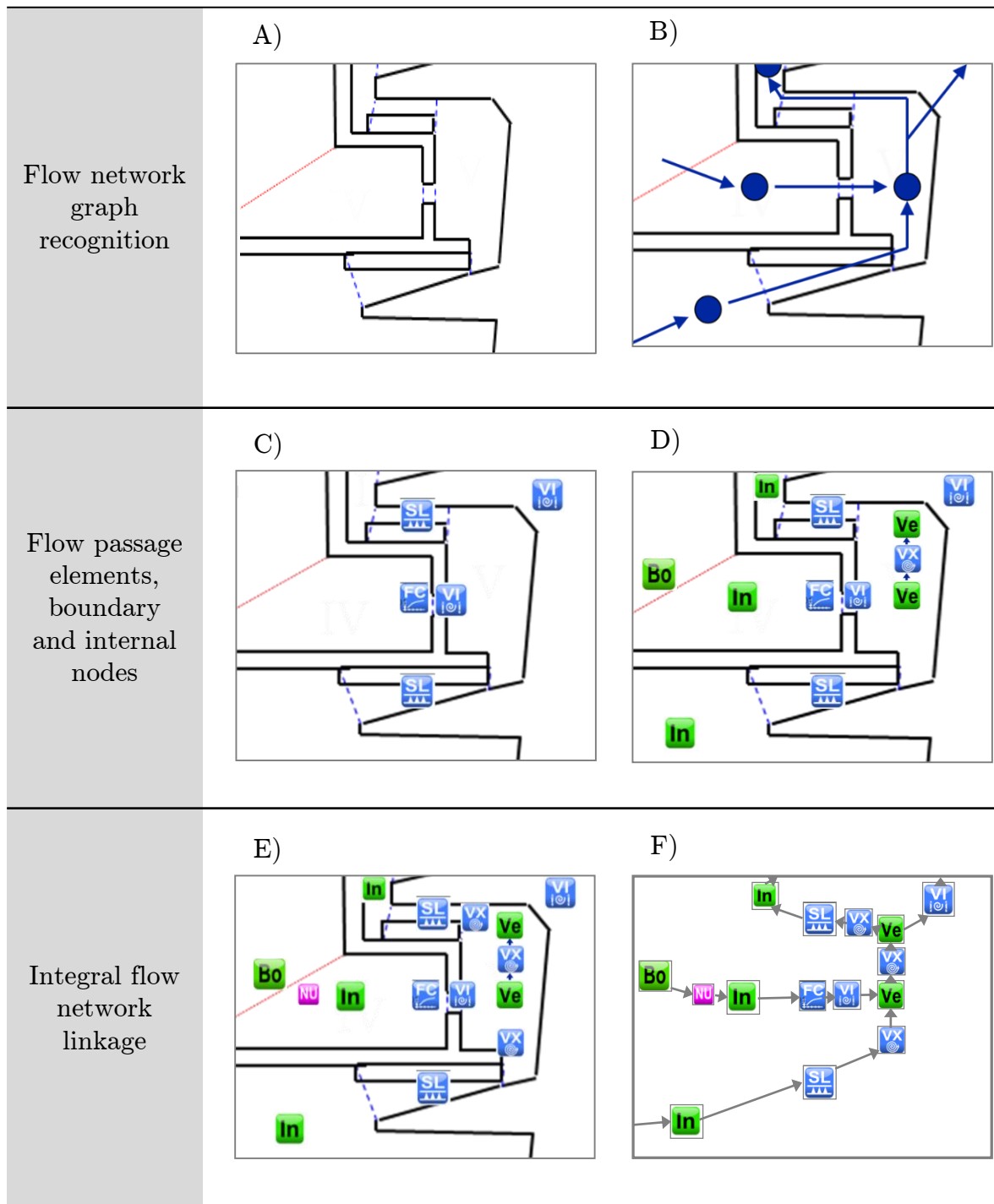


Figure 5.4.1.: Diagram of the 1D flow network model assembly procedure. A) Exemplary datum geometry of a rotor-stator cavity with a seal inlet, seal outlet, pre-swirl nozzle inlet, and rotor air holes outlet; B) Flow network graph; C) Added flow passage bits; D) Added boundary and internal nodes; E) Additional cavity bits; F) Linked flow network model.

flow network model.

## 5.5. Thermal FE-Model Construction

This section describes the details of the implemented functionality to enable the automatic generation of thermal FE-model inputs. The CSI procedure and necessary inputs have been already presented in Section 4.5.

The key steps of this process are the selection of a thermal boundary conditions scheme for a given design and the allocation of FE-model domains. The other part of the process involves exporting the additional data files for the thermal FE-model, such as the performance and SAS data file, in the correct format. These latter steps do not present an academic value and are therefore not described in detail, since the formatting of data files is very specific to the tools being used and is prone to changes in the near future.

### 5.5.1. Thermal boundary conditions template engine

The CSI programming data model nodes that represent features with solid-fluid interface need to capture thermal modelling information. These features are the ones that belong to the SAS flow network, i.e. cavities and flow passages (orifices, seals, cooling holes, etc.). The classes of flow network elements are thus equipped with a class interface to contain lists of thermal boundary conditions (BC's). At the same time, each thermal BC can have interdependencies to other thermal BC's, for example linking their mass flows or their outlet to inlet temperatures. A typical arrangement of thermal boundary conditions has been shown in Figure 3.4.1 on page 63. The thermal BC's and thermal modelling properties of each flow network feature are stored in an object "thermal-model", attached to each feature in the CSI data tree.

Each thermal BC contains a set of BC inputs that define the fluid-solid heat transfer mechanisms. The thermal BC inputs can be of the following types:

- a user defined function,
- a profile extracted from CFD models,
- an interdependency to another BC, or

- a parameter from the performance and secondary air system output file.

The thermal model objects are a type of directed graphs, where the flow network flow conjunctions are abstracted as nodes and the thermal boundary condition flows are abstracted as edges. In such, the thermal model of each feature retains at all times its flows-linkage information.

Regarding the application of CFD-enhanced boundary conditions, CFD extracted profiles of thermal functions (e.g. the *HTC*) can be stored in the template of a particular cavity. The CFD profiles can be defined as tables of specific values or parametric functions that adjust the profile to changes in the cavity operation or dimensions. A more detailed description of how the CFD data profiles are prepared can be found in the appendix Section A.2.

### Thermal modelling templates

In order to facilitate the creation of thermal models within the CSI environment, an XML-format database with template thermal models for each flow network feature has been made available. For expansion purposes, the management (adding and removing) of thermal model templates in the database is an available option for CSI thermal users (in practice thermal systems experts).

The list of applicable thermal model templates for a specific flow network category is automatically filtered based on the category type (e.g. rotor-stator cavity with pre-swirl inlet, axial-stator cavity, seal, cooling hole, etc.). Then, the template engine automatically initialises the thermal BC's for a specific design, resolving interdependencies, applying specific geometric parameter values, and mapping flow data from the SAS model outputs.

Moreover, the thermal model initialisation identifies the list of CAD geometry walls (via curve tags) that are associated to each thermal BC. The list of BC edges defines the linkage between thermal BC's and the geometry file. In some cases, the definition of a thermal BC might require a CAD curve to be split. For these cases, the CAD model is modified automatically via the CSI-CAD remote interface in order to accommodate the geometry file to the newly assigned thermal BC's.

New thermal model templates can be added to the database via exporting functionality of predefined thermal models in the CSI environment. As a future work recommendation, a version and tracking control system should be taken into account to keep record of the created

thermal model templates.

### **Interdependencies of the integral thermal model**

After the individual thermal models flow network features have been initialised, the integral thermal model of the subsystem needs to be linked together via the interdependencies in thermal boundary conditions.

This process involves updating the thermal BC's inputs of the individual thermal models with references to fluid properties of other thermal BC's (such as fluid temperature or mass flow). The BC interdependencies across thermal models of different flow features are resolved using the information stored in the CSI flow network directed multigraph, which has been described in Section 5.3.

### **5.5.2. Thermal FE-model domains allocation**

FE-model domains and their properties are stored as a list of data objects associated to each solid feature in the CSI data tree (e.g. disc body, disc arms, or solid block with orifice). Each domain is identified by a line or a series of lines that make it a unique solid area in the FE-model.

The CSI automated algorithm resolves the lines that identify a domain by considering the set of solid walls as an undirected graph. The algorithm then searches for closed solid wall loops, which define an enclosed solid domain. This results in the relation between a wall of an enclosed graph loop and its corresponding feature, since the solid wall is an object whose parent containing feature can be traced back in Java.

Once the list of FE-domains for each CSI data tree feature has been instantiated, the domains allocation syntax is exported into a data file, which is readable by the FE-tool. Given that the domain allocation and naming has been controlled from the CSI environment, the domain properties such as material or thickness can then be automatically updated in the data file that is sent to the FE-tool. This functionality would then enable automated optimisation studies to be performed with varying materials and kinematic properties.

---

# 6

## Application on an HP Turbine Subsystem

---

This chapter illustrates how the process developed can improve the preliminary design and analysis of engine subsystems by applying it to a realistic HP Turbine case. For demonstration purposes, an existing turbine design has been chosen, with the intention of verifying the outputs of the proposed automated process against available validated engine models. The chosen demonstration case focuses on the front SAS of a typical 2-stage HP turbine configuration used in corporate aviation engines.

First, the preliminary design of this turbine subsystem is replicated using the previously described CSI common design environment. Followed by the automatic construction of the corresponding CAD models. Secondly, the automated CSI work-flow is used to recognise and generate the SAS flow network model. Lastly, the thermal modelling scheme of each flow network feature is instantiated, the set of input data for the FE-model is generated, and the thermal FE-model is assembled and run. The automatically constructed models and their simulation results are compared against existing experimentally validated models of the selected turbine application case.

In the last phase of the investigation, a design variation study is performed. The purpose of this study is to demonstrate the preliminary design capability of the newly developed process.

The results of applying the advanced preliminary design process are discussed at the end of this chapter, highlighting the findings of this work.

## 6.1. Application Case Description

### The HPT subsystem

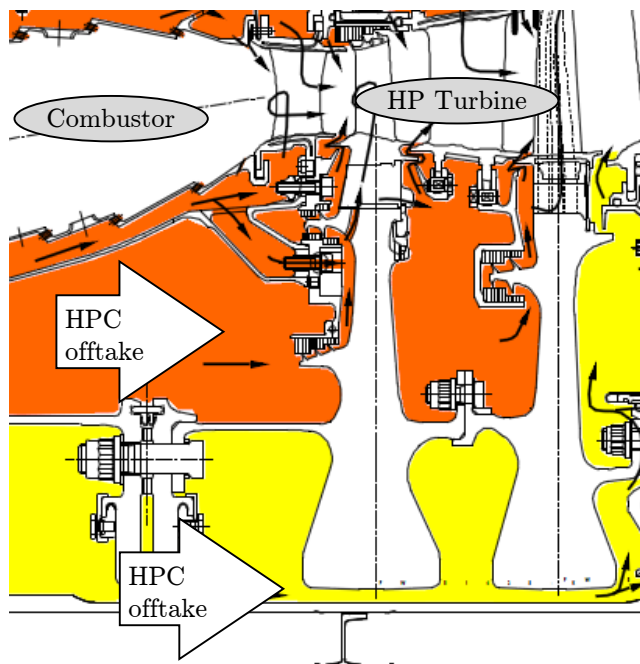
The exemplary application case of this work focuses on the front cavities of a typical aero engine HPT. The HPT components operate at high temperatures and rotating speeds in the engine, which makes their performance highly dependent on the flow field phenomena. Regarding the main annulus configuration of the selected case, this HP turbine subsystem includes the first stage rows of vanes, immediately after the combustor exit, the first row of rotor blades, the second row of vanes, and the second row of rotor blades. Usually, the HPT subsystem includes also the blades outer casing. However, this work did not take this component into account, as it focuses on the sub gas-path architecture of the turbine. Regarding the architecture of the disc assembly, each rotor blade is mounted around a rotor disc via a firtree blade-disc root. The discs transmit the turbine power to the compressor through a front drive arm with a bolted and curvic coupling. The two HPT discs are joined to each other via a bolted joint, and the rear disc is bolted via a drive arm to a short stub shaft that supports the rotating structure inside the rear bearing housing.

A description of the considered SAS features and their operation is presented in Table 6.1 on page 101. Figure 6.1.1 on page 101 shows a sketch of the HPT front SAS configuration, presenting a summary of the SAS cavities and features that will be relevant throughout the next sections. The main SAS passages in the front of the HPT consist of two labyrinth seals A and B that enclose a rotor-stator Cavity B with a pre-swirl nozzle inlet. The pre-swirl nozzle adapts the flow conditions for entry into the disc cooling holes of the blade cooling system. Additionally, a rim seal at the main annulus hub, outlet of Cavity A, controls the rim sealing flow and a micro-turbine in the blade root feeds the HPT interstage cavity with air from the front stage. It should also be taken into account that a moderately high mass flow in between the firtree lobes feeds the interstage cavity.

Table 6.1.: Description of the application case features and SAS configuration

SAS feature	Description	Operation
Cavity A	rotor-stator at rim	radial outflow
Cavity B	rotor-stator at mid radius	radial outflow
Cavity C	purely static walls	axial flow
Cavity D	rotor-stator at drive cone	axial flow
Seal A	labyrinth seal	feeds cavity B
Seal B	double labyrinth seal	feeds cavity A
Pre-swirl	skewed orifice	feeds cavity B
Firtree	micro-turbine and firtree slots	interstage flow
Blade cooling	Disc cooling air hole and blade cooling passages	radial outflow

A) 2-Stage HPT subsystem flows diagram



B) SAS flow network features

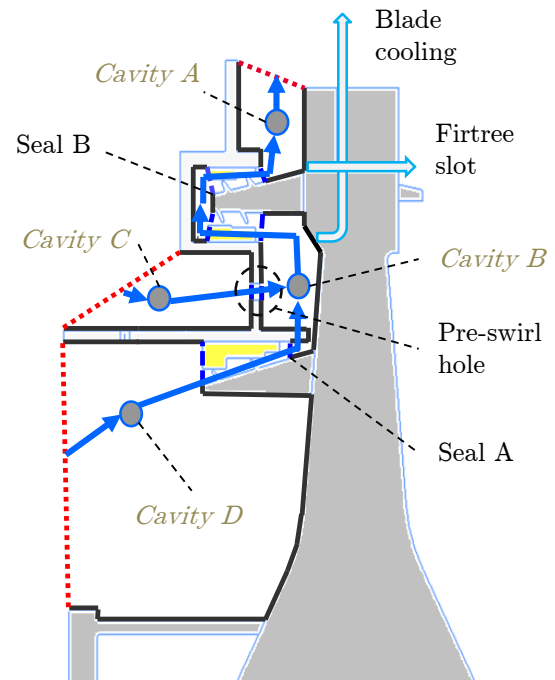


Figure 6.1.1.: A) Diagram of the HPT subsystem application case; and B) sketch of SAS cavities and flow passages as an abstraction of the flow network in the front of the first HPT stage.

There are five boundaries to the model. The inlet flow boundaries are the air flows that source from two separate off-takes in the high pressure compressor. The outer one of these flows, passes in between the combustor inner casings and leads through Cavity C to the pre-swirl nozzle. Additionally, the conditions of the air that sinks through the front and rear rim gaps

into the main annulus are taken as a boundary (outlets of Cavity A). The outlet conditions of the blade cooling flow are set also as a sink boundary. To close the subsystem, the interstage cavity conditions are set as the sink boundary for the micro-turbine and firtree flows.

### **Available engine data**

The following set of data for the validation of the application case was made available by courtesy of Rolls-Royce Deutschland Ltd & Co KG:

- performance deck for high power design point,
- main annulus geometry and through flow data,
- disc assembly geometry CAD model,
- validated SAS 1D flow network model and output data,
- HP turbine preliminary design and validated thermal FE-models,
- HP turbine thermal survey experimental data.

## **6.2. Rotors and SAS Design using the CSI environment**

This section deals with the demonstration of the CSI environment design capability. Herein, the process of building the rotors and SAS architecture is exemplified, with the subsequent automated generation of CAD models. As a starting point, it is assumed that the turbine main annulus design is frozen. This is a common assumption when the turbine blade rows geometry are fixed as an iteration of the preliminary design process or in the transition phase to detailed design. In this chapter, the outcome of the automated CAD model generation work-flow will be discussed and its fidelity compared with available former engine CAD models.

### **CSI common design environment**

The details of the process for the definition of a subsystem design have been described in Section 4.1. The application process starts by loading the engine performance data, the HP and LP turbine main annulus geometry and the aerodynamic data. Even though the application focuses on the HP turbine subsystem, the LP turbine aerodynamic data is needed as boundary



condition for the SAS sink flows. Figure 6.2.1 on page 105 shows the turbine main annulus design loaded into the CSI environment.

The CSI rotor design process begins with the selection of a disc assembly plug-in. Since the annulus design has been fixed, the number of rotor stages is also fixed. In this case, a disc assembly was chosen that could replicate the geometry of the available validated models; i.e. a 2-stage disc structure with bolted drive arms. The selected disc assembly plug-in from the CSI palette already contains an associated parametric and tagged CAD model. This CAD model has already been prepared with a high level of fidelity, featuring detailed disc body shape, fillets, and blends. Within the CSI environment, the user selects then the number, location and orientation (front, rear) of drive arms, as well as the design of the bolted joints (inwards, outwards, number of bolts, etc.). The disc body parameters can also be modified, including the rim, diaphragm and cob dimensions. At this point, it should be verified that the disc assembly has been assigned the proper material code and domain kinematic properties. Figure 6.2.1 on page 105 shows the CSI design after the rotor features have been added.

The SAS configuration process starts with the selection of compressor off-take stations that are necessary to feed the turbine needs. The main design requirement is to keep the SAS flows penalty to the turbine overall efficiency to a minimum. Within this application case, the off-take to sink configuration has been set to match the SAS of the available validated models. The sealing arrangement is then adjusted by adding seal arms to the discs and modifying their parameter values. In the next step, the disc firtree flows, the blade cooling arrangement, and the interstage micro-turbine flow are set. The next design step involves replicating the construction of the static structures surrounding the discs and adding the SAS flow passage features, such as the pre-swirl nozzle, seal honeycombs, and orifices. The fidelity of the static structures definition at this point is very basic, since these features act as a scenery to the subsequent simulation models. In this stage of the process, the material selection and kinematic domain properties for the static features should be fixed. Figure 6.2.1 on page 105 shows the CSI data model sketch after the SAS scenery has been added.

Another scenery feature that needs to be added to the subsystem is the LP spool shaft below the HPT discs. This simple horizontal block structure belongs to the LP spool, and it can be modelled with low fidelity as it serves mainly for enclosing the HP components and supporting the passage for the inner SAS flows.

The final preparatory step before the automated work-flows are able to run involves setting the CSI virtual boundaries<sup>1</sup>. The following virtual boundaries have been set for the application subsystem:

- HP compressor mid stage off-take air flowing to the HPT disc cobs.
- HP compressor last stage off-take air flowing through the drive-cone cavity.
- HP compressor last stage off-take air flowing to the pre-swirl nozzle.
- HP turbine sink into the rear bearing housing.
- HP turbine sink into interstage cavity.
- HP turbine sinks into the main annulus.

The above described CSI data model is used as the basis for the automated processes to follow.

---

<sup>1</sup>Virtual boundaries represent the boundaries of the modelled sub-system with the non-modelled environment, a more description can be found in Section 4.1.

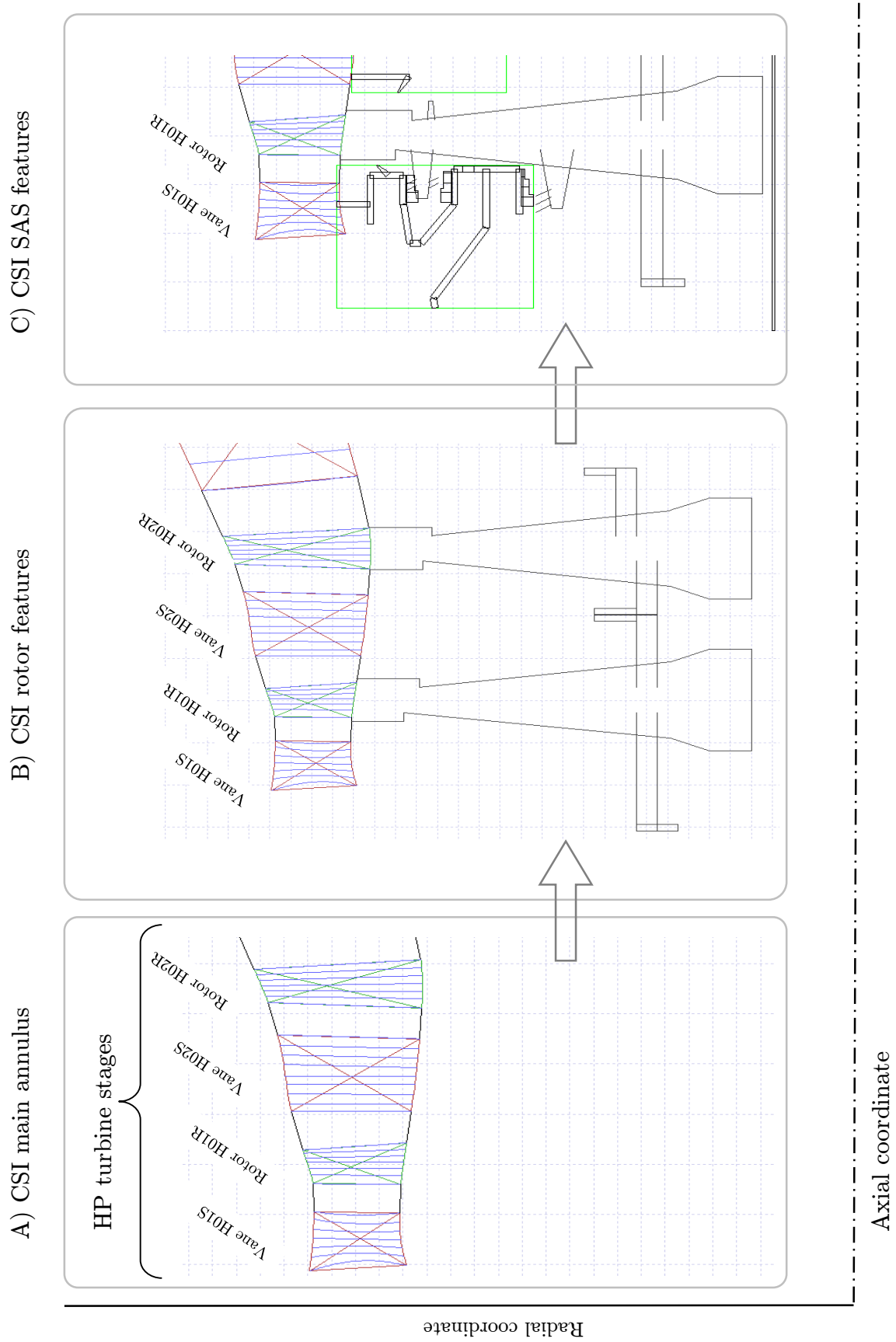


Figure 6.2.1.: CSI design definition process: A) Loaded main annulus design data; B) Added disc assembly; and C) Added static structure scenery, LP shaft and SAS features.

## CAD model generation

With the data model defined above, a CAD model of the subsystem can be automatically generated following the work-flow described in Section 4.3 with Table 4.1 on page 81. The resulting combined subsystem parts CAD model is shown in Figure 6.2.2 on page 106.

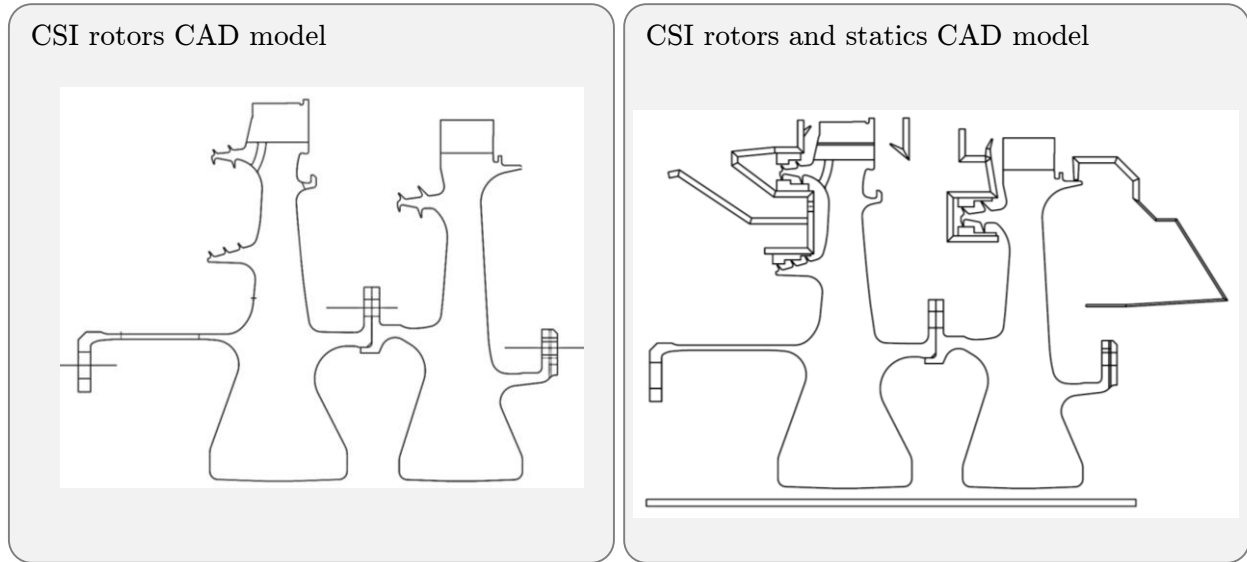


Figure 6.2.2.: 2D sketches of the CSI automatically generated CAD model, showing the geometry of rotors and the geometry of rotors with static structure scenery.

## Comparison to the available engine models

The output CAD geometry from the CSI environment compares well to the CAD models of the reference turbine, from here on called baseline models. As a main difference, the baseline preliminary design model had no static structures geometry, whereas the baseline detailed design model had a very accurate definition of the static structures. The CSI generated geometry presents an intermediate solution, where the static structures have been sketched in a premature level, since the structural and vibration analysis have not been performed yet. At the intended design stage, the simplistic CSI static structures have the purpose of assisting in the composition of the SAS flow network.

Furthermore, the automatically generated geometry of rotors contains the same level of detail as the baseline detailed design model. Some detailed 3D firtree features, which correspond to the detailed design phase, have not been applied in the automated process. However, if the project team would considered these features of importance, they could readily be included

in the automated process by applying a small modification to the CAD part file in the NBM plug-in of the disc assembly.

## 6.3. Automated SAS Model Construction and Results

This section deals with the demonstration of the CSI SAS flow network model generation capability. The process starts with the automated flow network recognition algorithm, followed by the automated construction of the 1D flow network model. As a starting point, it is considered that the CSI data model contains the design definition of the main annulus, rotors, and SAS features. The CSI generated 1D flow network elements and results are compared to the available validated engine 1D flow network model and output data.

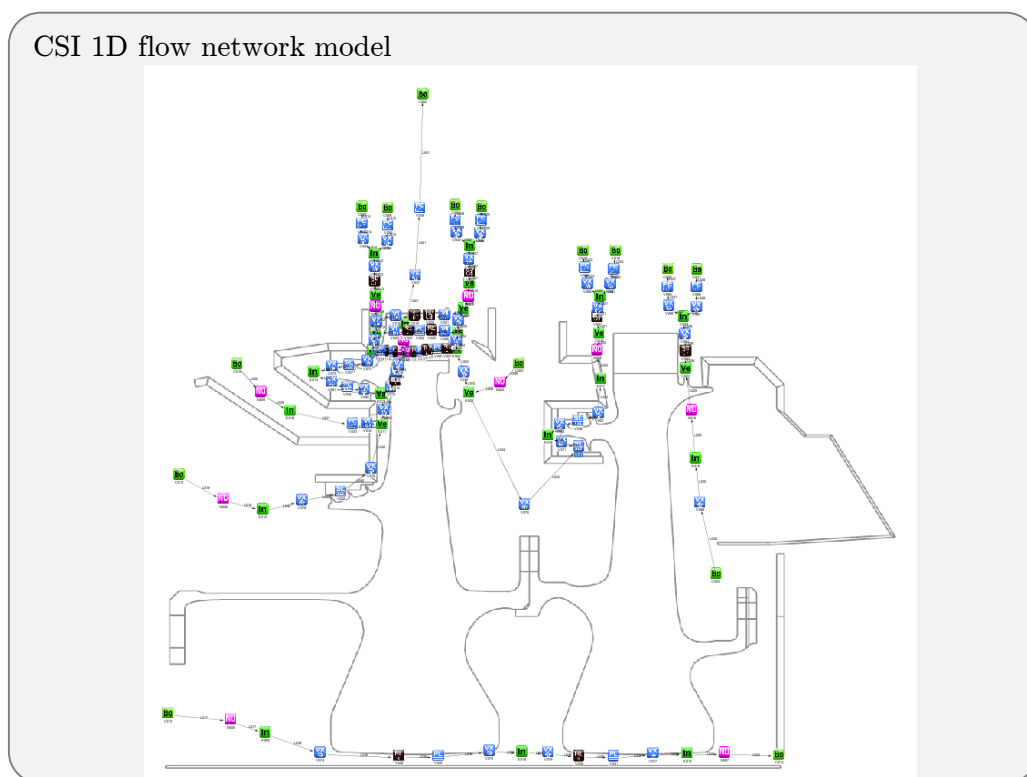


Figure 6.3.1.: Diagram showing the CSI automatically generated 1D flow network model over a 2D sketch of the HPT application case.

Table 6.2.: List of automatically extracted flow network information for the application case

<b>Cavities</b>	<b>Cavity description</b>	<b>Flow passages</b>
Cavity A	rotor-stator radial outflow	seal inlet
		rim boundary outlet
		firtree passage outlet
Cavity B	rotor-stator radial outflow	seal inlet
		pre-swirl nozzle inlet
		seal outlet
		cooling hole outlet
Cavity C	static axial flow	off-take boundary inlet
		pre-swirl nozzle outlet
Cavity D	rotor-stator axial flow	off-take boundary inlet
		seal outlet
Cavity E	inner firtree flows conjunction	disc post cooling hole inlet
		blade cooling boundary outlet
		firtree lobes slots inlet
		micro-turbine outlet
		firtree lobes slots outlet

### Flow network recognition results

The flow network recognition process is performed with the automated work-flow described in Section 4.4 Table 4.2 on page 83. The results of applying the algorithm are the list of flow network cavities and their connecting flow passages, shown in Table 6.2 on page 108. The algorithm automatically associates the list of CAD geometry curves that surround each cavity (as a dependency to a Java object with the curve tag and coordinates).

### Comparison of flow network elements and SAS analysis outputs

The flow network construction process is performed with the automated work-flow described in Section 4.4 Table 4.3 on page 84. The algorithm automatically creates the 1D flow network base file elements and maps its parameter values, based on the information collected from the flow network recognition process. In summary, the resulting CSI generated 1D flow network model is shown in Figure 6.3.1 on page 107.

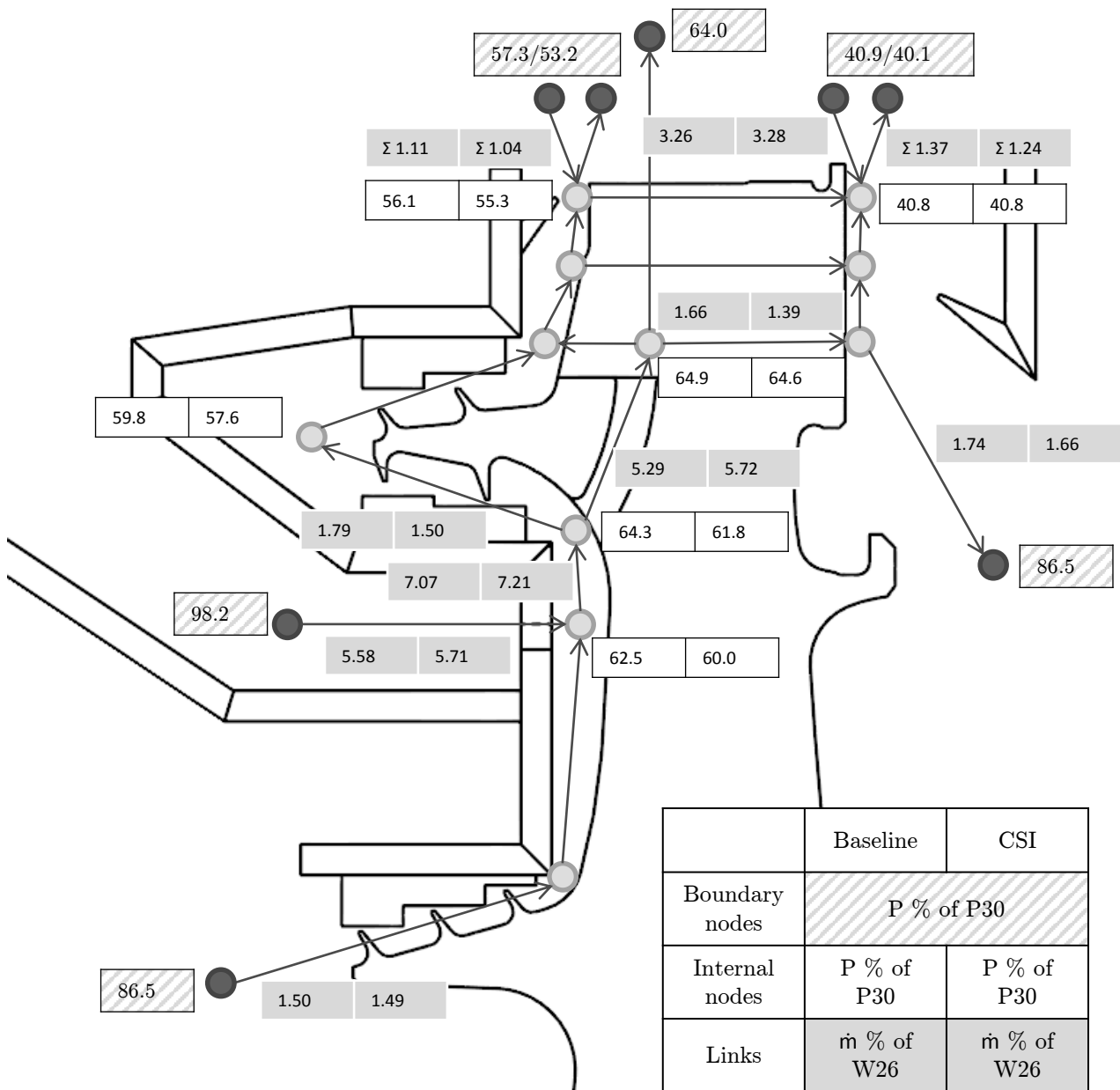


Figure 6.3.2.: Comparison of HPT front 1D flow network model output link mass flows and node pressures from the CSI automatically generated model vs. the validated reference model. Mass flows are shown normalised as % of W26 and pressures are shown normalised with P3.

The 1D flow network outputs presented in focus within this work are the mass flows and pressures in the flow network links and nodes. Figure 6.3.2 on page 109 shows a back-to-back comparison of the CSI model output against the validated model. The link mass flows have been normalised with the core engine compressor main annulus mass flow (W26) and the node

pressures have been normalised with the HP compressor outlet pressure (P3). It should also be noted that at the rim boundary nodes, there are two pressure values being shown, corresponding to the minimum and maximum of the hub pressure wave distribution. In accordance, the double link mass flow is shown as the sum of egress minus hot gas ingestion. In this application case, the sum is positive, meaning that the net mass flow at the rim is outwards, towards the main gas path.

In general, the mass flows at the network links between the CSI generated data and the validated data are in good agreement, with some moderate differences (below 10%) in the interstage cooling feed system. The node pressures are also well matched, with the highest difference (still below 5%) at the disc inlet of the blade cooling passage. Further discussion on the automated process outcomes is put forward in Section 6.6.

### **Flow network windage and pumping power losses**

The previously described 1D flow network model can be employed to assess the HPT subsystem windage and pumping power losses. A physical understanding of these factors has been presented in Section 3.2. Now, the rotor-stator windage and channel pumping powers that result from the CFD-enhanced 1D flow network model generated with the CSI approach are compared to the previously available preliminary design results.

In the flow network, each bit represents a known fluid thermodynamic effect, e.g. vorticity, sealing, pipe loss or hole's discharge. Additionally, heat transfer and power terms into the fluid can be implemented and calculated inside every network bit (e.g. windage effects in vortex bits). The 1D-cavity bits in the network that calculate windage power, swirl and thus total temperature changes have been enhanced with data extracted from parametric CFD calculations. The fundamentals of the CFD-enhanced approach and how windage profiles are generated are described in Section A.3. For the application case treated in this work, the CFD was pre-run on the front HPT pre-swirl rotor-stator cavity. As a result, generalized surrogate functions were extracted that can be used for the same cavity type in any new designs. These CFD-surrogates can be used as long as the cavities of the new design are analogous to the pre-run cavity. The surrogate CFD functions should be newly generated for designs with completely new cavity morphology.

Figure 6.3.3 on page 111 shows the windage and pumping power results of the CFD-enhanced



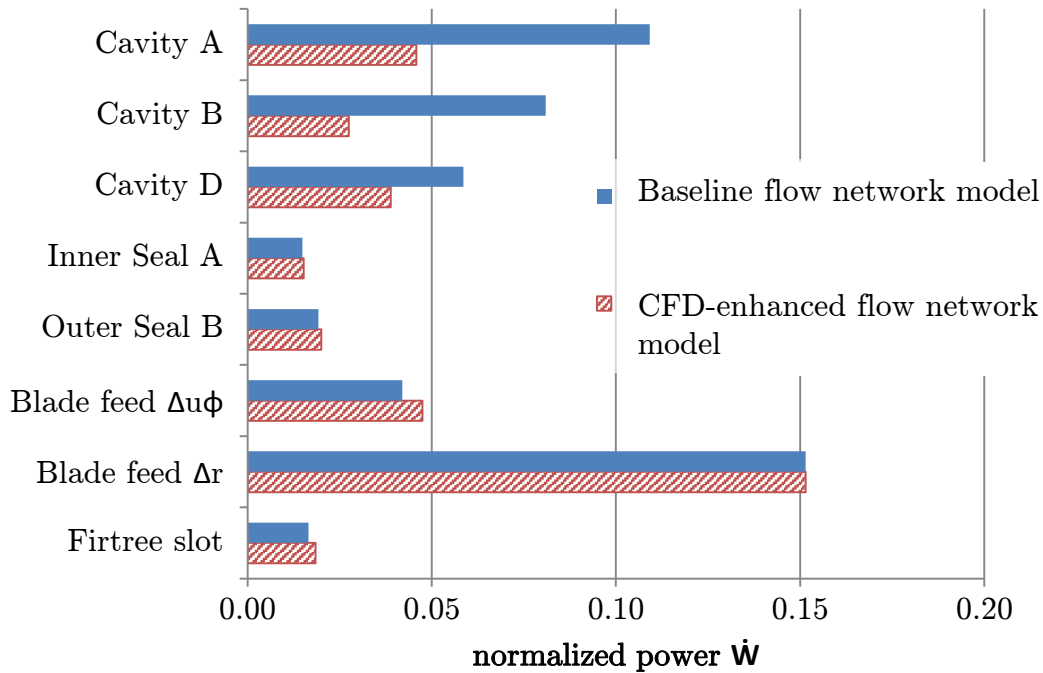


Figure 6.3.3.: Comparison of the front HPT SAS windage and pumping powers calculated with the enhanced flow network model and the previous preliminary design model. The power splits are normalized with  $\dot{W}_{SAS}$ .

flow network in comparison to the previous preliminary design calculation. In the shown figure, the power splits are normalised with the whole power loss of the HPT front SAS  $\dot{W}_{SAS}$ , as calculated with the previous preliminary design model. In addition to the values shown in Figure 6.3.3 on page 111, the pumping power of the blade cooling flow to the turbine blade rows gas path accounts for 48% of the front HPT SAS power losses  $\dot{W}_{SAS}$ . This contribution takes into account the radius change from the blade root to a mean main annulus exit radius. It has been omitted from the figure, because it would show the other contributions too small in the scale.

The CFD-enhanced calculated windage power splits of the rotor-stator cavities are smaller than the ones from the original preliminary design calculation. This in turn has an effect on the swirl velocity of the fluid entering the rotating channels. When the swirl decreases, the blade feed and firtree pumping power increases moderately. Considering the whole system, the integral power loss of the front HPT SAS calculated with the enhanced 1D flow network adds up to 0.83% of the overall HPT power, including the full blade cooling pumping power. The difference

to the previous preliminary design calculation is 12%, which translates into 0.1% of the overall turbine efficiency.

The presented comparison does not show which prediction is more accurate. Given that subsystem power splits cannot be practically measured experimentally in engine testing, the validation of these power split results would need to rely on temperature predictions with these new windage power assumptions. Thus, the accuracy of the CFD-enhanced thermal functions employed in this work will be demonstrated with the thermal analysis results in Section 6.4.

## 6.4. Automated Thermal FE-Model Construction and Results

This section deals with the demonstration of the CSI thermal FE-model generation capability. The process starts with the automated thermal FE-model inputs generation process, followed by the automated thermal FE-model construction and solver. As a starting point, it is considered that the CSI data model contains already the design definition of main annulus, rotors, and SAS features, as well as the flow network definition (Graph of cavities and flow passages) and the SAS output data. In the next part of the section, the CSI generated thermal FE-model inputs and results are going to be compared with the reference validated thermal FE-model.

### Automated thermal FE-model inputs

The generation of thermal FE-model inputs is performed with the automated work-flow described in Section 4.5 Table 4.4 on page 85. The resulting files after applying the automated process are listed below:

- the geometry definition file (2D \*.igs format),
- the journalising file (\*.jnl) including domain allocation, domain properties, mesh settings, analysis settings, and boundary conditions,
- the engine performance definition file (\*.bdd) including the analysis cycle, performance and aerodynamic data.

The geometry file is the result of exporting a 2D cross section of the CAD model in the appropriate format for the FE-tool (in this case \*.igs). Thus, the accuracy of the FE-model 2D

Table 6.3.: Ramp times and conditions of the application analysis cycle

Ramp	Condition	time (s)
1	stop	0
2	idle	5
3	idle	2000
4	high power	2007
5	high power	4000
6	idle	4015
7	idle	6000

geometry is as good as the one already shown in Figure 6.2.2 on page 106.

Regarding the analysis cycle, a so called squared operation cycle has been considered. The FE-tool will then solve the model through a transient time marching steady-state calculation. The cycle ramp times and conditions are shown in Table 6.3 on page 113.

The CSI automated algorithm to allocate and initialise the FE-model domains is able to replicate almost exactly the domain splits of the validated model. The CSI generated FE-model geometry highlighting the different domains is shown in Figure 6.4.1 on page 114, and it contains as much detail as any typical turbine FE-model.

It should also be noted that a turbine detailed design model contains typically a larger number of dummy-block domains, used for the detailed modelling of recirculation flows and leakages. Such high fidelity of recirculation modelling is usually out of scope in the preliminary design phase. Nonetheless, the CSI generated FE-model does contain some dummy-block domains to be able to simulate the most relevant recirculation flows, which demonstrates that the automated domain allocation algorithm is able to cope with all required modelling complexity. In addition, this algorithm automatically assigns the material, thickness and kinematic definition properties to the solid domains. This functionality enables the future application of automated optimisation strategies to select these properties.

The CSI algorithm to generate the thermal boundary conditions is one of the most complex parts of the work-flow, since it needs to take into account know-how from multiple disciplines: the design, engine performance, SAS flow network, and thermal modelling best practice. The results of applying the CSI automated process demonstrate that it captures the same complexity of structure and type of thermal boundary conditions as the previous manual process. The

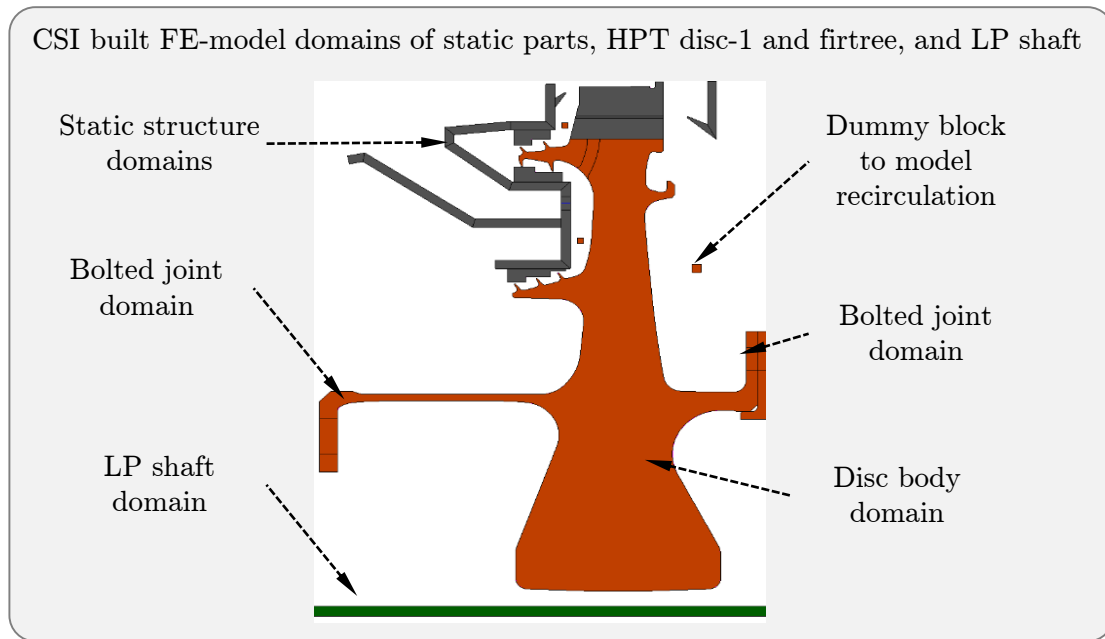


Figure 6.4.1.: Comparison of the HPT first-stage FE-model domains between the CSI generated, the reference preliminary model and the reference detailed design model.

automatically generated list of thermal boundary conditions replicates very nearly the validated thermal modelling scheme of the reference model. Some differences exist, which concentrate in the firtree area and the pre-swirl nozzle domains. These differences are due to the simpler representation of the firtree and pre-swirl nozzle features in the preliminary design models. Additionally, some of the cavity thermal boundary conditions in the CSI-generated model have been updated with the CFD-enhancement method, which is further explained in the appendix Section A.3. Figure 6.4.2 on page 115 shows the CSI-generated thermal boundary conditions applied onto the FE-model. For academic purposes, the comparison focuses on the front HPT cavities of the application case.

Regarding the CFD-enhanced thermal boundary conditions, the differences between the reference and the CFD-enhanced thermal modelling lie not only on the thermal inputs, but also on the orientation and type of thermal boundary conditions (e.g. after CFD analysis, a new recirculation zone has been introduced). The CFD-enhanced thermal modelling modifications include: stream directions, modelling of flow recirculation, mass flow distribution, swirl number, heat transfer coefficients, and heat pick up due to windage effects.

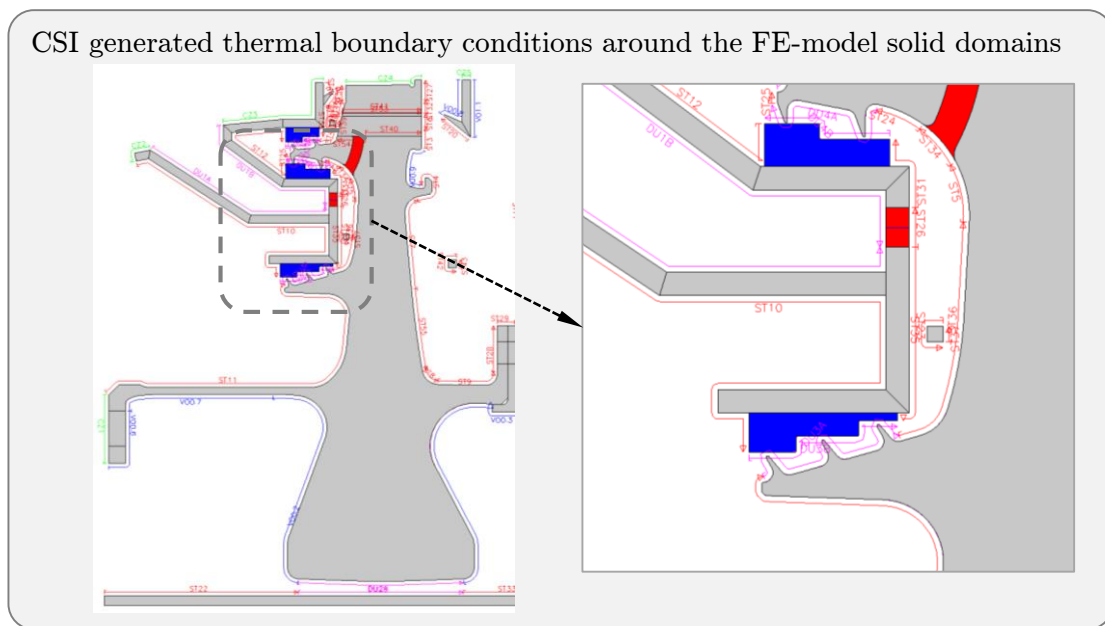


Figure 6.4.2.: Scheme of CSI generated FE-model thermal boundary conditions on the first HPT stage.

With all required inputs available, the final steps are the assembly of the thermal FE-model, the mesh generation and the solver processes, which are carried out with the work-flow described in Table 4.5 on page 86. The prediction of the thermal field that results at the end of these automated processes is discussed below.

### CFD-enhanced thermal FE-model results

The results of the thermal FE-model consist of the temperature distribution across solid domains, as well as of heat flux and fluid temperatures along the thermal boundary conditions. These results are typically analysed over a transient operating cycle, which in this application case considers a square cycle with acceleration and stabilisation phases between idle and high power operating conditions.

It is important for the understanding of the results to point out that the reference validated thermal FE-model was originally matched to a few thermocouple locations along the HPT disc walls. Figure 6.4.3 on page 117 shows the location of these thermocouples in the HPT front rotor-stator cavity that has the pre-swirl nozzle inlet and the disc cooling air holes outlet. The following results discussion will especially focus on this cavity.

In order to compare the temperature field resulting from the manual thermal modelling process to the CSI automated process, temperature results are shown in detail for the high power operating condition, as well as transient temperatures along the square cycle for one of the thermocouple points. Figure 6.4.3 on page 117 shows the temperature distribution over the first HPT stage rotor and static parts at the high power condition, when applying the CSI CFD-enhanced thermal boundary conditions. The temperature field has been normalised with the temperature of the incoming coolant flow  $T_{C^{ref}}$  from the HP compressor off-take flow, which flows into the pre-swirl rotor-stator cavity through the inner seal. A more detailed explanation on how the CSI generated model was enhanced with CFD extracted data can be found in the appendix Section A.3.

The temperature field that results from the thermal FE-analysis provides a valuable understanding of the heat transfer phenomena in the HPT subsystem. This temperature gradient across the disc radius is critical to the design for optimal component lifing. In a typical operating condition, the HPT disc cobs are cooler than the disc post, with a gradient that is controlled by the SAS cooling flows distribution. The impingement jet from the pre-swirl nozzle has a cooling effect in the area around the entry to the blade cooling air holes. However, the amount of cooling is a critical design parameter, since lower temperatures at local areas can lead to thermal gradients that deteriorate the disc's structural behaviour.

Now focusing on the pre-swirl rotor stator cavity, Figure 6.4.4 on page 118 shows the temperature deviations to the validated model along the rotor wall radius at high power condition. These temperature deviation results are normalized with the deviation of the previous preliminary design model at the location of thermocouple *RP1*. The curves in Figure 6.4.4 on page 118 thus present the uncertainty of models to the experimentally validated solution: one being the CFD-enhanced model uncertainty and the other one being the previous preliminary design model uncertainty.

The rotor wall temperature prediction with the CFD-enhanced thermal inputs is much closer to the validated data. The previous preliminary design thermal inputs led to results with deviations 4 to 7 times higher than the CFD-enhanced inputs. Not only is the temperature at the thermocouple location closer to the experimental data with the new technique, but also the surface distribution of temperatures runs smoother in between thermocouple points.

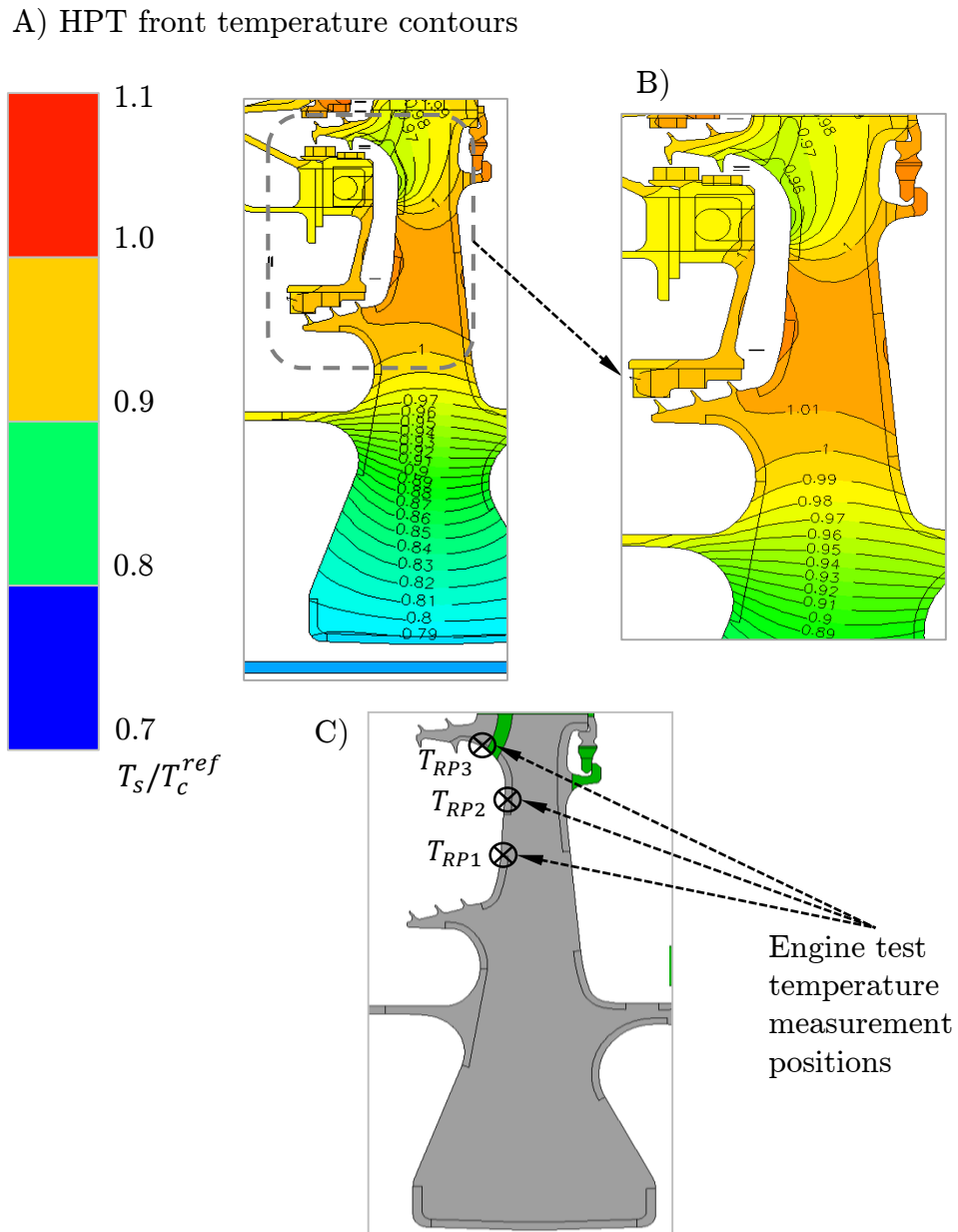


Figure 6.4.3.: A) Normalised temperature contours at high power condition, resulting from applying the CFD-enhanced thermal boundary conditions to the reference detailed design thermal FE-model; B) Shows detail on the temperature field at the pre-swirl rotor-stator cavity area; and C) shows the temperature measurement locations from the reference engine test data.

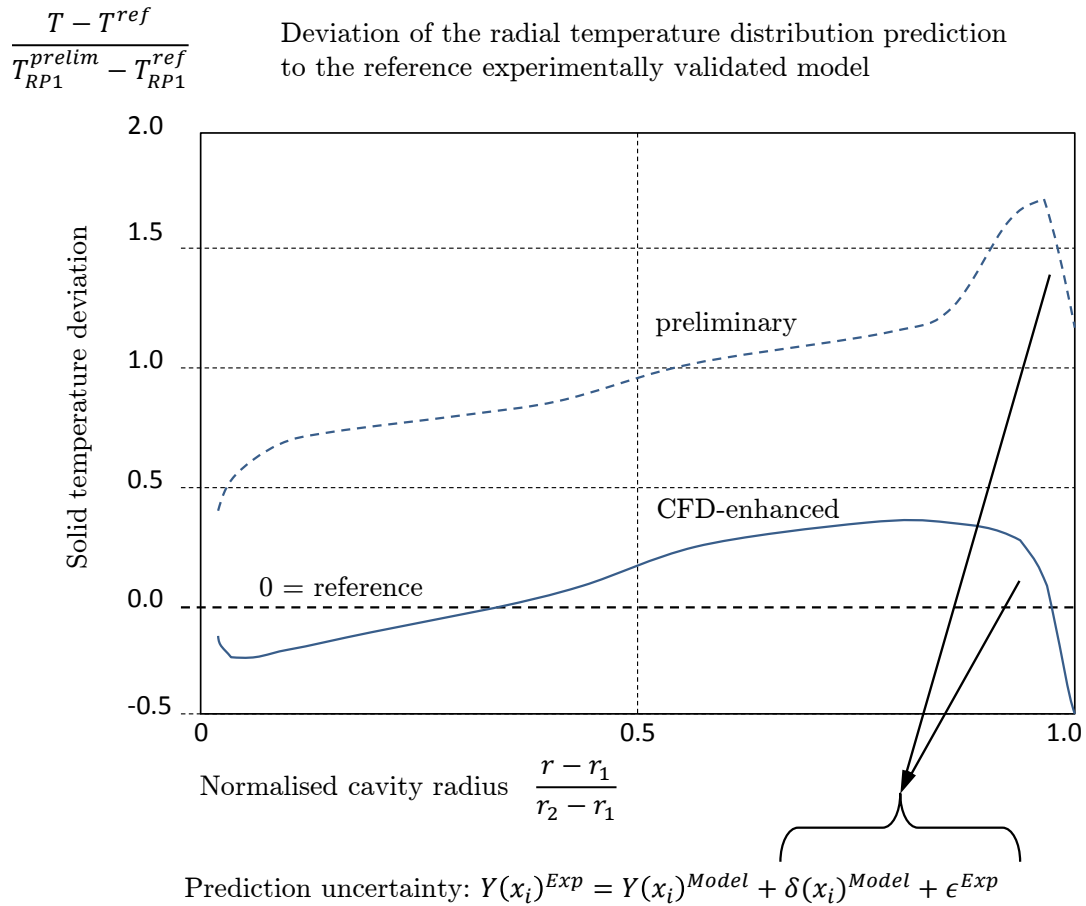


Figure 6.4.4.: Comparison of the pre-swirl cavity's rotor wall temperature prediction from the CFD-enhanced to the reference preliminary model, plotted as deviation to the experimentally validated model. The values are normalised with the temperature deviation at the thermocouple location  $RP1$ . The engine cycle conditions correspond to the stabilised high power operating condition.



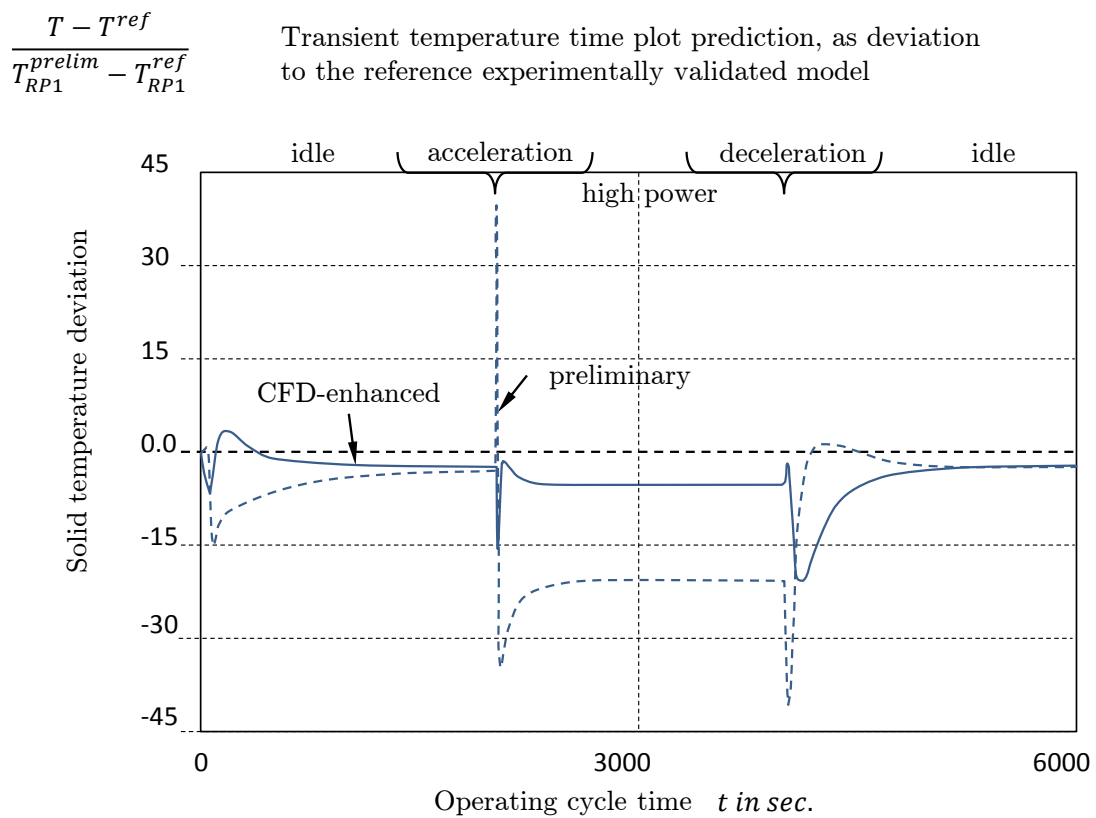


Figure 6.4.5.: Comparison of the time dependant temperature prediction at location  $RP1$  from the CFD-enhanced to the reference preliminary model, plotted as deviation to the experimentally validated model. The values are normalised with the temperature deviation at the thermocouple location  $RP1$ .

Figure 6.4.5 on page 119 presents the transient evolution of the uncertainty in the models at one of the rotor wall radial locations (*RP1*). Since the thermal inputs carry a correlation to operation and air system parameters, they are updated as the speed, air system pressures and mass flows vary along the different cycle time steps.

The deviations to the experimental data at the high power stabilised condition in Figure 6.4.5 on page 119 are the same as in Figure 6.4.4 on page 118, only with inverted sign. However, the uncertainty of the previous preliminary design model is a factor of 2 higher during the cycle transients than the uncertainty of the CFD-enhanced model. It should be noted that the CFD-enhanced prediction at deceleration phase is still not fully accurate, with a high peak of normalized uncertainty.

As a direct conclusion of this uncertainty analysis on the temperature predictions, there is some gained confidence on the CFD-enhanced thermal functions and therefore also on the SAS power splits from the CSI process, which were previously shown in Figure 6.3.3 on page 111.

## 6.5. Design Variation Study

This section presents an evaluation of how SAS design variations typical of the preliminary design phase can influence the HPT power losses. The CSI-generated flow network model with CFD-enhanced windage functions has been used to predict the power losses of the HPT subsystem, while varying an array of the SAS design parameters. Taking the reference front HPT SAS configuration as the baseline geometry (see Figure 6.1.1 on page 101), the following variations are applied in the parameter study:

- scaling of the main annulus inner rim radii (constant axial gaps),
- widening of radial rotor-stator cavity gaps,
- modification of pre-swirl system radius and skew angle,
- modification of seal radii,
- variation of operation speed.

Each design parameter has been varied from the baseline in a bandwidth of  $\pm 10\%$ . The parametric investigation in this work focuses on turbine power losses and disc ventilation flows.

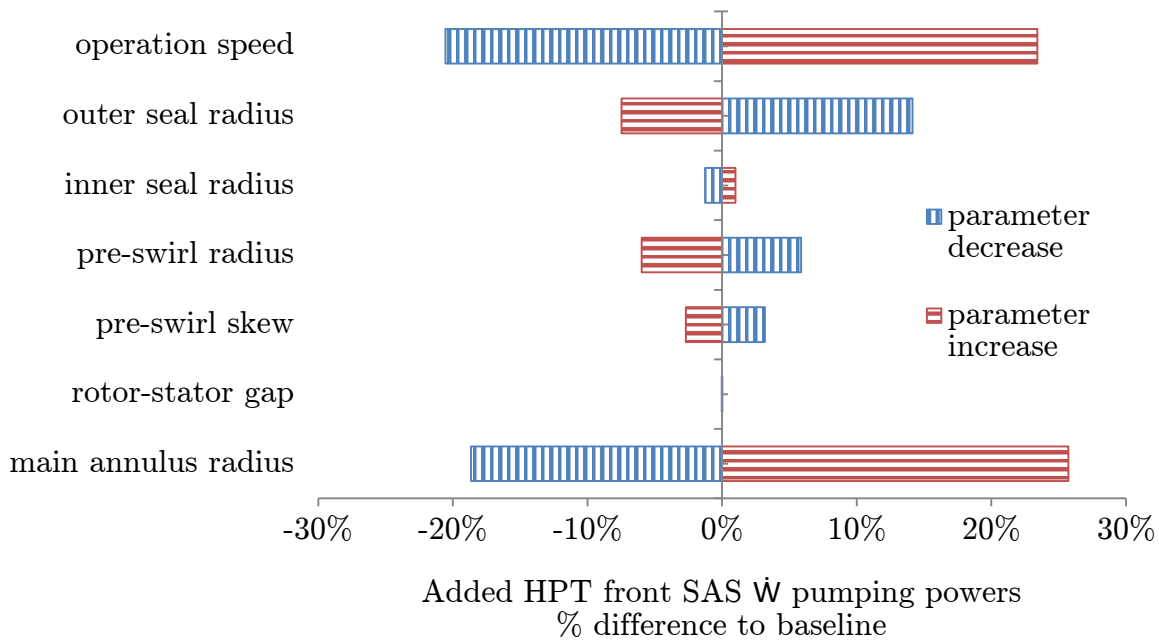


Figure 6.5.1.: Percentage impact of each SAS design variation of  $\pm 10\%$  on the power loss of the whole HPT front SAS. The baseline whole HPT front SAS pumping and windage power  $\dot{W}_{SAS}$  is the addition of the individual feature powers, presented in Figure 6.3.3 on page 111.

Nonetheless, it should be mentioned that the proposed variations would have consequences in engine bearing loads, performance, manufacturing costs, and robustness. A realistic design should take trade-offs for all of these disciplines into account.

Figure 6.5.1 on page 121 shows the impact of each parameter on the integral pumping and windage power of the front HPT SAS  $\dot{W}_{SAS}$ . The main annulus radii changes, which are common during the engine concept phase, have the highest impact on the subsystem power loss. The turbine rim line modifications shift the radial position of the cavities below, leading to variations of the rotor wall area that directly affect the viscous heating surface. The seal radii changes also imply higher surface and rotor wall tangential speed, thus higher windage.

The operation speed of the turbine evidently has a high impact on the integral power loss, since the pumping power  $\dot{W}$  is proportional to  $\Omega^2$  for the channels and the windage power is proportional to  $\Omega^3$  for the cavities. A parameter that has shown smaller impact is the rotor-stator cavity gap, at least in the parameter range where it has been varied. When increasing the gap, the cavity behaves more like a free disc system. The recirculation effect lessens and

the windage power slightly rises.

The pre-swirl nozzle radius has a moderate impact on the added subsystem powers  $\dot{W}_{SAS}$ . It has a negative correlation, where a higher radius reduces the losses. Even though a higher pre-swirl nozzle radius increases the windage in the pre-swirl cavity, it also benefits the inlet conditions to the blade cooling system. The optimisation of the pre-swirl system should be treated carefully, as its operation also depends on the off-take pressure conditions of the compressor where the air comes from.

In summary of these results, the assessed SAS design changes have a considerable impact on the overall HPT power  $\dot{W}_{HP}$ . For example, the +10% scaling of main annulus radius leads to around 0.2% change of the total HP power due to pumping needs. The positions of the seals and pre-swirl also have a considerable impact, which could be used on the benefit of a design optimization. Further conclusions about the methodology used to produce these results are drawn in the following chapter.

## 6.6. Results Discussion

The newly developed CSI common design environment has been used to demonstrate the preliminary design modelling of a HP turbine subsystem. An existing turbine design has been chosen to verify the outputs of the proposed automated process against available validated engine models. In such, the preliminary design definition of the reference turbine subsystem has been reproduced using the newly developed CSI tool. Then, the automated work-flows have then been used to generate the corresponding CAD models, to recognise the subsystem flow network, to generate the SAS 1D flow network model, and to generate the thermal FE-model. The automatically constructed models and their simulation results have been compared against the experimentally validated models of the reference turbine case. Upcoming is a discussion of the results to each part of the work.

### Subsystem Design

The following conclusions can be drawn from the application of the CSI processes to the preliminary design definition of the reference HP turbine case:

- The CSI environment facilitates a more agile design process of the rotors and SAS features, where the parameters of the various disciplines are integrated and can be interconnected.
- Every design feature of the subsystem has been stored in XML format as an object in a programmable Java based data tree. The benefit of this approach is that the design data or parts of it can now be readily transferred, reused or modified. Furthermore, since the design data is stored as Java objects, which have interdependencies to one another, it is easier to manipulate the data with programmable algorithms that aid the engineering processes.
- The CSI CAD model generation process can automatically assemble a geometry model containing a high fidelity definition of the rotors and a low fidelity definition of static structures with SAS features. The automatically generated HPT rotors geometry is analogous to the geometry of the reference detailed design CAD model.
- Some CAD differences can be found in the discs firtree area, associated to the higher level of 3D detail definition proper of the production design phase. The CSI generated static structure geometry was not present in the previous preliminary design model. On the other hand, the static geometry in the detailed design model has much higher fidelity than the CSI-generated one. Nevertheless, the CSI static structures definition is sufficient to capture the complexity of the SAS layout needed to build the flow network.

### SAS modelling

The application of the CSI automated SAS modelling process has led to the following results:

- The CSI algorithm for flow network recognition is able to resolve the relevant flow passages and cavities of the given HP turbine design. The automated process can even recognise complex multi passage features, such as the turbine disc firtree with blade cooling passages and a micro-turbine interstage flow.
- It has been demonstrated that the automated work-flow can generate a high fidelity SAS 1D flow network model. Its results of node pressures and link mass flows have been compared against data from the reference validated engine model. There is good agreement between both sets. Some differences exist between both models, which seem to be caused by the somewhat different boundaries of the subsystem and the fine detailed

leakage flows in the validated model.

- The CSI generated 1D flow network model has been enhanced with power and heat functions within the individual flow elements. Some of these power functions have been derived from CFD analysis data. This functionality has then been used to calculate the subsystem pumping and windage power splits.
- The difference on estimated HPT front power loss between a previous preliminary design calculation and the CFD-enhanced flow network is 12%. These power losses add up to 0.83% of the overall HP power.

### **Thermal FE-modelling**

The application of the CSI automated thermal FE-modelling process and the CFD-enhanced thermal modelling methods has led to the following results:

- It has been demonstrated that the thermal FE-model inputs can be automatically generated with the CSI automated work-flows.
- The FE-model geometry file is exported from the automatically generated CAD model, featuring its same level of fidelity. As a new functionality, the CSI process can resolve automatically the FE-model domains allocation. The domain properties such as material, speed, or thickness, are then captured in the Java definition of the design and associated to each individual feature. This functionality enables the automatic control of material selection and kinematic properties.
- Moreover, the performance, aerodynamics and cycle data for the FE-model can also be automatically managed within the CSI environment. Here, the SAS flow network model outputs can now be mapped into the SAS features in the Java data tree. This further enables the SAS data to be automatically mapped into the thermal boundary conditions.
- A key function of the CSI work-flow is the automatic generation of the thermal boundary conditions. This is not trivial, since the process needs to take into account the physical understanding of how features affect flows. It has been demonstrated that a high fidelity set of thermal boundary conditions can be automatically generated. As an added capability, these boundary conditions are able to carry CFD-enhanced thermal inputs.
- The temperature results of the CSI-generated thermal FE-model are in good agreement

with the reference validated model prediction. The CSI CFD-enhanced thermal results improve the prediction of the previous preliminary design model. The improvement can be seen in both the radial gradient of temperatures for a given operating condition and in the transient evolution of a point temperature across the analysis cycle.

- More specifically, the results indicate that the temperature prediction deviation to the validated data of the previous modelling techniques is 4 to 7 times higher than the deviation of the CFD-enhanced thermal model. When analysing the transient behaviour of the rotor through accelerations between idle and high power, the temperature prediction of the model with CFD-enhanced inputs is even 10 times closer to the test data than the prediction from the traditional method.
- The reference validated model had been matched to the engine test data at discrete points (thermocouple locations). However, in between measurement points there is still a model prediction uncertainty in the validated model. Therefore, which technique truly represents the real rotor surface temperature distribution is still uncertain. Nevertheless, the CFD-enhanced technique provides a deeper physical understanding of the flow heat transfer phenomena.

### Design variations study

The design variation study performed with the CSI work-flow has helped to assess the impact of the SAS parameters in the subsystem pumping and windage power needs. This assessment has led to the following results:

- The CSI environment enables parameter studies to be performed, where a parameter modification can be propagated to the rest of subsystem features. Such functionality can provide a better understanding of the impact of the design parameters on the general subsystem performance outputs, such as the integral subsystem pumping and windage power losses.
- It was found that rim line radii scaling and operation speed are the biggest contributors to the HPT SAS power losses. Moreover, the effect of the rotor-stator cavities' windage should not be underestimated in designs with very large radial cavities, since it has a very strong dependency to the radial height of a cavity:  $r_2^5 - r_1^5$ .

- This investigation focused on HPT front SAS variations, which lead to deviations on HP overall power in the order of 0.1%. When considering the complete SAS of an aero engine, there is a relevant overall power optimization potential for the gas turbine community.



---

# 7

## Conclusions & Outlook

---

This work illustrates the proof of concept of a novel process for the preliminary design of aero engine subsystems, focused on the automation of the design and analysis of turbine components. The research began with the review of previous work and the preparation of the scenario to set the purpose for this work. It was followed by the development and implementation of the newly automated process, and it ends with the application of the process to a real turbine design in order to validate the implemented advanced common design environment.

In the final section, an outlook is given with future steps to continue this research. The future perspective includes a proposal to apply the newly developed methods to the concept design phase of further subsystems and arising aero engine technologies.

### 7.1. Conclusions

The combination of geometry, secondary air system, and flow field thermal parameters involves such a large number of variables that traditional manual design evaluation can rarely optimise all characteristics of the system in the short time frame of the preliminary design phase. The application of parametric studies using probabilistic and optimization algorithms opens the possibility to search for multi-disciplinary optimised designs. In this framework, a large number of parameters and their interdependencies can be adjusted in such a way that aero engine

subsystems could be greatly improved. However, a key prerequisite for applying such algorithms is the automation of the engineering work-flow to drive the design and analysis models. This work has concentrated on the integration and automation strategy of the design and analysis tools.

Regarding the design and analysis disciplines to simulate the aero engine, the state of the art in virtual engine methods has reached a mature state. The current tools offer high level of fidelity and are able to capture the fine detail of heat transfer phenomena in the cavities of the secondary air system. However, these tools have until now required a careful manual set up of many model data sets, which made this task one of the most time-restricting in the preliminary design phase of an aero engine.

Within this work, a common preliminary design environment has been developed that captures in one platform the integral subsystem design data: main annulus aerodynamic design, rotors design, SAS layout, parametric CAD models, flow network definition, flow network simulation results, detailed cavity flow CFD analysis, and thermal analysis via the FE-method. The missing engineering disciplines, planned for future work, are the structural analysis, lifing, and cost management of the subsystem components.

### **Conclusions of the automated CAD modelling process**

The automation of CAD model generation has been solved with a combination of three previous strategies, i.e. the parametric sketch design, the standard UDF's approach, and the CAD programming approach. Within the newly developed CSI environment, parametric sketch CAD models can be loaded as plug-ins, which act as enhanced UDF's with a Java NBM interface. The CAD geometry of turbine rotors can be loaded as one of these plug-ins, including high fidelity of curves, fillets, and detailed features. The CAD geometry of static structures is built from individual blocks, with a connection logic that is specified by the user. To finalise the process, the automated programming CAD approach is applied to merge geometry blocks, trim model lines and produce a clean geometry model suited for the thermo-mechanical analyses.

### **Conclusions of the automated flow network recognition and modelling process**

A key step in the process of generating secondary air system and thermal models is the recognition of the subsystem flow network. This process has been automated by making use of the

CSI data model object oriented capabilities and the storage of flow network data in the form of a directed multi-graph.

The availability of flow network data in graph format enables the management of SAS flows, cavities and flow passages within the programming environment. This capability, joined with a database of standardised flow network elements, enables the automated assembly of 1D flow network models. The intention behind this approach is to facilitate the engineering end user the ability to rapidly perform flexible modifications of the SAS layout.

### **Conclusions of the automated thermal FE-modelling process**

An additional advantage of the graph with flow network features is the management of thermal modelling schemes for each cavity and flow passage type. Again, joining this capability with a database of thermal modelling templates has made the automatic generation of thermal boundary conditions possible. Since the thermal boundary conditions are now associated to flow network graph objects, their interdependencies can automatically be resolved and updated when design modifications are introduced.

Furthermore, the CSI data objects that represent thermal boundary conditions have been implemented with the ability to carry flow field data profiles from CFD analysis. This permits the use of CFD-enhanced thermal functions, which have been proven to improve the accuracy of temperature prediction during design stages where no engine test data is available.

In order to automatically generate the thermal FE-model inputs, data sets from all previous disciplines need to be combined. Having the integral subsystem data gathered in a common design environment facilitates this process. The last step in the automation challenge is to export each set of data in the correct format readable by the FE-tool. To complete the thermal FE-model inputs, the CSI work-flow automatically resolves the FE-domain allocation, allowing the end user to flexibly modify the material and kinematic properties.

### **Conclusions of applying the process to a real HP turbine design**

The newly developed CSI environment has been applied to reproduce the preliminary design and model generation of an existing HP turbine internal system.

The results of the automated process have been compared to the available experimentally validated SAS and thermal FE-models of the chosen reference design. The CAD geometry of

turbine rotors from the automated process compares very well to the detailed design geometry. The automated static structures CAD geometry is rudimentary, but it fulfils the purpose of providing a frame for building the SAS flow network.

Regarding the SAS 1D flow network model results, the nodal pressures and link mass flows from the automatically generated model are in good agreement with the validated data. There are some result differences within acceptable tolerances for the preliminary design phase, which are attributed to the calibration of subsystem boundaries.

Moreover, the results of the automated CFD-enhanced thermal model present an improvement with respect to the previous preliminary design model. Both, the rotor surface heat transfer profile and the transient evolution of temperatures, are better replicated by the CFD-enhanced thermal model, when compared to the available validated model prediction that had been matched to engine test data.

As a finding of the application, having the possibility to gather design data from the various engineering disciplines in one data model has proven a valuable aid for the management of design modifications. Furthermore, the process of CAD, SAS and thermal FE-model generation, which previously lasted weeks, can now be performed in less than 1 hour. However, this gained agility can only be expected once the standard features database contains the adequate set of data for the attempted design. Otherwise, the database preparation time needs to be taken into account, which for a full new design could suppose a time period in the order of the traditional process. Nevertheless, as the database is expanded, more and more designs can be automated. Thus, unlike in the traditional process, the CSI environment and database approach makes full usage of work re-usability benefits.

In the last part of the research, the CSI automated work-flow has been used to perform a SAS design variation study of the reference HP turbine. This study demonstrates some of the CSI design modifications ability and it helps to understand the behaviour of the subsystem when design variations are introduced. As a conclusion of the study, it has been realised that there is big room for optimising the performance of the aero engine subsystem, and it is also clear that the user of the engineering process must always maintain close communications with the engineering stakeholders, so that the automated approach does not forget the assumptions behind the design criteria.

## 7.2. Outlook

The next step for this research is the deployment of the simulation environment and automated work-flows in the application of an aero engine component optimisation. This would involve applying the CSI process to new component design systems of aero engines. The following future work proposals are recommendations to continuously improve the CSI engineering process:

- For the developed processes to be of practical use, it is crucial to continue the extension of the standard feature databases with the parametric CAD model NBM plug-ins, the SAS flow network elements, and the thermal modelling templates with further CFD analysis data.
- The fidelity of the automated geometry generation process can only be as good as the template CAD models stored in the database. Therefore, improved parametric CAD models of further components would have a direct benefit in the outcomes of the CSI work-flows.
- Regarding the modelling of the SAS, an identified potential functionality is the automatic loading of existing full engine 1D flow network models into the CSI Java data model. This would enable the user to integrate former models without necessarily going through the automated flow network process. Additionally, the interface process between the 1D flow network model and the thermal FE-model could be further improved. This has been solved in the current work with a parameter interface file (BDD file), but the communication between the two models could be solved with direct programming linkage.
- In relation to the FE-model capabilities, the combination of 2D and 3D geometry for thermal and structural analysis is considered as high potential. This would enable thermo-mechanical analysis to be performed with mixed critical features defined in high 3D fidelity together with less relevant features defined in 2D.
- To further improve the automation of the process, it would be recommended to implement a programming-driven extraction of CFD analysis profiles and translation into traditional thermal boundary conditions. Furthermore, there is an interest to automatically deliver the inputs and solve the interfaces for a fully coupled transient simulation of the 1D flow network model, the thermal FE-model, and multiple cavity CFD models. This capability

would enable the transient convergence of running clearances and gaps with very high accuracy.

- In a further engineering step, the developed common design environment could be extended with the functions to handle structural analysis, vibrations, component lifing, and a life-cycle cost calculation unit.

As the state of the art in virtual engine systems advances, the methods which used to be considered adequate for detailed design move into the category of preliminary design. The detailed design methods are substituted with new ones of higher accuracy and the preliminary design methods benefit from the experience of the detailed design legacy.

---

# A

## Appendix on Applied Thermal FE-Modelling

---

## A.1. Categorisation of thermal boundary conditions

In thermal FE-analysis, thermal boundary conditions are used to simulate the conditions of the fluid around the solid geometry that is to be meshed and resolved. The most common thermal boundary condition types are presented below.

- Prescribed heat flux: application of a known heat flux or heat flux distribution.
- Prescribed temperatures: Application of a known temperature or temperature distribution, which typically comes from a measurement on a component test.
- Convecting zone: Assumes a region of infinite heat capacity. The fluid temperature will not change regardless of the heat transfer to the solid components.
- Thermal void: In contrast to a convecting zone, a thermal void can be considered as a region of negligible heat capacity. It represents a region with a uniform temperature which is in equilibrium with its surroundings. The heat flux can however vary along the void contour.
- Stream: represents a finite flow of fluid with given direction and a finite heat capacity. A stream is able to absorb heat from one location on the surface and transport it to another. The change of fluid temperature along the edge is calculated considering the convection heat transfer and additional energy inputs, such as windage.
- Duct: similar to a thermal stream, with the difference that a duct is defined on two edges of narrow passages. As a result, heat can be exchanged between both surfaces and can be transported via the flow.
- External radiation: used to simulate radiative heat transfer from a source outside the model. The temperature of this source is not influenced by the heat transfer to or from it.
- Internal radiation: applied on internal model edges which are able to receive and transmit radiative heat from themselves to other boundaries.
- Thermal contact: used to apply full or partial heat conduction on an interface.



## A.2. CFD-enhanced Thermal FE-Modelling

There are four basic flow field properties that carry the information of how heat transfer occurs between solid and fluid domains: the mass flow  $\dot{m}$ , the swirl number  $\beta$ , the heat transfer coefficient  $HTC$ , and the heat pick up rate  $HPU$  due to rotational power (i.e. windage). The fundamentals of flow phenomena in rotor-stator systems of the SAS have been presented in Section 3.2.

These four flow field properties can be extracted from 3D CFD simulations and implemented as inputs to the thermal FE-model via the boundary conditions. In the approach presented in this work, each of the four thermal properties is built from three part functions, as it is exemplified in (A.2.1) for the  $HTC$ . The three part functions are defined as follows:

1. dependency to the geometry profile extracted from CFD:  $f^{input}(x_i)$ ,
2. correlation to engine operation parameters:  $g^{input}(\Omega)$ ,
3. dependency to cavity topology via a factor from the parametric CFD simulations, which scales the input when dimensions are varied:  $Fc^{input}(cavity)$ .

$$HTC = f^{HTC}(x_i) \cdot g^{HTC}(\Omega) \cdot Fc^{HTC}(cavity) \quad (\text{A.2.1})$$

The CFD analysis is pre-run on cavities where the local flow field phenomena are relevant to the heat transfer modelling of the system. As a result from the CFD analysis, generalised surrogate functions are extracted that can be used for the same cavity types in any new designs. These CFD-surrogate models are used as long as the cavities of the new design are analogous to the pre-run cavities. The surrogate CFD functions should be newly generated for designs with completely new cavity topology. To exemplify this methods, an application of CFD-enhanced heat transfer functions is demonstrated for the topology rotor-stator cavity in Section A.3.

## A.3. Rotor-Stator cavity application of CFD-enhanced thermal functions

As an example application of the CFD extracted heat transfer functions, this section describes the process followed for a turbine rotor-stator cavity with a seal inlet, a seal outlet, a pre-swirl

nozzle inlet, and rotor cooling air holes outlet. A diagram of this cavity can be seen in Figure 3.4.1 on page 63. Before describing the process for this particular cavity, it should be noted that the methods for extraction of heat transfer functions from CFD analysis are very case dependant. As such, the methods presented here are well suited for the flow field of this example cavity, but should be treated with care for other types of SAS cavities.

In order to extract the flow field functions  $f^{input}(x_i)$  from the pre-run CFD model, some post-processing needs to be performed. The mass flow and swirl ratio distributions can be directly extracted from the CFD output by applying post-processing planes to areas of flow streams or recirculation. The outwards mass flow rate in a recirculation zone can be determined by integrating the fluid density times radial velocity across the axial direction at the radial location of the recirculation centre. (A.3.1) presents the ratio of rotor side mass flow over cavity inlet mass flow, which is greater than 1 in a rotor-stator cavity with recirculating mass flow. The swirl ratio at every radial position can be calculated as the mass-weighted averaged swirl ratio across the radial plane:  $\beta = \frac{u_\varphi}{\Omega \cdot r}$ .

$$\frac{\dot{m}_{rotor}}{\dot{m}_1} = \frac{(|\rho \cdot u_r \cdot A| + \rho \cdot u_r \cdot A)}{2 \cdot \dot{m}_1} \quad (\text{A.3.1})$$

The *HTC* and windage *HPU* functions require some more post-processing from the CFD output. The *HTC* in this application case can be determined via Reynolds analogy, (A.3.2), and the windage power input is calculated as the moment of the wall shear stresses, (A.3.3).

$$HTC = \frac{\tau_\varphi(r) \cdot c_p(r)}{u_\varphi(r) \cdot Pr^{0.4}} \quad (\text{A.3.2})$$

$$HPU = \tau_\varphi(r) \cdot r \cdot \Omega \quad (\text{A.3.3})$$

As an example of the CFD extracted heat transfer functions, Figure A.3.1 on page 137 shows the windage profile along rotor radius of the example turbine rotor-stator cavity. The plot compares three windage functions: the raw CFD extracted data, the traditional preliminary design windage function, and the new CFD-enhanced windage function. The piece-wise linear function that approximates the CFD data, rather than the raw CFD data itself, is what will be implemented in the thermal boundary conditions of the FE-model. An analogous plot is shown

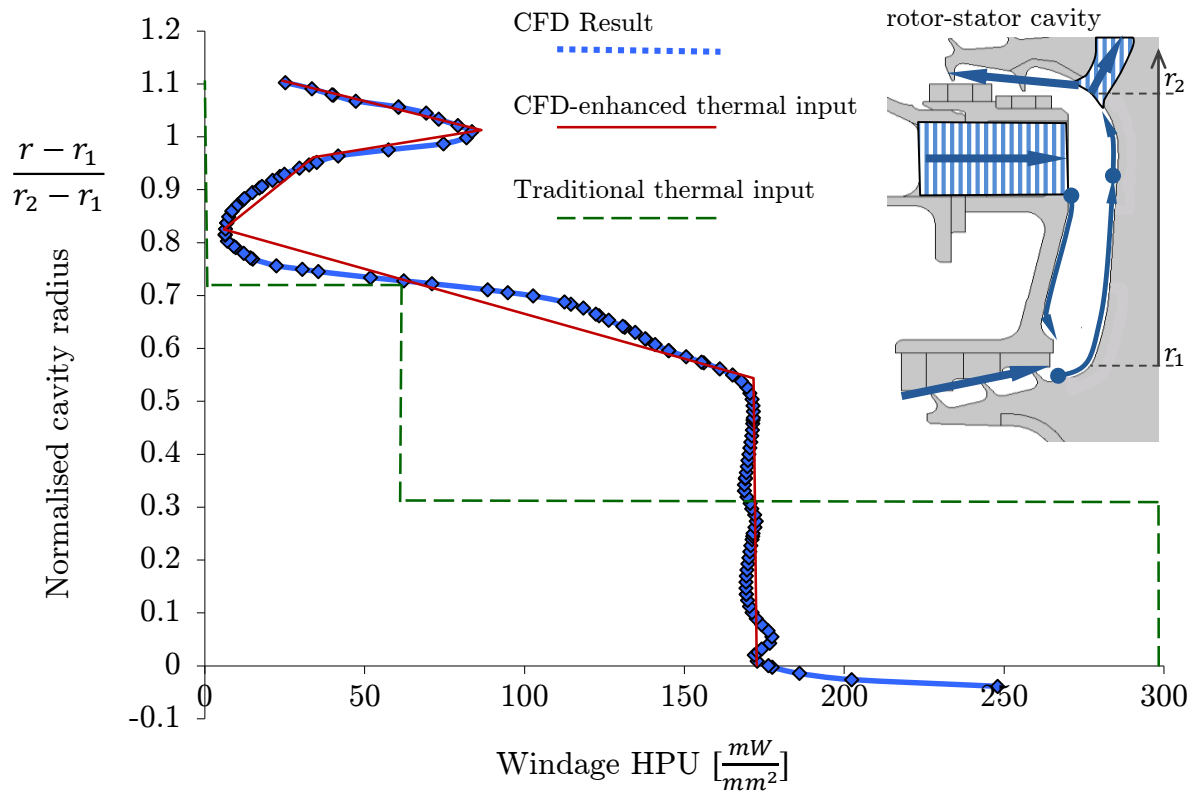


Figure A.3.1.: Radial distribution of rotor windage  $HPU$  in a typical HP turbine front rotor-stator cavity.

in Figure A.3.2 on page 138 for the  $HTC$  profile along rotor wall radius of the example turbine rotor-stator cavity. It should be pointed out that no direct CFD  $HTC$  profile data is shown at the zones where the pre-swirl nozzle impingement and the cooling holes inlet are located, since the Reynolds analogy is not valid in areas where the tangential velocity tends to null.

The  $HTC$  radial profile from Figure A.3.2 on page 138 is then combined with the functions of operation and cavity topology dependency, as described in (A.2.1). Regarding the dependency to operation parameters, so called  $g^{input}(\Omega)$ , the scaling functions for each thermal input and their implications are described in Section A.4.

Finally, the functions of cavity topology  $Fc^{input}(cavity)$  are generated through a DOE set of analyses with a parametric CFD process. This parametric CFD surrogates can be a polynomial approximation as in (A.3.4) or (A.3.5), where the coefficients are chosen to best fit the CFD results across the design space of the cavity parameters ( $x_i$  being one of the cavity dimension parameters normalized with its baseline value  $x_{i,BL}$ ). In REY VILLAZON, J. M. et. al. (2013)

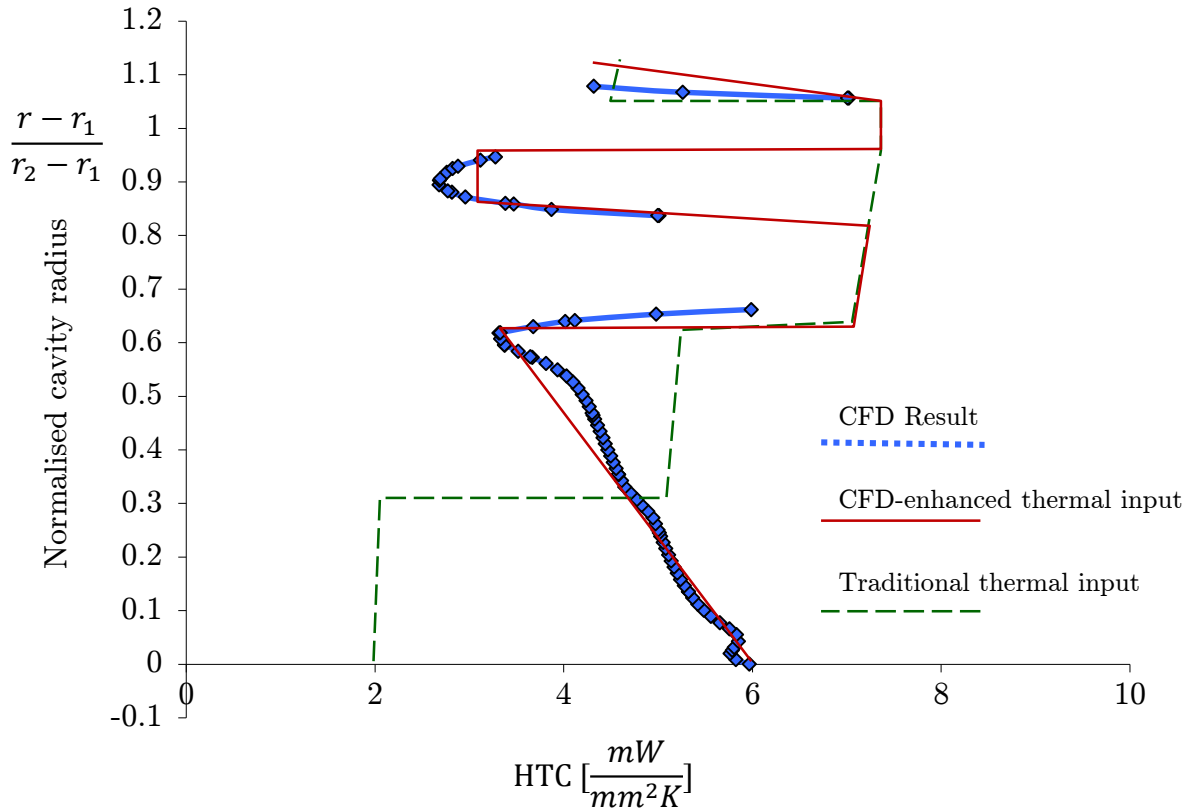


Figure A.3.2.: Radial distribution of  $HTC$  in a typical HP turbine front rotor-stator cavity.

can be found a more detailed description of how a parametric CFD process can be set up to generate the CFD-enhanced heat transfer functions.

$$F_C^{HPU} = C_0 + \sum_{i=1}^n C_i \cdot \frac{x_i}{x_{i,BL}} \quad (\text{A.3.4})$$

$$F_C^{HTC} = D_0 + \sum_{i=1}^n D_i \cdot \frac{x_i}{x_{i,BL}} \quad (\text{A.3.5})$$

## A.4. Cycle scaling of CFD-enhanced thermal boundary conditions

In order to prepare scaling rules for thermal functions extracted from CFD analysis data, it is necessary to assess the changes in the cavity flow field when the operating condition of the

engine is changed. In case that the flow field is significantly changed for different operating conditions, simple scaling equations will not be valid and different sets of CFD data will have to be used to create the CFD-enhanced thermal functions. However, it is common in most turbine rotor-stator cavities that the flow field is only slightly modified in between the typical operating conditions. For these cases, it is possible to use simple scaling equations to extrapolate the CFD-enhanced thermal functions along the engine operating cycle.

Following is a description of cycle scaling rules for the four fundamental thermal functions: the mass flow  $\dot{m}$ , the swirl ratio  $\beta$ , the heat transfer coefficient  $HTC$ , and the heat pick up rate  $HPU$  due to rotational power.

The local mass flows in a rotor-stator cavity, including the recirculation mass flow, can in most cases be scaled with the cavity through flow. For the application HP turbine front rotor-stator cavity, shown in Figure 3.4.1 on page 63, the cavity inlet mass flow through the inner seal is a good variable to drive the local mass flows when operating conditions are changed. In this sense, the ratio of recirculation to inlet cavity mass flows can be assumed constant, thus scaling the recirculation flow with the cavity inlet mass flow along the engine cycle.

The swirl ratio distribution is very dependent on the cavity type being analysed, and thus, the scaling factor for a cavity category cannot be read across for other cavity categories. In the example cavity, the swirl ratio distribution remains mostly unchanged through the operation of the engine (except for very low start up speeds). Therefore, a time-constant swirl ratio distribution is a fair approximation for this case. It should be noted that when the swirl ratio remains constant, the fluid tangential velocities are scaled with the rotational speed of the turbine.

For the  $HTC$ , the traditional correlations dependent on the  $Re$  number that are available in the literature can be used as the scaling rule for the operating condition. This implies using the  $HTC$  radial profile from the CFD analysis, but scaling the profile with an adequate correlation, such as the forced convection from a free disc with turbulent flow from DORFMAN (1963), shown in (A.4.1).

$$HTC = 0.0267 \cdot Pr^{0.6} Re^{0.8} \frac{\lambda}{r} \quad (\text{A.4.1})$$

The windage  $HPU$  function scaling equation can be derived taking into account the correlations

of the moment coefficient  $c_m$ , as defined in (3.2.12). For a typical rotor-stator cavity under turbine high power operating conditions, the  $HPU$  is a function of the operational parameters, as in (A.4.2). Thus, the scaling rule for the  $HPU$  can be expressed as in (A.4.3).

$$HPU = f(r) \cdot \Omega^2 \cdot r^2 \cdot \frac{\dot{m}}{A} \quad (\text{A.4.2})$$

$$HPU = HPU_{ref-op} \cdot \frac{(\dot{m} \cdot \Omega^2)}{(\dot{m} \cdot \Omega^2)_{ref-op}} \quad (\text{A.4.3})$$

As a final note, the scaling rules for CFD-enhanced thermal boundary conditions present a quick and low fidelity method to extrapolate CFD results along the engine cycle. However, a method of better accuracy, computational resource permitting, would be to use transient thermal-CFD coupling that resolves the fluid-solid heat transfer problem with more physical detail across all time points of the engine operation.

## Bibliography

---

ALEXIOU, A. and MATHIOUDAKIS, K.

Secondary Air System Component Modeling for Engine Performance Simulations. *Journal of Engineering for Gas Turbines and Power* 131(3), 2009, P. 031202.

ANTINORI, G.; MULLER, Y.; DUDDECK, F. and FISCHERSWORRING-BUNK, A.

Statistical Methods for a Stochastic Analysis of the Secondary Air System of a Jet Engine Low Pressure Turbine. In: *Proceedings of the ASME Turbo Expo 2013: Turbine Technical Conference and Exposition*. New York and N.Y: ASME, 2013, P. V03AT15A009.

ATKINSON, K. E.

*An introduction to numerical analysis*. 2. Inlage. New York NY u.a: Wiley, 2004.

AUNGIER, R. H.

*Turbine Aerodynamics: Axial-flow and Radial-flow Turbine Design and Analysis*. New York: ASME Press, 2006.

BAGSHAW, D.; ALIZADEH, S.; MABILAT, C. and LEWIS, L.

CFD-FE Automation and Thermo-Fluid Characterisation of an IP Turbine Cavity. In: *Proceedings of the ASME Turbo Expo 2010: Turbine Technical Conference and Exposition*. New York and N.Y: ASME, 2010.

BAYLEY, F. J. and CONWAY, L.

Fluid friction and leakage between a stationary and rotating disc. *ARCHIVE: Journal of Mechanical Engineering Science 1959-1982 (vols 1-23)* 6(2), 1964, P. 164–172.

BAYLEY, F. J. and OWEN, J. M.

The Fluid Dynamics of a Shrouded Disk System With a Radial Outflow of Coolant. *Journal of Engineering for Power* 92(3), 1970, P. 335.

BERTHOLD, M.

*Turbine Inner Cavities Flow Field Characterisation and Scaling Methods for Preliminary Design: Diplomarbeit.* 2012.

BISCHOFF, T.; VOIGT, M.; CHEHAB, E. and VOGELER, V.

Probabilistic Analysis of Stationary Gas Turbine Secondary Air Systems: GT2006-90261. In: *Proceedings of the ASME Turbo Expo 2006: Turbine Technical Conference and Exposition.* New York and N.Y: ASME, 2006.

BRÄUNLING, WILLY J. G

*Flugzeugtriebwerke: Grundlagen, Aero-Thermodynamik, ideale und reale Kreisprozesse, Thermische Turbomaschinen, Komponenten, Emissionen und Systeme.* VDI-Buch, Berlin and Heidelberg: Springer-Verlag Berlin Heidelberg, 2009.

BROPHY, F.; MAH, S. and TURCOTTE, J.

Preliminary Multi-Disciplinary Optimization (PMDO) an Example at Engine Level. In: NATO SCIENCE AND TECHNOLOGY ORGANIZATION (Editor), *RTO-EN-AVT-167 - Strategies for Optimization and Automated Design of Gas Turbine Engines.* 2010.

CHAKRABARTI, A.; SHEA, K.; STONE, R.; CAGAN, J.; CAMPBELL, M.; HERNANDEZ, N. V. and WOOD, K. L.

Computer-Based Design Synthesis Research: An Overview. *Journal of Computing and Information Science in Engineering* 11(2), 2011, P. 021003.

CHAQUET, J. M.; CORRAL, R.; PASTOR, G.; PUEBLAS, J. and COREN, D. D.

Validation of a Coupled Fluid/Solid Heat Transfer Method: GT2011-45951. In: *Proceedings of the ASME Turbo Expo 2011: Turbine Technical Conference and Exposition.* New York and N.Y: ASME, 2011.

CHAUDHARI, V.; MONIZ, T.; NAIKTARI, C.; WASLO; D.; KANASE and M.

Integrated Preliminary Design Approach for Turbomachinery Design: GT2011-45546. In: *Proceedings of the ASME Turbo Expo 2011: Turbine Technical Conference and Exposition.* New York and N.Y: ASME, 2011.

CHEW, J. W. and HILLS, N. J.

Computational fluid dynamics for turbomachinery internal air systems. *Philosophical trans-*



*actions. Series A, Mathematical, physical, and engineering sciences* 365(1859), 2007, P. 2587–2611.

CHEW, J. W. and HILLS, N. J.

Computational fluid dynamics and virtual aeroengine modelling. *Proceedings of the Institution of Mechanical Engineers, Part C: Journal of Mechanical Engineering Science* 223(12), 2009, P. 2821–2834.

CIAMPOLI, F.; CHEW, J. W.; SHAHPAR, S. and WILLOCQ, E.

Automatic Optimization of Preswirl Nozzle Design. *Journal of Engineering for Gas Turbines and Power* 129(2), 2007, P. 387.

CLAUS, R.; EVANS, A. and FOLLEN, G.

Multidisciplinary propulsion simulation using NPSS. In: *4th Symposium on Multidisciplinary Analysis and Optimization*. 1992.

CROSS, H.

*Analysis of flow in networks of conduits or conductors, University of Illinois bulletin*, Volume v. 34, no. 22. Urbana and Ill: University of Illinois, 1936.

DAILY, J. W. and NECE, R. E.

*Roughness and chamber dimension effects on induced flow and frictional resistance of enclosed rotating disks, Technical report*, Volume no. 27. [Cambridge and Mass.]: Hydrodynamics Laboratory, Dept. of Civil and Sanitary Engineering, Massachusetts Institute of Technology, 1958.

DEBUCHY, R.; PONCET, S. and ABDEL NOUR, F.

Experimental and numerical investigation of turbulent air flow behaviour in a rotor-stator cavity. *Proceedings of the 8th European Turbomachinery Conference* 2009.

DI MARE, L.; KULKARNI, D. Y.; WANG, F.; ROMANOV, A.; RAMAR, P. R. and ZACHARIADIS, Z. I.

Virtual Gas Turbines: Geometry and Conceptual Description: GT2011-46437. In: *Proceedings of the ASME Turbo Expo 2011: Turbine Technical Conference and Exposition*. New York and N.Y: ASME, 2011, P. 347–358.

DIXON, J. A.; VERDICCHIO, J. A.; BENITO, D.; KARL, A. and THAM, K. M.

Recent developments in gas turbine component temperature prediction methods, using com-

putational fluid dynamics and optimization tools, in conjunction with more conventional finite element analysis techniques. *Proceedings of the Institution of Mechanical Engineers, Part A: Journal of Power and Energy* 218(4), 2004, P. 241–255.

DORFMAN, L. A.

*Hydrodynamic resistance and the heat loss of rotating solids.* [1st english ed.] Inlage. Edinburgh: Oliver & Boyd, 1963.

DYE, C.; STAUBACH, J. G.; EMMERSON, D. and JENSEN, C. G.

CAD-Based Parametric Cross-Section Designer for Gas Turbine Engine MDO Applications. *Computer Aided Design and Applications, Ryerson University* (Vol. 4, Nos. 1-4), 2007, P. 509–518.

EDMUNDS, T.

Practical three dimensional adaptive analysis. In: *Proceedings of 4th International Conference on Quality Assurance and Standards.* 1993.

EUROPEAN COMMISSION

*Flightpath 2050: Europe's vision for aviation.* Luxembourg: Office for Official Publications of the European Communities, 2011.

FLASSIG, P.

*Unterstützende Optimierungsstrategien zur robusten aerodynamischen Verdichterschaufelauslegung.* Berichte aus der Luft- und Raumfahrttechnik, Aachen: Shaker, 2011.

GANINE, V.; JAVIYA, U.; HILLS, N. J. and CHEW, J. W.

Coupled Fluid-Structure Transient Thermal Analysis of a Gas Turbine Internal Air System With Multiple Cavities. *Journal of Engineering for Gas Turbines and Power* 134(10), 2012, P. 102508.

GOSMAN, A. D.

*Transfer of heat in rotating systems, HTS,* Volume 75,12. London: Imperial College of Science and Technology, Dep. of Mechanical Engineering, 1975.

GRASSELT, D.

*An Automated Process for CFD Investigation of Jet Engine Generic Cavities: Application to the Non-ventilated Turbine Interstage Cavity: Diplomarbeit.* 2011.

HAN, J. C.; DUTTA, S. and EKKAD, S.

*Gas turbine heat transfer and cooling technology. 2.* Inlage. Boca Raton and Fla: CRC Press, 2013.

HESELHAUS, A.; VOGEL, T. and KRAIN, H.

Coupling of 3D-Navier-Stokes External Flow Calculations and Internal 3D-Heat-Conduction Calculations for Cooled Turbine Blades. In: *AGARD-CP AGARD Conference Proceedings, Heat Transfer and Cooling in Gas Turbines.* 1992.

HILLS, N. J. and CHEW, J. W.

Computational fluid dynamics and virtual aeroengine modelling. *Proceedings of the Institution of Mechanical Engineers, Part C: Journal of Mechanical Engineering Science* 223(12), 2009, P. 2821–2834.

JESCHKE, P.; KURZKE, J.; SCHABER, R. and RIEGLER, C.

Preliminary Gas Turbine Design Using the Multidisciplinary Design System MOPEDS. In: *ASME Turbo Expo 2002: Power for Land, Sea, and Air.* 2002, P. 75–84.

JONES, M. J.; BRADBROOK, S. J. and NURNEY, K.

*A Preliminary Engine Design Process for an Affordable Capability.* Ft. Belvoir: Defense Technical Information Center, 2003.

KÁRMÁN, T. V.

On laminar and turbulent friction. *Zeitschrift für angewandte Mathematik und Mechanik*, 1921, Vol. 1, No. 4 1092, 1946.

KUPIJAI, P.; BESTLE, D.; FLASSIG, P. M. and KICKENWEITZ, D.

Automated Multi-Objective Optimization Process for Preliminary Engine Design: GT2012-68612. In: *Proceedings of the ASME Turbo Expo 2012: Turbine Technical Conference and Exposition.* New York and N.Y: ASME, 2012, P. 87–96.

KURZKE, J. T.

*Gasturb Version 8.0 - Gasturb version 8.0 - User's Manual.* München, 1998.

KUTZ, K. J. and SPEER, T. M.

Simulation of the Secondary Air System of Aero Engines. *Journal of Turbomachinery* 116(2), 1994, P. 306.

LYTLE

*The numerical propulsion system simulation: A multidisciplinary design system for aerospace vehicles.* Cleveland and Ohio, 1999.

MAJUMDAR, A.

*A generalized fluid system simulation program to model flow distribution in fluid networks, [NASA contractor report],* Volume NASA/CR-207793. Washington and DC and Springfield and Va: National Aeronautics and Space Administration and National Technical Information Service, distributor, 1998.

MATTINGLY, J. D.; HEISER, W. H. and PRATT, D. T.

*Aircraft engine design.* 2. Inlage. AIAA education series, Reston and VA: American Institute of Aeronautics and Astronautics, 2002.

MERKLER, R. S.; STAUDACHER, S. and SCHMIDT K. J.

Modellierung Des Luftsystems Von Turboflugtriebwerken Für Die Anwendung In Leistungssyntheseprogrammen: DGLR-2003-006. In: *Deutscher Luft- und Raumfahrtkongress 2003.* 2003, P. 817–824.

MILLER, D. S.

*Compressible internal flow, BHRA fluid engineering series,* Volume v. 10. [Cranfield]: BHRA Fluid Engineering, 1984.

MILLER, R. G. and SORRELL, S. R.

The future of oil supply. *Philosophical Transactions of the Royal Society A: Mathematical, Physical and Engineering Sciences* 372(2006), 2013, P. 20130179.

MILLWARD, J. A. and EDWARDS, M. F.

Windage Heating of Air Passing Through Labyrinth Seals. *Journal of Turbomachinery* 118(2), 1996, P. 414.

MULLER, Y. and MONNOYER DE GALLAND, F.

*Coupled thermomechanical fluid-structure interaction in the secondary air system of aircraft engines: Contribution to an integrated design method.* [S.l.]: [s.n.], 2009.

MÜNZBERG, H.-G. and KURZKE, J. T.

*Gasturbinen - Betriebsverhalten und Optimierung.* Hochschultext, Berlin [etc.]: Springer Verlag, 1977.

NOURI, B.; LEHMANN, K. and KÜHHORN, A.

Automated CAE Process for Thermo-Mechanical Lifting Prediction of a Parameterized Turbine Blade with Internal Cooling. In: *ECCOMAS 2014 Proceedings*. 2014.

ORACLE

Java. 2014. URL <http://www.java.com/en/about/>.

OWEN, J. M. and ROGERS, R. H.

*Flow and heat transfer in rotating disc systems: Rotor-Stator Systems (Vol. 1), Mechanical engineering research studies : Engineering design series*, Volume 1. Taunton and New York: Research Studies Press and Wiley, 1989.

OWEN, J. M. and ROGERS, R. H.

*Flow and heat transfer in rotating-disc systems: Rotating Cavities (Vol. 2), Mechanical engineering research studies Engineering design series*, Volume 2. Taunton and New York: Research Studies Press and Wiley, 1995.

PAHL, G.; BEITZ, W.; BLESSING, L.; FELDHUSEN, J.; GROTE, K.-H. and WALLACE, K.

*Engineering Design: A Systematic Approach*. Third edition  
Inlage. London: Springer-Verlag London Limited, 2007. URL  
<http://site.ebrary.com/lib/alltitles/docDetail.action?docID=10230457>.

PANCHENKO, V.; MOUSTAPHA, H.; MAH, S.; PATEL, K. and DOWHAN, M. J.

*Preliminary Multi-Disciplinary Optimization in Turbomachinery Design*. Ft. Belvoir: Defense Technical Information Center, 2003.

PETERS, A.

*Assessment of propan propulsion systems for reduced environmental impact*. 2010.

PRADO, P.; PANCHENKO, Y.; TRÉPANIER, J.-Y. and TRIBES, C.

Preliminary Multidisciplinary Design Optimization System: A Software Solution for Early Gas Turbine Conception. In: *ASME Turbo Expo 2005: Power for Land, Sea, and Air*. 2005, P. 213–220.

RAMERTH D. L.; MIRZAMOGHADAM A. V.; KIRATSINGH A. and BANDA G.

A Probabilistic Secondary Flow System Design Process for Gas Turbine Engines: GT2010-22071. In: *Proceedings of the ASME Turbo Expo 2010: Turbine Technical Conference and Exposition*. New York and N.Y: ASME, 2010.

REED, R. C.

*The superalloys: Fundamentals and applications.* [nachdr.] Inlage. Cambridge: Cambridge Univ. Press, 2008.

REY VILLAZON, J. M.; BERTHOLD, M. and KÜHHORN A.

Adaptive Flow Field Thermal Modeling Techniques for Turbine Rotor-Stator Cavities: GT2013-94845. In: *Proceedings of the ASME Turbo Expo 2013: Turbine Technical Conference and Exposition.* New York and N.Y: ASME, 2013.

REY VILLAZON, J. M.; WEISS, T. and KÜHHORN A.

A Parametric Impact Study Of The Geometry, Air System And Thermal Boundary Conditions On The Life Of A Two-Stage High Pressure Turbine: GT2012-68453. In: *Proceedings of the ASME Turbo Expo 2012: Turbine Technical Conference and Exposition.* New York and N.Y: ASME, 2012.

RIEG, F.; ALBER-LAUKANT, B. and HACKENSCHMIDT, R.

*Finite Elemente Analyse für Ingenieure.* 4. Inlage. München: Hanser, Carl, 2012.

RIGBY, D. L. and LEPICOVSKY, J.

Conjugate heat transfer analysis of internally cooled configurations: 2001-GT-0405. In: *ASME Turbo Expo 2001: Power for Land, Sea, and Air.* 2001.

ROLLS ROYCE

*The jet engine.* [6th ed.] Inlage. London: Rolls-Royce, 2005.

ROSIC, B.; DENTON, J. D. and PULLAN, G.

The Importance of Shroud Leakage Modeling in Multistage Turbine Flow Calculations. *Journal of Turbomachinery* 128(4), 2006, P. 699.

ROYAL AERONAUTICAL SOCIETY (Editor)

*Concurrent engineering and CALS.* London: Royal Aeronautical Society, 1995.

SANDBERG, M.; TYAPIN, I.; KOKKOLARAS, M.; ISAKASSON, O.; AIDANPAA, J.-O. and LARSSON, T.

A Knowledge-based Master-model Approach with Application to Rotating Machinery Design. *Concurrent Engineering* 19(4), 2011, P. 295–305.

SCHABER, R.

*Numerische Auslegung und Simulation von Gasturbinen.* München: Technische Universität München, 2000.

SCHOBEIRI, M. T.

*Turbomachinery flow physics and dynamic performance: Turbulent Flow and Modeling in Turbomachinery.* 2. Inlage. Berlin: Springer, 2012.

SIMULIA

Isight. 2014. URL <http://www.3ds.com/products-services/simulia/>.

STARKE, C. and SCHIFFER, H.-P.

Inclusion of an Estimation Method for Heat Losses in the Design Phase of High-Pressure Turbines. In: *Proceedings of the ASME Turbo Expo 2011: Turbine Technical Conference and Exposition.* New York and N.Y: ASME, 2011, P. 1597–1608.

STRICKER J. M.

The Gas Turbine Engine Conceptual Design Process - An Integrated Approach. *Symposium of the Applied Vehicle Technology Panel on Design and Methods for Aircraft Gas Turbine Engines* 1998.

STRICKER J. M. and NORDEN, C. M.

Computerized Preliminary Design of Turbomachinery: ASME 91-GT-391. *Proceedings of the ASME Turboexpo* 1991.

SUN, Z.; CHEW, J. W.; HILLS, N. J.; BARNES, C. J. and GUIJARRO-VALENCIA, A.

3D Coupled Fluid-Solid Thermal Simulation of a Turbine Disc Through a Transient Cycle: GT2012-68430. In: *Proceedings of the ASME Turbo Expo 2012: Turbine Technical Conference and Exposition.* New York and N.Y: ASME, 2012.

THEODORSEN, T. and REGIER, A.

*Experiments on drag of revolving disks, cylinders and streamline rods at high speeds, NACA WR, Volume L-226.* Langley Field and VA: Langley Memorial Aeronautical Laboratory, 1944.

TURNER, A. B.; LONG, C. A.; CHILDS; P.R.N.; HILLS, N. J. and MILLWARD, J. A.

A review of some current problems in gas turbine internal air systems: 97-GT-325. In: *ASME Aeroengine Congress.* 1997.

TYACKE, J.; TUCKER, P.; JEFFERSON-LOVEDAY, R.; RAO VADLAMANI, N.; WATSON, R.; NAQAVI, I. and YANG, X.

Large Eddy Simulation for Turbines: Methodologies, Cost and Future Outlooks. *Journal of Turbomachinery* 136(6), 2014, P. 061009.

ULLENBOOM, C.

*Java ist auch eine Insel: Das umfassende Handbuch ; [aktuell zu Java 7 ; Programmieren mit der Java Platform, Standard Edition 7 ; Java von A bis Z: Einführung, Praxis, Referenz ; von Klassen und Objekten zu Datenstrukturen und Algorithmen]*. 10. Inlage. Galileo computing, Bonn: Galileo Press, 2012.

VERDICCHIO, J.; CHEW, J. W. and HILLS, N. J.

Coupled fluid/solid heat transfer computation for turbine discs: 2001-GT-205. In: *ASME Turbo Expo 2001: Power for Land, Sea, and Air*. 2001.

VERES, J. P.

Flow of a Gas Turbine Engine Low- Pressure Subsystem Simulated. 1999.

VIRR, G. P.; CHEW, J. W. and COUPLAND, J.

Application of Computational Fluid Dynamics to Turbine Disk Cavities. *Journal of Turbomachinery* 116(4), 1994, P. 701.

WALSH, P. P. and FLETCHER, P.

*Gas turbine performance*. 2. Inlage. Malden and MA: Blackwell Science, 2008. URL <http://dx.doi.org/10.1002/9780470774533>.

WENZEL, V.; CHRIST, A.; JAGENBERG, J. T.; STRANG, D.; ANDERL, R. and BORNKESSEL, T.

Functional Shape Elements Integrating Design and Manufacturing Knowledge. In: *Smart Product Engineering*. Berlin and Heidelberg: Springer Berlin Heidelberg, 2013.

WILFERT G. and SIEBER J.

New Environmental Friendly Aero Engine Core Concepts. *ISABE* 2007.

WILLENBORG, K.; KIM, S. and WITTIG, S.

Effects of Reynolds Number and Pressure Ratio on Leakage Loss and Heat Transfer in a Stepped Labyrinth Seal. *Journal of Turbomachinery* 123(4), 2001, P. 815.



WYSONG, R. R.; PRINCE, T. C.; LENAHAN, D. T.; CANEY, R. D. and KEITH, J. S.

*Turbine Design System: A preliminary design system for turbines.* Ft. Belvoir: Defense Technical Information Center, NOV 1978.

WYSONG, R. R. and TABAKOFF, W.

*A computer program for the detailed design of free vortex turbines.* Ft. Belvoir: Defense Technical Information Center, JUL 1965.

ZIMMERMANN, H.

Some Aerodynamic Aspects of Engine Secondary Air Systems. *Journal of Engineering for Gas Turbines and Power* 112(2), 1990, P. 223.

## Publications

Rey Villazon, J. M., Wildow, T., Kühhorn, A., Benton, R., Eydam T. Advanced Turbine Preliminary Design Environment for the Automatic Generation of Secondary Air System Models. Proceedings of the ASME Turbo Expo 2015, Paper GT2015-42661, 15 – 19 June, Montreal.

Rey Villazon, J.M., Kuehhorn, A. Adaptive CFD-Enhanced Windage Modelling for Aero Engine Turbine Rotor-Stator Cavities. Joined 11th World Congress on Computational Mechanics (WCCM XI), 5th European Conference on Computational Mechanics (ECCM V), 6th European Conference on Computational Fluid Dynamics (ECFD VI) conference, 21-25 July 2014 Barcelona.

Rey Villazon, J. M., Wildow, T., Kühhorn, A., Benton, R., Göhler, M. Impact of the Secondary Air System Design Parameters on the Calculation of Turbine Discs Windage. Proceedings of the ASME Turbo Expo 2014, Paper GT2014-26050, 16 – 20 June, Düsseldorf.

Rey Villazon, J. M., Weiss, T., Guijarro Valencia, A. Introduction to Fluid-Structure Coupled Analyses of Turbomachinery using FE and CFD Methods. Tutorial Session at the ASME Turbo Expo 2014, 19th June, Düsseldorf

Rey Villazon, J. M., Berthold, M., Kühhorn, A. Parametric Thermal Modeling Techniques for Turbine Rotor-Stator Cavities. 6. Dresdner Probabilistik-Workshop. Technische Universität Dresden, 10.-11. Okt. 2013.

Rey Villazon, J. M., Berthold, M., Kühhorn, A. Adaptive Flow Field Thermal Modeling Techniques for Turbine Rotor-Stator Cavities. Paper GT2013-94845, Proceedings of ASME Turbo Expo 2013, June 3-7, San Antonio, Texas, USA. Awarded Rolls-Royce Deutschland Innovationsspreis 2013.

Rey Villazon, J. M., Kühhorn, A., Weiß, T. A Parametric Impact Study of the Geometry, Air System and Thermal Boundary Conditions on the Life of a Two-Stage High Pressure Turbine. Proceedings of the ASME Turbo Expo 2012, Paper GT2012-68453, 11. - 15. June 2012, Copenhagen.

# Lebenslauf

Geburtsdatum/ -ort: 10. September 1982 / Madrid, Spanien

Familienstand: verheiratet; Staatsangehörigkeit: Spanisch

Email: jm.reyvillazon@gmail.com

## Beruflicher Werdegang

Seit 11/2014: Lead-Ingenieur Thermal-Systeme. Advanced Aviation Technology. GE Aviation. München, Deutschland.

05/2010 – 09/2014: Wissenschaftlicher Mitarbeiter. Projekt ViT3. Brandenburgische Technische Universität Cottbus in Kooperation mit Rolls-Royce Deutschland Ltd & Co KG. Cottbus & Dahlewitz, Deutschland. Lehrstuhl für Strukturmechanik und Fahrzeugschwingungen (SMF).

11/2009 – 02/2010: Freiwilligenarbeit. UONCRE. Quininde, Ecuador.

10/2007 – 09/2009: Entwicklungsingenieur im Bereich Thermofluidodynamik. Rolls-Royce Deutschland Ltd & Co KG. Dahlewitz, Deutschland.

02/2007 – 10/2007: Entwicklungsingenieur im Bereich Strukturanalyse. ITP Industria de Turbopropulsores. Bilbao, Spanien.

07/2006 – 12/2006: Diplomarbeit im Bereich Rotordynamik von Flugantriebe. Rolls-Royce Plc. Civil Aerospace. Derby, Vereinigtes Königreich.

06/2005 – 9/2005: Praktikum im Bereich Triebwerksauslegungsmethoden. ITP Industria de Turbopropulsores. Madrid, Spanien.

## Ausbildung

09/2000 – 06/2006: Studium an der Universidad Politecnica de Madrid (UPM). Spanien. Diplom-Studiengang: Luft- und Raumfahrttechnik. Abschluss: Dipl.-Ing.

09/1999 – 06/2000: Gymnasium Colegio Valdeluz. Madrid, Spanien. Abschluss: Allgemeine Hochschulreife Selectividad (entspricht Abitur).

09/1996 – 06/1999: Walt Whitman High School. Potomac, Maryland, U.S.A.